UNIVERSITY OF HULL

Experimental and theoretical studies of surface and volume changes in dielectrics induced by long-pulse RF CO_2 laser irradiation

by

A. L. Marchant, BSc.

being a thesis submitted for the
degree of Doctor of Philosophy

in the
Faculty of Science
Department of Physics

March 2012

"What we need are clearly defined areas of doubt and uncertainty."

D. N. Adams

Abstract

This thesis describes research into infrared (IR) laser irradiation and damage of four commercially significant polymers: polyimide (PI), polyether ether ketone (PEEK), polyethylene terephthalate (PET) and polypropylene (PP). Many research groups have studied the laser ablation and irradiation of polymers, but they have focussed mainly on ultraviolet and pulsed infrared sources. There appears to be little published data for laser irradiation of polymers with IR lasers operating with pulse durations in the range 50μs to 1ms.

Laser coupling to polymers is strongly dependent on the absorption coefficient at the emission wavelength. These properties are widely known and used to inform experimental practice but the absorption coefficient used in the literature is usually that measured at room temperature and low power. In this way it does not truly represent typical experimental conditions. It is also commonly assumed that the laser wavelength is constant. In this work the laser wavelength has been determined as a function of time during a typical pulse for a radio frequency (RF) excited CO_2 laser. It was found that the emission wavelength could move from as short as 10.53μm to as long as 10.63μm during a 200μs duration pulse. This alone was seen to affect the absorption coefficient of the polymers studied. The absorption coefficient as a function of polymer temperature was measured over all wavelengths. This allowed any changes in the optical coupling during laser heating to be inferred. The change in absorption coefficient as a function of temperature was determined as being -0.40$cm^{-1}K^{-1}$, 0.86$cm^{-1}K^{-1}$, 0.48$cm^{-1}K^{-1}$

and 0.04cm^{-1}K^{-1} for PI, PEEK, PET and PP respectively at a wavelength of 10.59μm.

The threshold fluence for damage was determined as a function of the laser pulse duration. Damage included any permanent change to the polymer surface and in this way took into account decomposition and melting, as well as ablation. Together with the absorption coefficient data, this allowed the energy densities to be calculated. For PI and PEEK these were found to be 2.4kJ/cm^3 and 1.9kJ/cm^3 respectively and agreed with existing data. The threshold energy density was 0.1kJ/cm^3 for PET and 0.2kJ/cm^3 for PP. These results were smaller than those expected from the literature due to melting rather than ablation taking place.

The threshold fluence for each polymer was found to be mostly independent of laser pulse duration over the range investigated. The small thermal diffusivity of the materials was thought to be the reason for this. Calculations using solutions to the heat diffusion equation and a rate limited thermal decomposition model were found to be consistent with the experimental results. Some initial calculations of the effect of including the temperature dependent absorption coefficient indicated that this does indeed affect the temperature profile during and after the laser pulse.

It has been shown that the RF CO_2 laser is suitable for polymer processing, particularly for applications where spot size and high resolution etching are not an issue. Laser marking, cutting and hole-drilling would be acceptable applications for this laser which offers more choice in terms of duty-cycle and pulse duration than the pulsed TEA CO_2 alternatives. Quantification of the thermal and optical

properties and the interaction between these two parameters could be extended to other polymers and it is expected that similar behaviours would be observed.

Acknowledgements

I would like to thank my supervisor, Dr Howard Snelling, for his help, advice and patience throughout my studies as an undergraduate and a PhD student. He has been an interested and encouraging supervisor and friend. I am very grateful for his ideas, insights and the hard work he has put in.

I would also like to thank Marie-Cappucine Pope, Steve Myers, Tony Sinclair, Ian Dobson, Graham Randerson and David Stavenau for their time, support and helpful advice during some of the experiments performed throughout my PhD. I could not have done it without you!

Special thanks go to my fellow PhD students, both past and present. I am very grateful for the friendship and understanding you have given.

I would like to thank my family and friends for their love and support during my studies. Particularly my parents, Karen and Peter, and my sister Emily. You have offered a shoulder to cry on as well as many encouraging words along the way. A special thank you to Karl, who has been a constant source of support throughout my degree and PhD.

Finally, to my partner David, thank you for being there. You have been my rock.

Contents

Chapter 1

Introduction

The laser irradiation of polymers has been very well covered in the literature for ultraviolet (UV) lasers. Many research papers are available and there are a number of extensive reviews of existing literature [1–3].

Due to the limitations of the UV lasers from an industrial standpoint, infra-red (IR) sources have become much more prevalent in industry especially in low value and high volume markets. Understanding the processes involved in the interaction between IR photons and polymers is therefore an important area for research. The studies covering the use of pulsed lasers have been reviewed and contrasted in publications which bridge the gap between UV and IR pulsed sources [4]. Literature concerning the carbon dioxide (CO_2) laser irradiation of polymers has focussed mainly on the pulsed transversely excited atmospheric pressure (TEA) laser [5–9].

This thesis gives an account of the long pulse CO_2 laser irradiation of polymers, which has received significantly less attention than the short pulse TEA CO_2 counterparts. The aim of the work was to study and better understand the process of laser induced surface and volume changes in this regime. The laser used in this work was a radio frequency (RF) excited CO_2 laser and the polymers studied were polyimide (PI), PEEK, PET and polypropylene (PP). These materials were selected due to being both prevalent in industry and differing in optical and thermal parameters. Laser ablation is of interest for these polymers for many applications including marking and cutting and the RF CO_2 laser offers advantages over other

laser sources due to the cheap operation costs, the use of non-toxic gases and greater efficiency.

The polymers used here have been studied in the literature over a wide range of laser wavelengths and pulse durations. This thesis aims to begin to fill the gap in current research for IR lasers operating at pulse durations in the range of approximately 50–500μs. In particular, the threshold fluence for ablation and damage and the effects of temperature rise on the optical coupling to these materials have been studied in detail.

In Chapter 2 a literature review is presented which gives an overview of the research which has already been carried out using lasers to irradiate polymers. A description of the various mechanisms of ablation is given. The industrial context of laser ablation is also discussed, with particular focus on ablation and surface modification in the IR laser regime. Additionally, the introduction to each chapter briefly discusses the literature pertaining to the work that follows.

Chapter 3 describes characterisation of the laser being used in this work. Calibration of the laser pulse duration and energy per pulse is shown. The operating wavelength is determined both in a time integrated fashion and as a function of time during a typical laser pulse. The optical absorption coefficient is most often used at a fixed laser operating wavelength, which is appropriate as an estimation. However, if the wavelength of the laser changes, the optical coupling to the polymer may also be affected.

In Chapter 4, the thermal and optical properties of PI, PEEK, PET and PP are

investigated with a view to better understanding the changes in each polymer during long pulse laser irradiation. The decomposition temperature for each polymer is determined using thermo-gravimetric analysis (TGA) to allow this characteristic to be used in model calculations. The IR optical absorption coefficient is then investigated using Fourier transform infra-red (FTIR) spectroscopy both at room temperature and as a function of increasing temperature. The wavelength results found in Chapter 3 are used to study the change in optical absorption both during heating and as a function of laser operating wavelength. To further the work in this chapter, the transmission of the laser light through each polymer is measured and compared to the data of the absorption coefficient as a function of laser wavelength and polymer temperature.

Chapter 5 describes the surface and volume changes of each polymer after focussed irradiation with the laser described in Chapter 3. Single laser pulses of different pulse duration and energy are used. Measurements of the damage sites allow the threshold fluence for damage of each polymer to be determined as a function of laser pulse duration. The damage sites are also studied in more detail using scanning electron microscopy (SEM). A PP damage site is studied with white light interferometry with a view to profiling the whole damage site.

In Chapter 6, the results obtained in Chapters 4 and 5 (and to a certain extent Chapter 3) are analysed using the heat diffusion equation and a rate limited thermal decomposition model. Both numerical and semi-analytical solutions are compared and used to calculate the threshold fluence as a function of the laser pulse duration based on material properties. The outcome of the modelling is compared

to experimental results. A discussion and some calculations using the temperature dependent absorption coefficient are included to determine the importance of this parameter in analysing the process theoretically.

Finally, in Chapter 7, an overview of all findings is given and conclusions are drawn about the results obtained in the thesis as a whole. Some proposed work that could follow on from this study is discussed.

Chapter 2

Literature Review

2.1 Laser ablation of polymers

The interaction of photons with a polymer can lead to a variety of reactions ranging from changes in the polymer surface to complete decomposition [1]. The ultraviolet (UV) laser ablation of polymers was first reported in 1982 by Srinivasan et al [10] and Kawamura et al [11].

Since these first publications, the ablation of a wide variety of polymers using a range of different laser sources has been studied extensively in the literature. There have also been a number of reviews and books covering the work in the years following the first papers. The UV ablation of polymers has been reviewed in a number of papers, including those by Yeh [12], Dyer [2], Srinivasan et al [13], Lippert et al [1] and more recently Bityurin [14]. Said-Galiev et al [15] and Bityurin [14] give a review of the IR ablation of polymers, with IR lasers receiving much less attention than lasers operating in the UV regime [16]. Specifically, polymer research using CO_2 lasers has focussed primarily on the transversely excited atmospheric pressure (TEA) CO_2 laser [6, 7, 9, 17–23].

The UV laser ablation of polymers has been studied over a wide range of materials, including polymethyl methacrylate (PMMA), polyurethane (PU), polyimide (PI), polyethylene terephthalate (PET), polycarbonate (PC), polyether ether ketone

(PEEK), polytetrafluoroethylene (PTFE) and many others [24, 25]. In the IR, a similar range of polymers have been investigated.

Despite the plethora of publications, there is still discussion about the interaction of lasers with polymers and the specific mechanisms of laser ablation [2, 22, 26].

Laser ablation is defined as material removal by high-intensity laser irradation [27]. A threshold fluence gives an indication of the laser energy per unit area which has to be exceeded to begin significant removal of material [24]. The threshold fluence is usually expressed in units of J/cm^2 and in general decreases with increasing absorption coefficient. The absorption coefficient is a measure of the absorptive power of a material and is specific to wavelength and is generally expressed in units of cm^{-1}. It follows that a characteristic optical absorption depth is the reciprocal of the absorption coefficient and therefore with increasing absorption coefficient the energy of a laser pulse is deposited into a smaller volume.

The product of the absorption coefficient and the threshold fluence is known as the energy density, or ablation enthalpy [2], and is thought to be mostly constant for a given polymer [2, 24], provided that the mechanism for material removal is thermal in nature. It follows that as the absorption coefficient increases, the energy is deposited into a smaller volume and the fluence required to overcome the ablation threshold is reduced. In contrast, a small absorption coefficient would result in the energy being deposited over a large volume and therefore a higher fluence would be required to overcome a threshold for ablation.

The threshold fluence is generally determined by measurements of etch depth.

Laser pulses are used to ablate the material and the ablated depth is measured and divided by the number of pulses used. This gives the etch depth per pulse, which is seen to depend on the laser fluence. The relationship between the etch depth per pulse (x), the laser fluence (F), the threshold fluence for ablation (F_T) and the effective optical absorption coefficient (α_e) is often seen to follow equation 2.1 [2, 24].

$$x = \frac{1}{\alpha_e} ln \left(\frac{F}{F_T} \right) \tag{2.1}$$

It follows from equation 2.1 that if the etch depth per pulse is plotted as a function of the natural logarithm of the laser fluence, that the gradient would equal the reciprocal of the effective absorption coefficient. This absorption coefficient differs from that measured at low power, as changes in the polymer due to temperature rise, density and chemical alterations and non-linear effects are not taken into account during low power absorption measurements [24].

Shown in figure 2.1 is a typical and simplified graph obtained from a polymer etch experiment where Beer's law, and therefore equation 2.1, is applicable. The etch depth per pulse as a function of the natural logarithm of the laser fluence is plotted and the threshold fluence is also indicated.

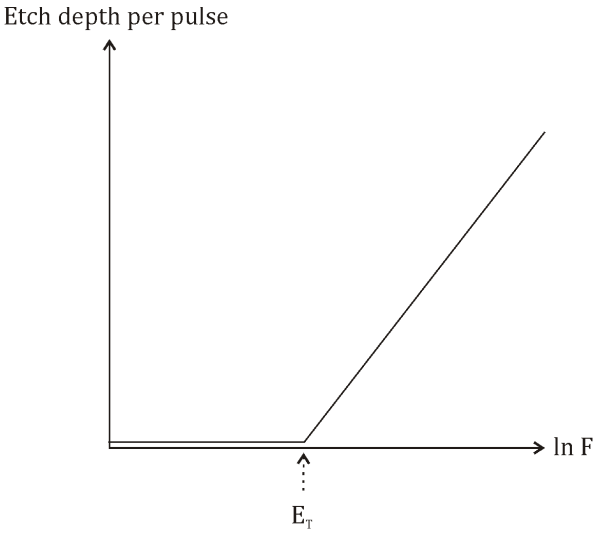

FIGURE 2.1: Etch depth per pulse as a function of the natural logarithm of the laser fluence. The threshold fluence for ablation is indicated on the graph. Adapted from [24].

Other methods have been used to determine the etch rate which are more sensitive than averaging the etch depth over a number of pulses. Although this method gives a fairly accurate representation of the process as a whole, it does not take into account the individual contribution of each pulse to the overall ablation rate. Sensitive techniques such as atomic force microscopy (AFM) and weight loss measurements by quartz crystal micro-balances can detect changes in materials in the initial stages of ablation, without the need for averaging the effect over many pulses. Dumont et al [28] gained more information about the behaviour of polyimide around the threshold fluence by measurement of the weight per successive pulses from 248nm and 308nm lasers, using a quartz crystal micro-balance. A difference between the ablation rate of the first pulse and that of subsequent pulses was detected; a subtle effect which would not have been made clear had multiple pulses been used. Similarly, in a study by Küper et al [29] laser pulses with wavelengths ranging from 193nm to 351nm were used to irradiate polyimide and the

ablation rate determined using a QCM.

Important considerations when measuring the threshold fluence of laser ablation are incubation effects and the plume of ablation products, resulting from material leaving the polymer surface. Incubation is the process by which earlier pulses, which do not ablate the material, change the chemical composition or introduce defects which effectively increase the absorption coefficient and therefore allow ablation to proceed. Chemical and physical defects caused by the laser radiation can influence microscopic interactions between the laser and material [27]. Experimental etch rates differ from the behaviour described by equation 2.1 because the later part of the laser beam must pass through the plume, which has a different absorption coefficient to the bulk material [2, 24]. Equation 2.1 then becomes [2, 24]:

$$x = \frac{1}{\alpha_p} \ln\left(\frac{\alpha_p F}{\alpha_e F_T} - \frac{\alpha_p}{\alpha_e} + 1\right) \tag{2.2}$$

In equation 2.2, α_p is the absorption coefficient of the plume. In the case where both the absorption coefficient of the plume and the bulk are the same, equation 2.2 reduces to equation 2.1. When $\alpha_p > \alpha_e$ the etch rate is seen to rise less rapidly and when $\alpha_p < \alpha_e$ the etch rate rises more rapidly [2, 24]. Despite the complicated effects that are seen during ablation, it is generally accepted that equation 2.1 gives a useful guideline to determine the threshold fluence for ablation [2].

2.2 Mechanisms of ultraviolet laser ablation of polymers

There has been much debate over the fundamental mechanisms of ablation using UV lasers [24]. Two processes are generally considered: bond breaking processes via a direct photochemical route or a highly localised thermal reaction (photo thermal ablation) [1, 24].

Photochemical ablation is based on the absorption of photons of sufficiently high energy that result in direct bond breaking of the polymer, where material is ejected due to repulsive forces between species [2]. UV photons have energies in the range 3.5–7.9eV and it is generally accepted that the absorption of UV photons results in electronic excitation of the polymer being irradiated [13] and in reference [3] UV photon energies are shown to correspond to molecular bonds commonly found in organic polymer materials. One possible outcome of the absorption of UV photons is that the excited electronic state can undergo decomposition in that state, which would be a purely photochemical reaction [13]. In terms of removal of material, the local particle number density in the irradiated volume increases due to bond breaking and this is accompanied with a rise in pressure. The pressure is released as a shock wave that ejects polymer material, usually as gas and monomers [3]. The reaction step which results in the breaking of bonds, and therefore polymer ablation due to photochemical processing, happens on a time scale which is faster than the time required for thermalisation of the excited state [27].

Equation 2.3 can be used to estimate the fluence required to achieve photochemical ablation. In this equation, n is the number of bonds per unit volume which must be broken to result in material removal, $h\nu$ is the photon energy, η is the quantum yield for breaking the bonds, α is the absorption coefficient and R is the reflectivity.

$$F_T = \frac{nh\nu}{\eta\alpha(1-R)} \tag{2.3}$$

The first investigation of the mechanism of UV laser ablation of polymers was based on the idea that a polymer can be seen as a simple molecular solid [30] and the bonds could be directly broken by UV photons due to the process described above. This interpretation of the ablation mechanism was further supported by the observed precision of the ablated regions and a lack of detectable thermal damage of the polymer [3, 13]. In equation 2.3, the calculated fluence exceeds that found experimentally in most cases [2] and in order to successfully predict the threshold fluence from this equation, η must be approximately unity.

It was noted by Braun et al that etch rate measurements did not allow the specific mechanisms of UV laser ablation to be deduced from this method of measurement [17]. Photochemical models for ablation are discussed in detail by Buerle [27] and have been developed and reviewed by a number of research groups [14, 31].

Evidence then came to light that heating due to absorption of UV laser photons could also occur [31–33]. Photo-thermal ablation with UV laser irradiation is brought about when the absorbed laser energy produces an elevated temperature sufficient to decompose the material [2]. In this process, the excited electronic

states resulting from the absorption of UV photons undergo internal conversion to vibrational modes and subsequent decomposition is mostly thermal in nature [2, 13]. This relaxation is thought to occur on a time scale that is short compared with the laser pulse [2], with the electronic energy relaxing into heat during a time of 10^{-12} to 10^{-13}s [15]. Using equation 2.4 [2], the threshold fluence for a photo-thermal mechanism can be estimated. Here, C is the specific heat of the polymer, R is the reflectivity, T_R is the initial surface temperature and T_D is the temperature at which significant decomposition, and therefore ablation, is achieved.

$$F_T = \frac{C(T_D - T_R)}{\alpha(1 - R)} \tag{2.4}$$

Another important consideration in the photo-thermal ablation mechanism is the rate limited nature of thermal decomposition of polymers. The rate at which volatile products are formed (k), varies with temperature (which could be estimated from equation 2.4) as shown in equation 2.5 below [2].

$$k = Ae^{\frac{-E_A}{KT}} \tag{2.5}$$

In this Arrhenius expression, T is the temperature and K is the gas constant. The pre-exponential factor and the activation energy for the decomposition process are given as A and E_A respectively and depend on the polymer. A threshold fluence arises from the fact that the rate k must be sufficiently high so that material

decomposition occurs on a time scale such that the material is still hot enough to drive the process.

Küper et al [29] studied the UV ablation behaviour of polyimide at low fluence with sources operating at 193, 248, 308 and 351nm. The results found in the work implied that there was evidence for both photochemical and photo-thermal processes. Other publications have come to the same conclusion, but without definitive results of which mechanism is dominant [22, 24].

It is generally accepted that UV ablation of polymers is a complex subject and discussion is ongoing as to the exact mechanisms and their relative contribution to the process [34].

2.3 Mechanisms of infrared ablation of polymers

The processes involved in ablation using IR lasers generally fall into the category of photothermal, similar to that described for UV lasers above but with a different absorption process. It is assumed that in the IR wavelength region, this is the dominant mechanism, which somewhat simplifies the interpretation of ablation using this category of laser. IR photons directly excite vibrational modes in the polymer [21]. This excludes photochemical bond breaking as a mechanism to be considered because photons from IR sources do not have sufficient energy to directly break chemical bonds in the polymers [3]. After excitation of the vibrational modes, the energy becomes thermal on a rapid time-scale of the order of 10^{-12}s [21]. Again, in terms of actual removal of material, bonds in the polymer

break due to the elevated temperature which exceeds some decomposition parameter. The resulting polymer fragments and gas phase species typically occupy a larger volume compared to the surrounding material and, with the generation of sufficient pressure, lead to the forwarded ejection of ablated material [35].

In a paper by Said-Galiev et al, the CO_2 laser ablation of polymers is reviewed extensively [15]. The cause of ablation is cited as being similar to strong thermal shock and therefore, processes of thermal or thermo-oxidative breakdown of the polymer are particularly applicable.

2.4 Laser ablation of PI, PEEK, PET and PP

The following tables give a summary of some of the existing data for PI, PEEK and PET for a number of different laser wavelengths and ablation regimes. In the tables, λ is the wavelength, τ is the laser pulse duration, α is the absorption coefficient at λ and F_T is the threshold fluence. The enthalpy of ablation discussed earlier is also given (ΔH). The absorption coefficient in the literature was found from low power measurements or from the etch rate graphs. The pulse duration is sometimes given for pulsed TEA CO_2 lasers as an initial spike followed by a long tail, each of which contain a portion of the laser pulse energy. The first duration given is the spike, which tends to contain in excess of 50% of the pulse energy and the number in brackets is the duration of the pulse tail where given. The citation for each set of data is also given. The parameters of interest here were not readily available in the literature for PP. Research into laser interactions with

this polymer has taken place but a complete picture in terms of the absorption coefficient and threshold fluence was not found.

TABLE 2.1: A summary of existing laser ablation data for PI

λ	τ (ns)	α (cm^{-1})	F_T (J/cm^2)	ΔH (kJ/cm^3)	Ref.
193nm	15	$34x10^4$	$14x10^{-3}$	4.8	[29]
193nm	9	$13x10^4$	$30x10^{-3}$	3.2	[32]
248nm	20	$24x10^4$	$37x10^{-3}$	8.9	[17]
248nm	25	$22x10^4$	$54x10^{-3}$	12.0	[36]
248nm	11	$14x10^4$	$31x10^{-3}$	4.3	[32]
248nm	15	$30x10^4$	$19x10^{-3}$	5.7	[29]
308nm	8	$8x10^4$	$42x10^{-3}$	3.4	[32]
308nm	15	$8.6x10^4$	$37x10^{-3}$	3.2	[29]
351nm	15	$3.6x10^4$	$84x10^{-3}$	3.0	[29]
9.17μm	100	840	3.6	3.0	[8]
9.2μm	80 (600)	2340	0.5	1.2	[7]
9.21μm	100	780	3.8	3.0	[8]
9.24μm	250	854	$850x10^{-3}$	0.7	[17]
9.25μm	100	1250	3.6	4.5	[8]
9.46μm	250	154	2.2	0.3	[17]
10.31μm	250	76	2.2	0.2	[17]
10.6μm	80 (600)	270	2.1	0.6	[7]

Table 2.2: A summary of existing laser ablation data for PEEK

λ	τ (ns)	α (cm^{-1})	F_T (J/cm^2)	ΔH (kJ/cm^3)	Ref.
193nm	20	$30.3x10^4$	$12.5x10^{-3}$	3.8	[37]
193nm	20	$23x10^4$	$35x10^{-3}$	8.1	[38]
248nm	25	$10x10^4$	$50x10^{-3}$	5.0	[36]
248nm	30	$10x10^4$	$45x10^3$	4.5	[37]
308nm	25	$10x10^4$	$70x10^{-3}$	7.0	[38]
308nm	8	$10x10^4$	$70x10^{-3}$	7.0	[39]
10.77μm	130 (3.5μs)	2670	5.7	15.2	[6]

Table 2.3: A summary of existing laser ablation data for PET

λ	τ (ns)	α (cm^{-1})	F_T (J/cm^2)	ΔH (kJ/cm^3)	Ref.
172nm	8	$11x10^4$	$29x10^{-3}$	3.2	[40]
193nm	9	$12x10^4$	$28x10^{-3}$	3.3	[32]
248nm	25	$16x10^4$	$30x10^3$	4.8	[36]
248nm	11	$10x10^4$	$30x10^{-3}$	3.0	[32]
308nm	8	$2x10^4$	$170x10^{-3}$	3.4	[32]
9.17μm	110	$2x10^3$	0.77	1.5	[9]

From the data summarised in tables 2.1, 2.2 and 2.3 a few important points should be noted. UV ablation results in the smallest threshold fluences, as would be expected due to the strong absorption by most polymers at these wavelengths. However, it is interesting to note that when conditions are favourable, that is, the wavelength of the laser is tuned to an absorption band in the polymer such that the absorption coefficient is high, modest threshold fluences are also observed for IR laser sources. The enthalpy is a parameter which gives an indication of the approximate threshold fluence that can be expected for a particular wavelength, if the absorption coefficient is known, and therefore provides a means to compare data from different sources. The enthalpy for ablation is seen to be fairly consistent for PI, PEEK and PET having values in the range 1–10 of kJ/cm^3. Exceptions to this do not appear to be linked directly to the absorption coefficient or the pulse duration.

The IR laser ablation of PI, PEEK and PET is discussed in the following sections, in order that some of the findings presented in tables 2.1, 2.2 and 2.3 can be evaluated in more detail. Available laser ablation publications for PP are also discussed. The UV ablation of polymers is not considered in as much detail here, as photochemical mechanisms are not expected to occur for irradiation by IR laser sources.

2.4.1 IR laser ablation of PI

The IR irradiation of polyimide was studied by Brannon et al in 1986, using a TEA CO_2 laser [7]. The laser was tuned to operating wavelengths of 9.2 and 10.6μm.

FTIR measurements showed that the polyimide was weakly absorbing at 10.6μm and strongly absorbing at 9.2μm, having absorption coefficients of 270cm^{-1} and 2340cm^{-1} respectively. Ablation at the more absorbing wavelength was shown to be cleaner and more precise, indicating that the absorption coefficient is an important consideration when attempting to understand the ablation mechanism in the IR region.

Similarly, Dyer et al [5] used a TEA-CO_2 to demonstrate small scale hole formation in Upilex polyimide. It was suggested that optical resolution rather than thermal effects limited the feature size attainable.

In work by Dyer et al [16], the laser ablation of polyimide (Kapton HN) with IR and visible wavelengths was investigated using a Nd:YVO_4 laser operating at 1064nm and 532nm. The absorption coefficient was 15cm^{-1} and 120cm^{-1} at 1064nm and 532nm respectively. After irradiation with multiple laser pulses at 1064nm, thermal degradation was seen to occur and resulted in an absorbing carbon layer. This had the benefit of increasing absorption and therefore reducing the threshold fluence for ablation. For a larger number of pulses, however, the carbon was seen to restrict the depth of etching due to absorption. Incubation effects were also noted and were attributed to carbon formation in early pulses which did not ablate the polymer. At the visible wavelength of 532nm, the threshold was seen to be lower, as expected due to the larger absorption coefficient. The temperature distribution was calculated assuming a surface laser source and there was seen to be good agreement between experimental data and theoretical modelling, implying a process dominated by a thermal mechanism [16].

In reference [22], a comparison was made between the irradiation of polyimide using KrF (248nm), frequency tripled Nd:YAG (355nm) and TEA CO_2 lasers. Similarly in [19], a comparison of laser ablation using TEA CO_2 and argon ion lasers was made and in a publication by Braun et al [17], ablation using KrF and TEA CO_2 sources was compared. The mechanisms of ablation in papers [19, 22] were seen to be different for IR and UV, as expected. In [17], the IR laser etching of polyimide was shown to produce etch holes which were qualitatively similar to those produced by the UV radiation. This is an important observation, meaning that good quality etching is indeed possible with IR sources if the absorption coefficient is sufficiently high and other laser parameters (such as pulse duration and beam size) are controlled appropriately [17].

2.4.2 IR laser ablation of PEEK

Sumiyoshi et al [6] studied the ablation of PEEK using a TEA CO_2 laser and demonstrated successful ablation with a strongly absorbed laser line. As with the results for Braun et al [17], it was noted that control of the pulse duration and absorption coefficient of IR sources, and the thermal properties of the polymer, led to a greatly improved etch quality.

In reference [23], irradiation of PEEK using a CO_2 laser resulted in little change to the polymer other than a decrease in the degree of crystallinity of the material. The amount of crystalline material was reduced by increasing the amount of laser treatment. In terms of applicability to industry, this study indicated that the chemical and mechanical properties of laser ablated PEEK were left unchanged.

This is an important study if IR laser ablation is to be used in industry where the mechanical and chemical properties are relevant to a particular application.

2.4.3 IR laser ablation of PET

In reference [9], successful etching of PET films by pulsed TEA CO_2 laser was demonstrated. It was found that the relationship between laser fluence and the etch depth was similar to that found for UV ablation of the same material, however the threshold was less well defined. The laser was tuned to a strongly absorbed wavelength in PET (9.17μm). Thermalisation of the absorbed energy was assumed to be rapid and on the time-scale of the decomposition of PET (10^{-7}s). Photoacoustic measurements showed that ablation of the material occurred between 150 and 200ns after the 1.8J/cm^2 laser pulse began (derived from the compressive signal associated with ablated material leaving the surface). This was seen to be consistent with the rate of thermal decomposition, calculated as being significant (6%) at 150ns at a laser fluence of 1.8J/cm^2 [9].

In a publication by Dadsetan et al [18] pulsed CO_2 laser-induced surface modification of PET (of 70μm thickness) was studied in terms of morphology, surface chemical structure and surface properties. Samples of PET were irradiated using wavelengths of 10.28μm, 9.58 μm and 9.25μm. The complicated surface microstructures observed were attributed to stress release in a melted surface layer, similar to those observed in reference [9]. Crystallinity of the irradiated region was shown to decrease, while amorphism of the PET surface increased and was shown to be accompanied by degradation of the polymer [18].

2.4.4 IR laser ablation of PP

The irradiation of polypropylene was studied by Bormashenko et al [41] using a CO_2 laser and it was noted that modest laser powers caused significant thermal effects to the material. There was seen to be a distinguishable threshold, although specific values were not given. The effects resulted in a change in the polymer structure, revealed by IR absorption spectra.

Few papers were found that presented work on the IR irradiation and ablation of polypropylene, particularly in the regime of interest. Femtosecond duration pulses were used in reference [42], however the interaction of very short laser pulses adds complexity to the mechanistic interpretation which is not applicable in this work.

2.5 Industrial context

Laser processing is of great importance in industry. Some uses of laser prepared and ablated polymers include insulating films in the micro-electronics industry [7], bio-compatible materials [18], wire insulation, coatings for heat exchangers and automotive parts [23]. Lasers can be used to drill, mark, cut and weld polymers for these applications and offer advantages over more mechanical systems such as higher efficiency and increased throughput. For example, Bormashenko et al noted the application of the laser marking of polypropylene at very high efficiency and speed for their findings in their publication [41]. The applications of laser micromachining in industry are reviewed extensively in a paper by Gower [4].

The advantages of UV laser processing of materials over other techniques are as follows [24]:

- Highly localised spacial interaction between the laser and polymer. The minimum feature size is set by diffraction and it is possible to obtain sub-micron definition.
- A definite threshold for significant material removal can be defined for materials and lasers of interest.
- Minimal heat affected zone.

The high resolution of UV laser ablation of polymers is an indication as to why laser processing in the UV regime has received more attention than the IR counterpart. In contrast to the UV laser, the CO_2 laser has the attractive feature of being an industry-accepted device with relatively low operating costs. Where resolution becomes less critical, these lasers have a valuable role in polymer micro-machining [8]. The advantages of these lasers in contrast to UV sources include higher pulse energies, increased efficiency, the use of non-toxic gases and long term maintenance free operation.

This author has not found any reference to the laser ablation of polymers using a radio frequency excited CO_2 laser with pulse durations in the approximate range of 50–500μs. Literature indicates how the materials will behave under laser irradiation using these pulse durations, but experimental evidence and analysis are required to understand the process fully and to determine whether longer-pulse

IR lasers are a useful tool for both scientific understanding of laser ablation and in the polymer machining industry.

The introduction to each chapter in this Thesis will provide additional context to the work being carried out.

Chapter 3

The RF CO_2 Laser System

3.1 Introduction

In this chapter, the various properties of a radio frequency excited carbon dioxide (RF CO_2) laser will be presented. The variable pulse duration of the laser has been measured and calibrated. The energy per pulse has been determined from measurements of the average power as a function of the laser repetition rate. In addition, the operating wavelength of the laser has been investigated both in a time integrated fashion and as a function of time during a laser pulse of approximately 200μs in duration.

3.2 The laser system

An RF CO_2 laser with a manufacturers quoted average output power of approximately 100W was used for the experiments presented here. A transistor-transistor logic (TTL) signal was used to enable and disable the RF power supply (which had a frequency of 81MHz and a peak to peak voltage of 100s of volts), allowing the pulse duration and repetition rate of the optical output to be controlled. The TTL pulses were generated either from a PC or a signal generator (Farnell Pulse Generator PH102). As the PH102 pulse generator offered more flexibility, this

system is exclusively described here. The TTL pulses generated in this way were monitored on an oscilloscope (HP Infinium 500MHz 2GSa/s).

The optical output of the laser was initially reflected from a long focal length cylindrical gold coated brass mirror to reduce beam divergence in one plane. The divergence was different in the horizontal and vertical direction due to the electrode configuration in the wave-guide structure of the laser [43]. The beam was then reflected from a plane gold coated brass mirror to a PC controlled motorised stage. The metal mirrors were not aligned in order to maintain the polarisation of the beam and no efforts were made to preserve the polarisation of the laser.

A schematic of the system is shown in figure 3.1.

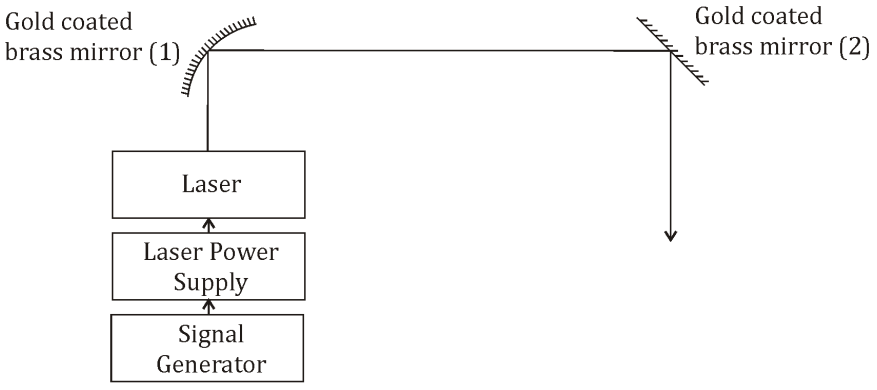

FIGURE 3.1: Schematic of the basic laser system used. The laser output was initially reflected from a long focal length cylindrical gold coated brass mirror (1) to reduce beam divergence in one plane as the output of the slab waveguide was astigmatic. The beam was then reflected from a plane gold coated brass mirror (2) to a PC controlled motorised stage.

3.3 Pulse duration measurements

The laser pulse duration was measured using a gold-doped germanium (Ge:Au) liquid nitrogen cooled detector. Germanium cannot operate as an intrinsic IR detector as its band gap is too wide at 0.67eV (corresponding to a photon wavelength of 1.85μm). When cooled to 77K, germanium can be used in devices for detecting wavelengths further into the infrared, but in order to detect CO_2 laser wavelengths (9-11μm) the germanium is doped with an impurity (in this case gold). The gold provides extra energy levels in the forbidden gap between the conduction and valance band. Longer wavelength, lower energy photons can excite electrons into these impurity levels and the holes left behind in the valance band are effectively swept out when an external bias is applied [44].

The detection system in this case consisted of the Ge:Au detector described above mounted on a cold finger cryostat, which was evacuated to a pressure of $5x10^{-5}$mbar. Liquid nitrogen was used to maintain a temperature of approximately 77K. The cryostat window was made of anti-reflection coated germanium. The experimental set-up used to determine the pulse duration and calibrate the system is shown in figure 3.2.

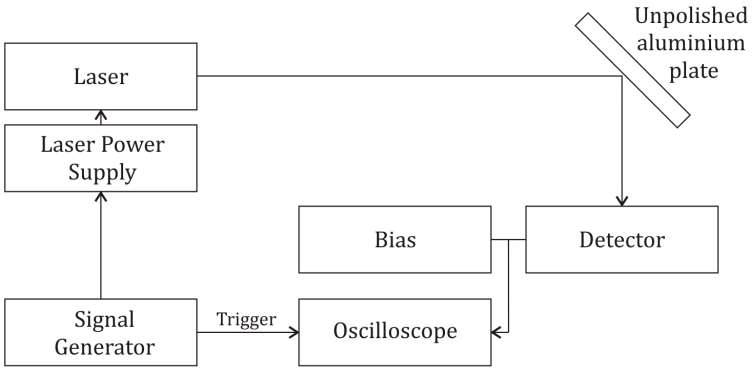

FIGURE 3.2: Schematic of the experimental set-up used to determine the laser pulse duration. A low level (approximately 100nW) of laser light was scattered from the unpolished aluminium plate onto the detector. A bias of -40V was used, supplied via a battery pack to reduce noise pickup. The detector bias unit was connected to the oscilloscope using a termination resistance of 6.8kΩ in parallel with the 1MΩ input impedance of the oscilloscope. The oscilloscope was triggered from the signal generator.

A bias unit (-40V) was used to extract the signal from the detector head and was connected to the oscilloscope via D.C. blocking capacitors. A battery pack was used to provide this, so as to reduce noise pickup. A low level of laser light was scattered from an unpolished aluminium plate onto the Ge:Au detector (approximately 100nW). A termination resistance of 6.8kΩ was used, in parallel with the 1MΩ input impedance of the oscilloscope. This was found to provide the most acceptable compromise between sensitivity and time resolution, as the recorded rise time did not change for values below 6.8kΩ and the signal size was sufficient for measurements to be made.

Figures 3.3 and 3.4 show two example pulse shapes obtained by using 200μs and 500μs duration TTL pulses from the signal generator.

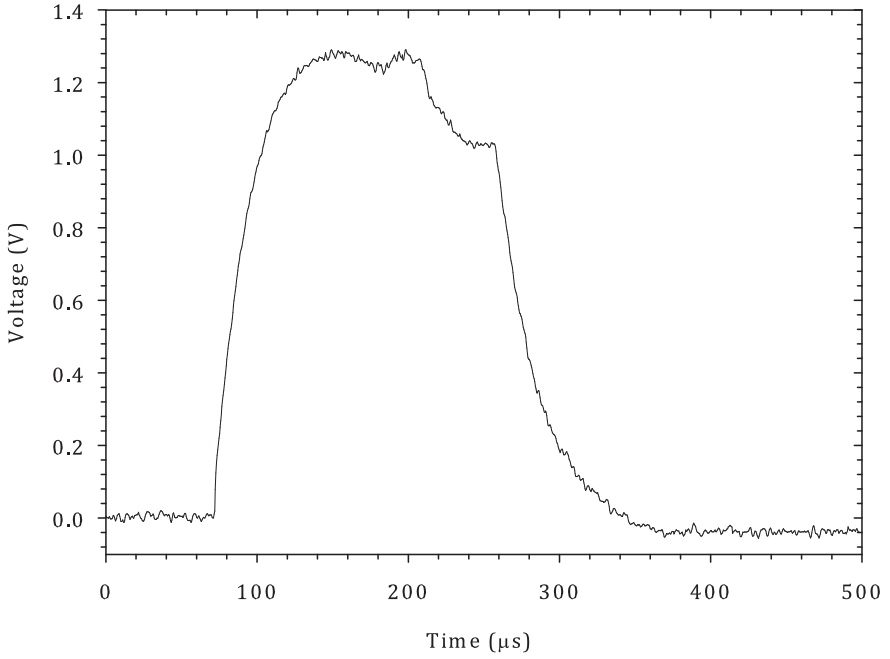

FIGURE 3.3: Laser pulse shape generated using a 200μs TTL pulse from the signal generator. A repetition rate of approximately 5Hz was used.

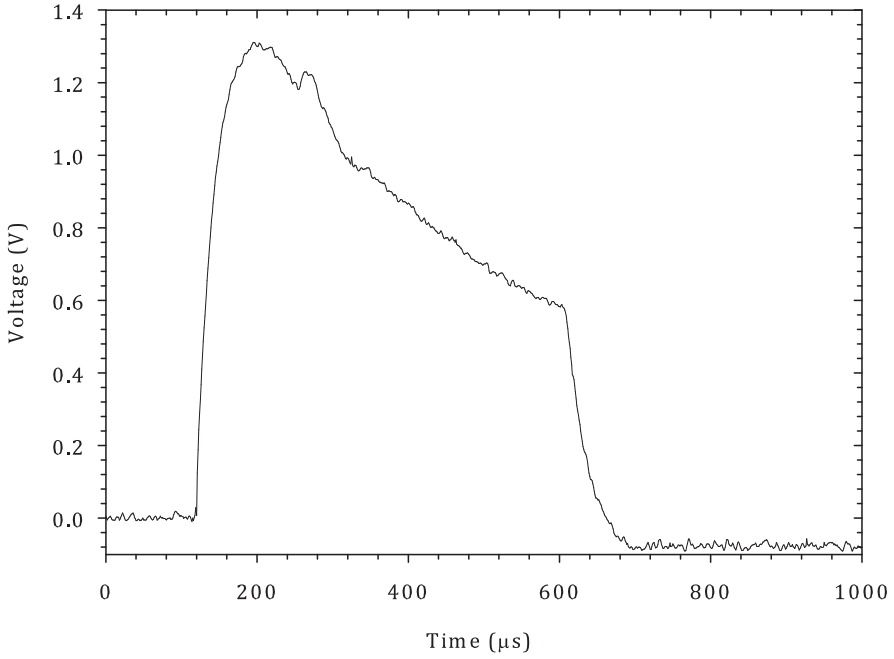

FIGURE 3.4: Laser pulse shape generated using a 500μs TTL pulse from the signal generator. A repetition rate of approximately 5Hz was used.

When using longer pulse durations ($\geq$300μs), the signal from the detector was seen

to decrease during the laser pulse and the signal voltage when the optical pulse ceased was negative with respect to the initial level. This behaviour was attributed to laser heating of the detector, which was thought to reduce the sensitivity. Figure 3.5 shows a laser pulse generated from a 1ms TTL signal and the recovery period. The dotted line indicates the signal level before the laser was incident on the detector.

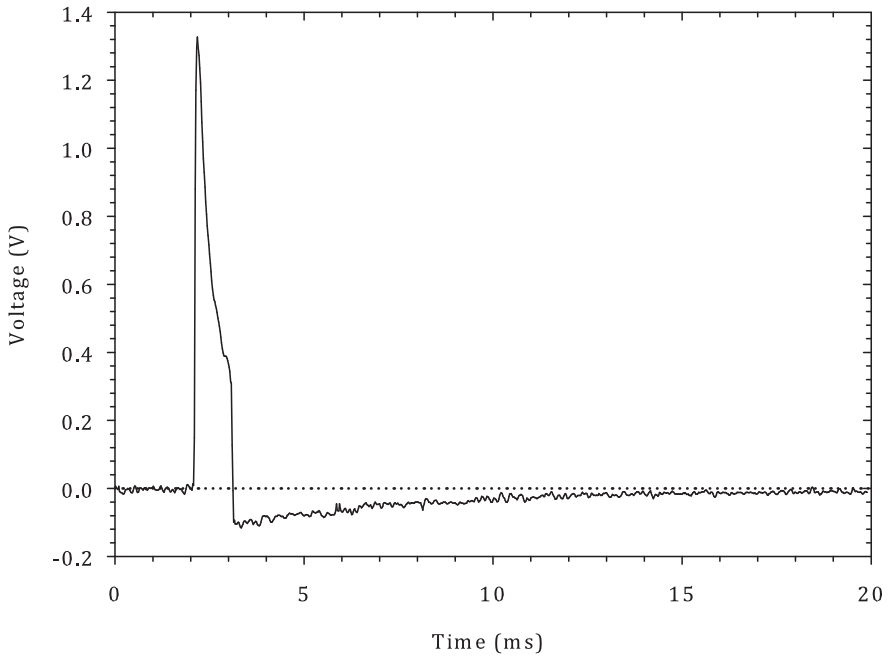

FIGURE 3.5: A laser pulse shape generated from a 1ms TTL pulse from the signal generator, showing detector recovery after the laser pulse had ceased. The laser was running at a low repetition rate of approximately 1Hz. The dotted line indicates the signal level before the laser pulse was incident on the detector.

In figure 3.5 the decrease in signal is obvious during the laser pulse and reaches its largest negative value at the end of the pulse. The signal was seen to recover before the next pulse, implying that the detector had cooled again.

The full width at half maximum (FWHM) of the pulse shapes were used to determine the pulse duration. These were used to produce a graph to calibrate between

the TTL pulse duration and the measured optical output, so that in future the optical pulse duration could be inferred from the TTL pulse duration of the signal generator. This is shown in figure 3.6.

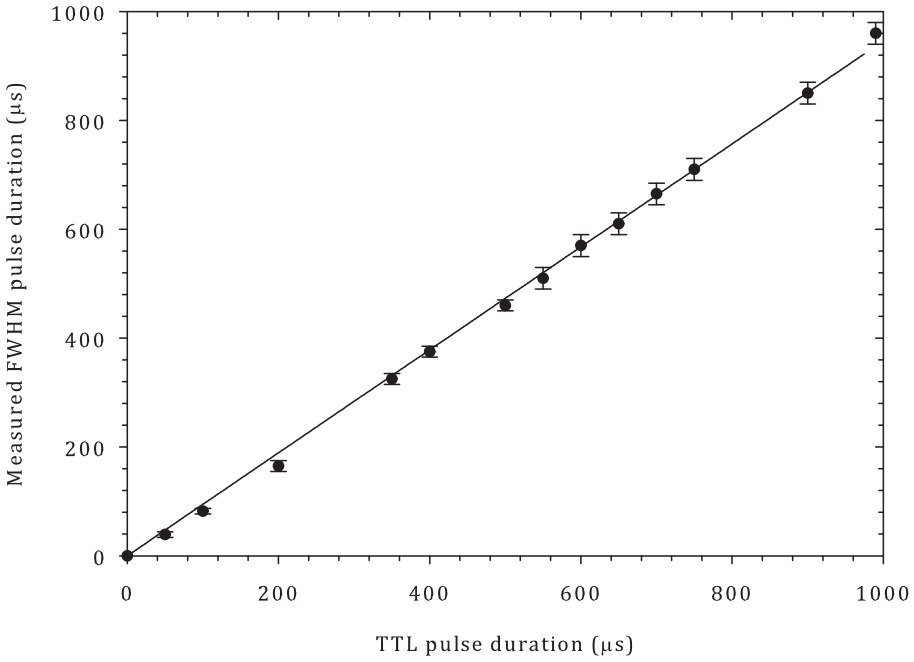

FIGURE 3.6: Calibration graph showing measured pulse duration as a function of the duration of the TTL control signal applied to the laser power supply.

The linear regression line in figure 3.6 has a gradient of 0.95. The pulse durations of the laser were consistently smaller than those from the signal generator and were delayed by approximately 20μs after the start of TTL pulse. This delay was attributed to the time taken for the laser to reach threshold for emission as a result of the build-up time of the RF field. The pulse duration of the laser was inferred from this graph for all future calculations, unless otherwise indicated. Calibration graphs were also produced when using the PC to generate the TTL signal and these were used when appropriate.

3.4 Power and pulse energy

The average power of the laser was measured as a function of laser repetition rate using a power meter (Coherent Labmaster Ultima). The power meter was mounted on the PC controlled stage shown in figure 3.1. The raw beam of the laser was positioned at the centre of the detector head. The consistency of the results across the area of the detector was checked and it was found that the power recorded was constant within the experimental uncertainty (approximately ±5%). The power was taken approximately one minute after the laser was switched on to allow stable operation. The results are shown in figure 3.7. In this figure the range of duty cycles encompassed is approximately 2–40%.

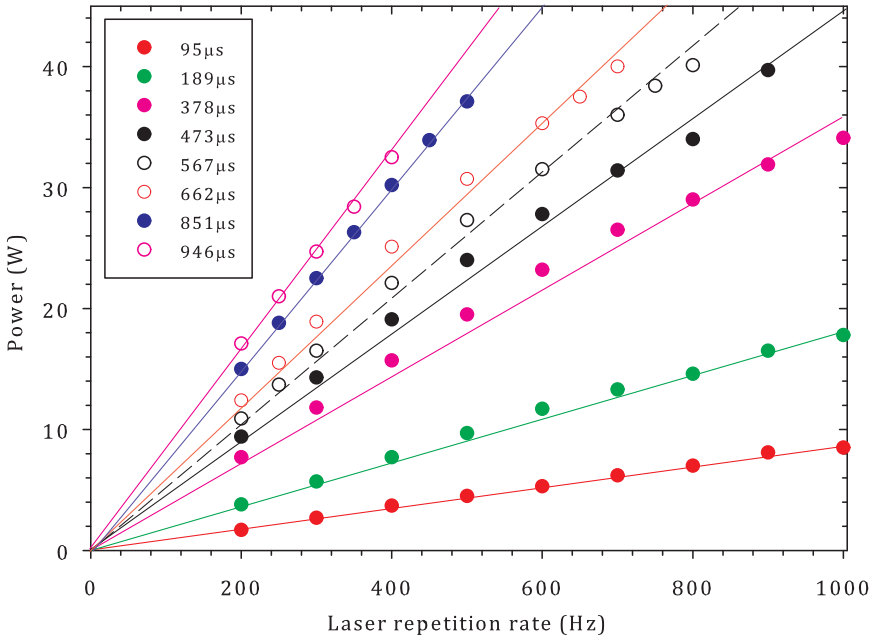

FIGURE 3.7: Average power as a function of laser repetition rate at various pulse durations. The pulse durations have been corrected using the calibration graph in figure 3.6.

Figure 3.8 shows a graph of energy per pulse as a function of pulse duration. The pulse durations plotted are those corrected using the results presented in figure 3.6 (or the calibration graphs for the PC controlled TTL pulses depending on which set of data was being analysed). This graph (and additional calibration graphs for the case of the PC controlled parameters) was used to determine the pulse energies for future experiments presented here.

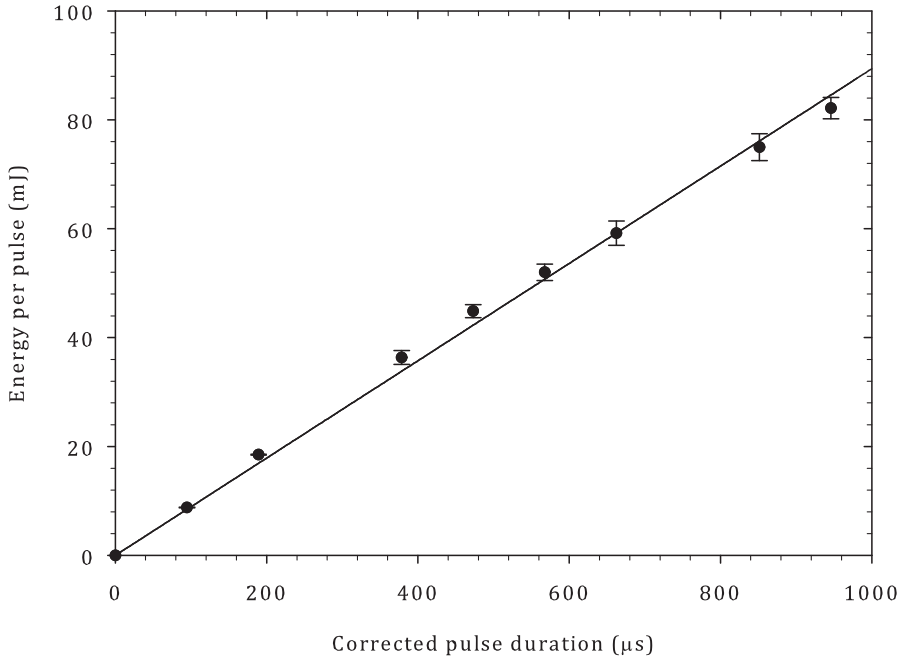

FIGURE 3.8: Energy per pulse as a function of laser pulse duration. The pulse energy was determined by consideration of the power measured as a function of repetition rate for each pulse duration. The pulse durations have been corrected using the calibration graph in figure 3.6.

The gradient of the linear regression line shown in figure 3.8 is 0.09mJ/μs. This corresponds to an average laser power of 90W. This is consistent with the manufacturers specifications as some loss was expected from the mirrors used to direct the beam to the stage where the power meter was positioned. This method of

determining the laser average power arose from the fact that the laser could not be run truly continuously, due to cooling requirements.

The laser pulse energy incident on the stage was controlled for selected pulse durations using sodium chloride attenuators aligned at 5.4 ° from the perpendicular to the beam propagation direction. The laser system including the attenuators is shown in figure 3.9.

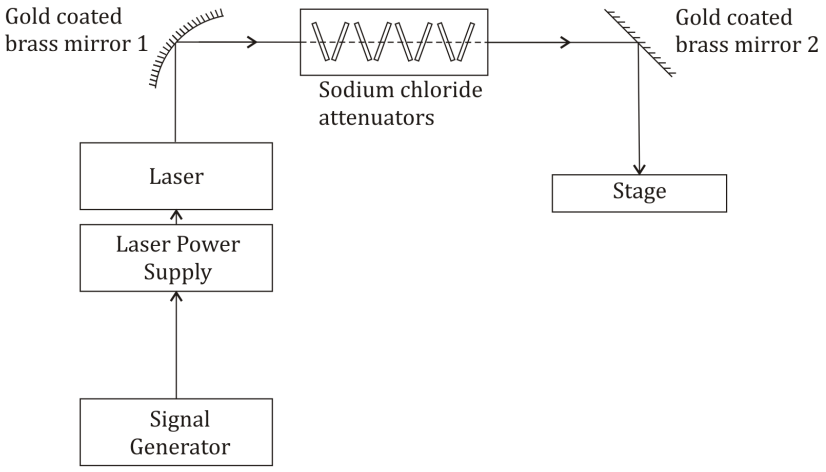

FIGURE 3.9: Schematic of the laser system set up including sodium chloride attenuators aligned at 5.4 ° from the perpendicular to the beam propagation direction. The rest of the system is the same as that shown in figure 3.1

The attenuators were used in pairs of opposing angles to conserve the beam path. The attenuators were added in the same order each time to ensure consistency. The transmitted power was measured for each pair of filters, which were added cumulatively, and the attenuation determined. Figure 3.10 shows the calibration curve for the attenuators. Assuming normal incidence, that the attenuation was based on reflection and that no absorption occurred and that the refractive index of NaCl is approximately 1.49 at the laser wavelength, the reflectivity was calculated as 3.8% per surface, meaning that for each attenuator the total reflectivity would

be approximately 7.5%. The line in figure 3.10 is therefore the theoretical result based on an attenuation of 7.5% per filter. This line was plotted assuming that the transmission (T) is proportional to the number of attenuators (x) and attenuation per filter (A_F) as shown in equation 3.1.

$$T = (1 - A_F)^x \tag{3.1}$$

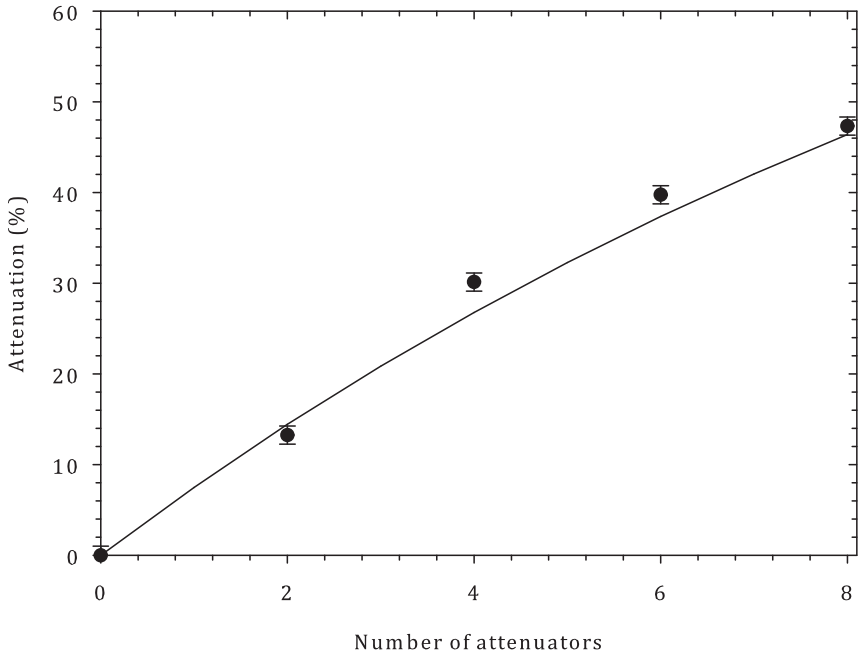

FIGURE 3.10: Calibration curve for the sodium chloride attenuators. The data points are derived from experimental data and the line is the theoretical calibration based on an attenuation of 7.7% per attenuator.

The calculated results agreed with results found experimentally and the calibration curve shown in figure 3.10 was used for all further calculations involving the attenuators. When not in use, the attenuators were kept warm and desiccated to avoid absorption of ambient moisture.

3.5 Wavelength

The CO_2 laser transitions involve the vibrational and rotational levels of the CO_2 molecule. There are three different quantized modes of vibrational states: symmetric stretching, bending and asymmetric stretching. These three vibrational modes are assigned quantum numbers. The usual notation used to indicate the vibrational mode is (abc), where a is number of quanta of the symmetric stretch mode, b is the number of quanta of the bending mode and c is the number of quanta of the asymmetric stretch mode. So, for example, one quanta of symmetric mode vibration is indicated by (100) [45]. The simplified modes of vibration are shown in figure 3.11.

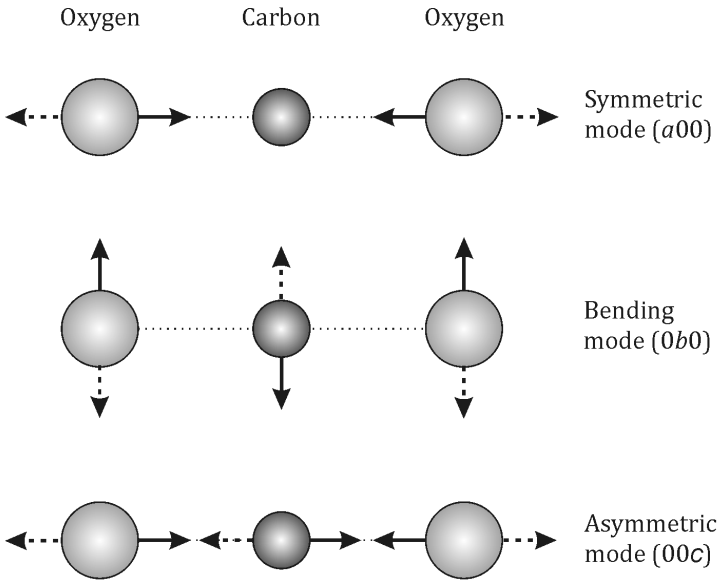

FIGURE 3.11: Simplified representation of the three vibrational modes of the CO_2 molecule. The symmetric, bending and asymmetric modes are assigned quantum numbers and are indicated in the figure by $(a00)$, $(0b0)$ and $(00c)$ respectively (adapted from [45, 46]).

Within the vibrational modes shown in figure 3.11 are multiple rotational states,

also quantized. That is, each vibrational state is separated into a number of closely spaced rotational levels. The rotational sublevels are assigned the rotational quantum number, J [45]. Selection rules mean that the rotational state either decreases or increases by only one quantum upon the transition from one vibrational level to another, that is $\Delta J = \pm 1$. The letters P and R represent transitions where the rotational quantum number within the vibrational mode increases or decreases by one quantum value, respectively. A simplified energy level diagram of the CO_2 molecule is shown in figure 3.12 [45, 47].

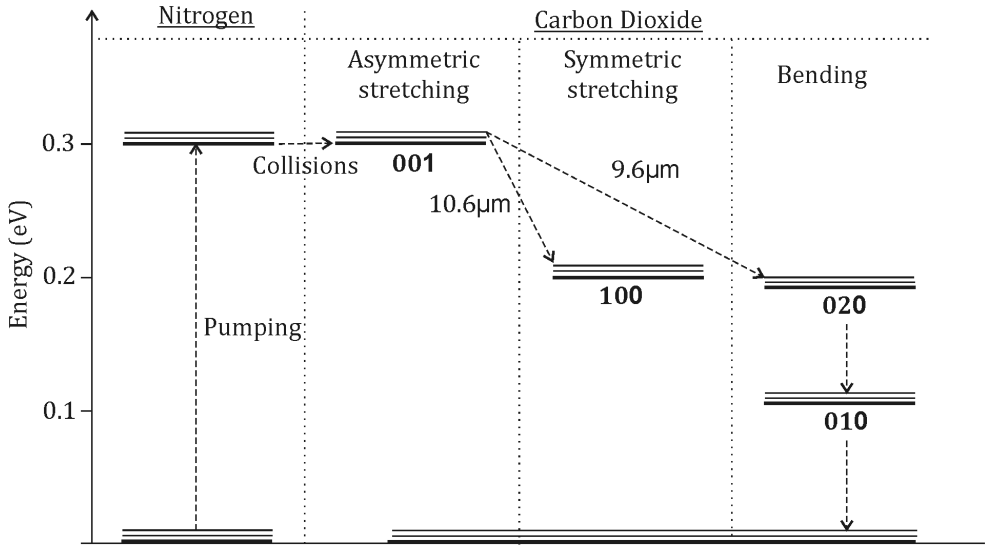

FIGURE 3.12: A simplified energy level diagram of the CO_2 molecule. Also shown is the metastable energy level of nitrogen which allows the asymmetric stretching mode, (001), to be populated via collisions. This vibrational mode then decays to one of either the bending or symmetric modes, resulting in the emission of a photon of wavelength 9.6μm or 10.6μm respectively. Rotational levels are shown with the vibrational modes (adapted from [45]).

Excitation of the CO_2 gas is a two-stage process involving nitrogen as an intermediary gas, as shown in figure 3.12. Direct excitation of the CO_2 molecule can also occur, but this process is much less efficient. The CO_2 is initially excited into the

asymmetric stretching mode (001). It is from this vibrational level that emission occurs. The lowest vibrational state of nitrogen is only $18cm^{-1}$ (0.0022eV) lower in energy than that of the asymmetric stretching mode in CO_2. This allows transfer between the metastable nitrogen level and the asymmetric stretching CO_2 energy level via collisions. As well as nitrogen, helium is added to the gas mixture. This increases the efficiency of the laser by deactivating the lower energy states of the CO_2 to the ground state (therefore maintaining the population inversion required for lasing). The helium also acts as a buffer gas to exchange waste heat to the laser cavity walls [45, 47].

Once a CO_2 molecule is in the asymmetric vibrational state, the molecule loses energy by decaying to one of either the bending or symmetric vibrational modes, as shown in figure 3.12. These two decay paths result in the highest optical gain laser transitions. The transition from the asymmetric to bending vibrational state (that is, the (001) to (020) transition shown in figure 3.12) results in the emission of a photon with a wavelength of 9.6μm. The asymmetric to symmetric decay pathway (the (001) to (100) transition shown in figure 3.12) leads to the emission of a photon with a wavelength of 10.6μm (or more specifically 10.59μm). Changes in the rotational state of the CO_2 molecule gives rise to other emission lines around these two main wavelengths. Shown in figure 3.13 is a discrete spectrum of the emission lines of the CO_2 laser [47, 48] arising from the transitions between rotational levels superimposed on the vibrational modes.

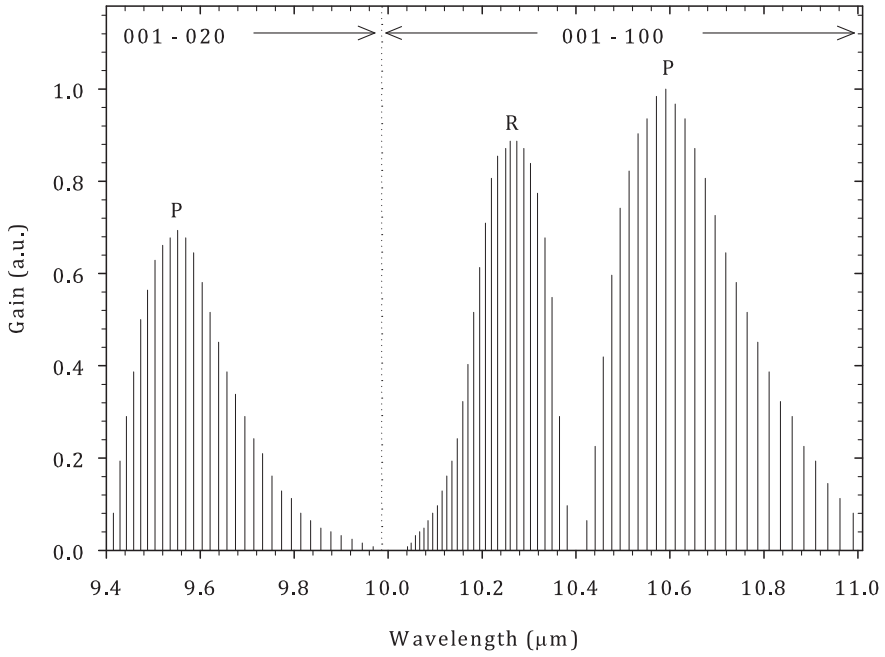

FIGURE 3.13: A spectrum of the discrete emission wavelengths from the CO_2 molecule showing the relative gain of each emission line. The vibrational and rotational transitions are indicated on the spectrum (replotted data from [47, 48]).

The wavelength of the laser used in this work was determined using a spectrometer (Optical Engineering, Inc., CO_2 Spectrum Analyser, Model 16-A). A schematic of the spectrometer [48] and experimental setup is shown in figure 3.14.

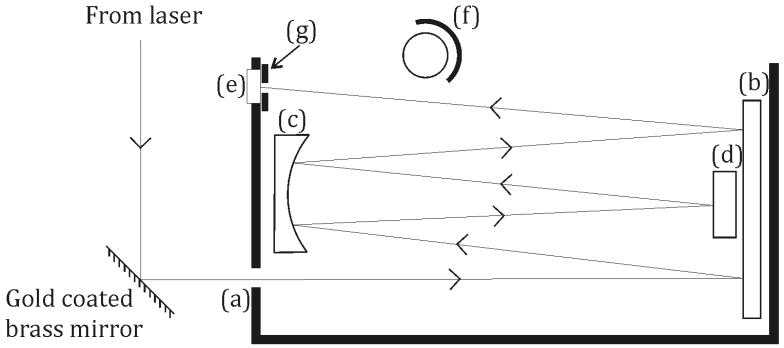

FIGURE 3.14: Experimental setup used to determine the emission wavelength of the laser. A gold coated brass mirror positioned at 45° to the beam path was used to direct the laser radiation into the spectrometer via the entrance slit (a). The beam was then reflected by a flat mirror (b) onto a concave mirror (c), which collimated the beam after the slit. The light was then diffracted by a diffraction grating (d), the first order lines reflected again by the concave mirror and focussed onto the spectrometer readout. The readout consisted of a thermally sensitive screen (e) illuminated by a UV lamp (f) and a scale (g).

The laser light was directed into the spectrometer using a gold coated brass mirror at 45° to the incident beam. After passing through an entrance slit, the laser light was reflected by a flat mirror, followed by a concave mirror which collimated the beam, correcting the divergence caused by the slit. The beam was then incident on a diffraction grating. The first order diffracted laser light was then incident on the curved mirror a second time, which focused the emission lines onto a readout scale. The readout scale consisted of a thermally sensitive screen illuminated by an ultraviolet lamp. When the lines of the laser were incident on the strip they caused darkening due to thermal bleaching and thus the wavelength and transition could be determined from the scale. Various emission lines were observed to oscillate in the wavelength range 10.53–10.63μm (P14–P24) for laser pulses of 189μs duration at a repetition rate of 75Hz. The strongest line was the 10.59μm (P20) line.

Initially the results were taken in a time integrated fashion using the fluorescent strip in the spectrometer, as described, but it was noted that the wavelength appeared to change during the laser pulse. Thus, time resolved measurements were performed to determine wavelength changes during the pulses. The experimental setup used is shown in figure 3.15.

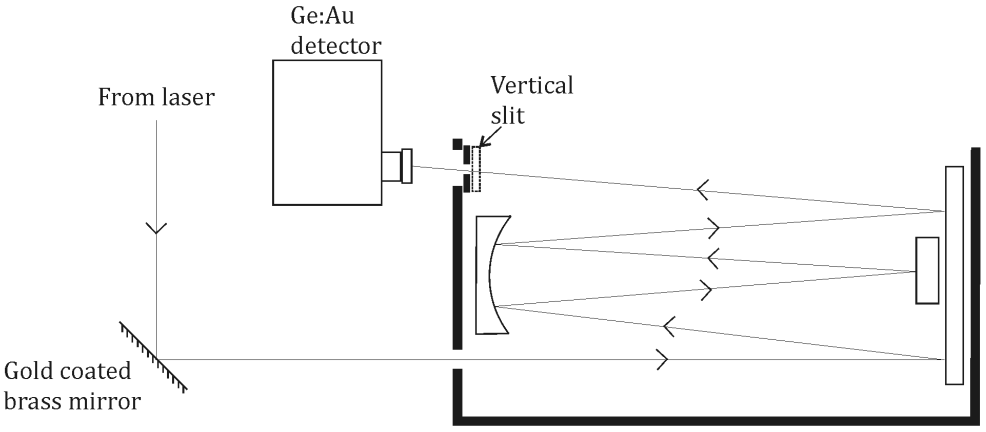

FIGURE 3.15: Experimental setup used to determine the wavelength of the laser as a function of time during the laser pulse. The Ge:Au detector was positioned where a line was detectable and a slit of approximately 0.5mm width was used, both to determine the laser transition and ensure only one line was being detected. The detector was used in the same manner as has been previously described.

This time the fluorescent strip was removed and the Ge:Au detector was used to measure the signal of each laser line. A slit approximately 0.5mm wide was used to ensure that the lines were measured individually. The slit also allowed the specific laser transition to be accurately determined from the scale in the spectrometer.

The time resolved wavelength results are shown in figure 3.16. The pulse duration of the laser was 189μs. It should be noted that the measurements of each wavelength were not taken simultaneously and therefore the results only give a

representation of how each wavelength evolved in time during the laser pulse on average.

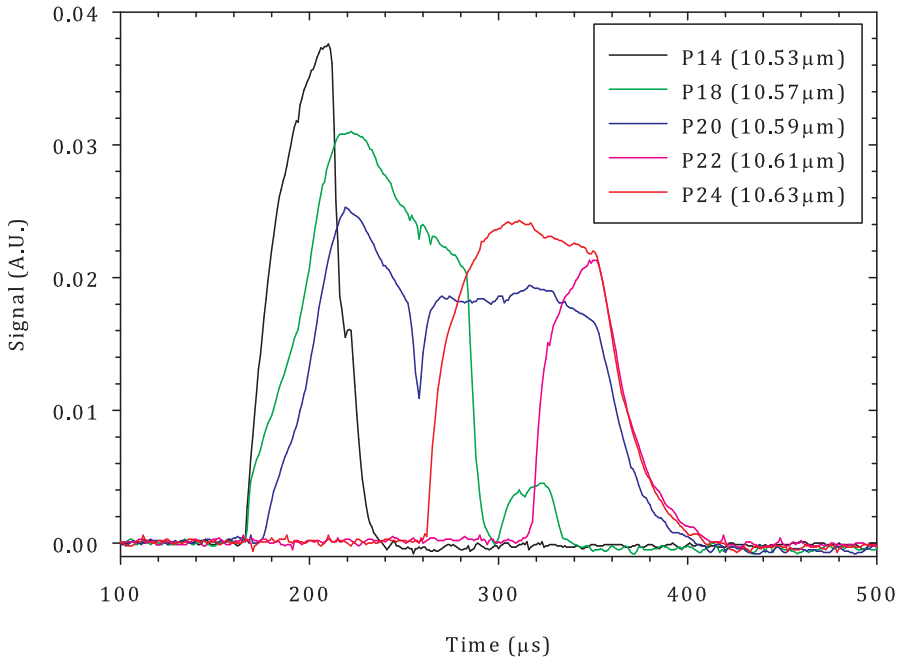

FIGURE 3.16: Graph showing time resolved wavelength measurements of the laser. It should be noted that the measurements were not made simultaneously and do not represent a single pulse breakdown of the wavelengths present. The measurements were made using the Ge:Au detector described previously. A slit of approximately 0.5mm width was used to ensure laser lines were measured individually and no averaging was used.

The graph in figure 3.16 clearly shows that the laser pulse was made up of different wavelength components that were present at different times during the pulse. The 10.59µm laser line was seen to be present during the majority of the pulse. The wavelength range measured was therefore 10.53–10.63µm (excluding 10.55µm) resulting from the P14, P18, P20, P22 and P24 rotational lines in the 001 to 100 vibrational transition. The P16 transition (10.55µm) was not observed in this

particular experiment but was seen to be present during the time integrated experiment. It will therefore be included in future calculations unless otherwise indicated.

Taking into account the spectrum shown in figure 3.13, the wavelength range corresponding to the highest gain lines for the P branch of the 001 to 100 vibrational transition is in agreement with the results obtained here.

3.6 Discussion and Conclusion

In this chapter the parameters of an RF-CO_2 laser system have been reported. Calibration of the laser pulse duration with respect to the pulse duration of the TTL pulses ensured that the pulse durations quoted are those which would arrive at the sample surface. Good correlation between the requested pulse duration (using a signal generator) and the pulse durations measured (using a Ge:Au liquid nitrogen cooled detector) was observed, with a calibration factor of 0.95. The pulse duration was calibrated between 50μs and 1ms (TTL) which corresponds to 47.5μs and 950μs (measured from the laser) and thus the laser could be reliably operated in this range with a well defined pulse duration.

The laser pulse duration and average power measurement led to the calibration of the energy per pulse. As expected from manufacturers specifications, the average power of the laser was found to be 90W (allowing for anticipated losses from the optical system). Using the laser pulse duration range above, this corresponds to a minimum energy per pulse of 4.3mJ and a maximum of 85mJ. The attenuators

that have been characterised in this chapter had a maximum attenuation of approximately 48%. Consequently, the laser could be operated with a range of pulse energies between 2.2mJ and 85mJ.

The wavelength of the laser was measured using a spectrometer. This was done in both a time integrated and time resolved fashion. It was found that the laser changed wavelength during the laser pulse. This line hopping is common and in a study by Plinski et al [49] a similar experiment was performed using a diffraction grating to separate the spectral contents of the pulse and photodetectors to measure the signal of each component. The hopping observed in the work was between laser wavelengths of 10.57μm and 10.65μm and during the laser pulse. This is similar to the effects noted here.

A range of emission wavelengths between 10.53μm and 10.63μm was observed. However, the most common wavelength recorded in both experiments was 10.59μm, which was present for the longest part of the pulse and gave the strongest signal when the pulses were measured in the time integrated experiment. It was decided that 10.59μm would be used for calculations, unless otherwise stated.

At a wavelength of 10.59μm the laser spot size was calculated for a 90mm focal length lens. This lens was used for further experiments where focussing of the beam was required. The spot size was determined from equation 3.2, where r is the focussed beam radius, λ is the laser wavelength, f is the focal length of the lens and ω_L is the beam radius at the entrance to the lens. In this case, ω_L was measured using the thermal response of fax paper to be approximately 2mm.

$$r = \frac{\lambda f}{\pi \omega_L} \tag{3.2}$$

The equation assumes that the beam quality factor, M^2 was equal to one and is therefore not shown in the equation. That is, the laser was assumed to be operating in the TEM_{00} [50].

Using equation 3.2, the approximate radius of the focussed beam was calculated to be 152µm at a laser wavelength of 10.59µm. This resulted in an area of approximately $7.3x10^{-4}cm^2$ at the focal point of the lens. Using the range of pulse energies above, the fluences available using a 90mm focal length lens at the focal point were in the range 3–116 J/cm^2. Considering the tables of results given in the literature review, this fluence range included the threshold fluences for ablation for PI, PEEK, PET and PP.

Chapter 4

Thermal and Infra-red Optical Properties of PI, PEEK, PET and PP

4.1 Introduction

In this chapter, the infrared optical and thermal properties of a selection of polymers has been investigated. The polymers selected were Polyimide Kapton HN (PI), poly(ether ether ketone)(PEEK), poly(ethylene terephthalate)(PET) and poly(propylene) (PP). The decomposition temperature of each material has been determined by thermo-gravimetric analysis (TGA) in air. The optical absorption coefficient of each material has been measured at room temperature and as a function of temperature using fourier transform infrared (FTIR) spectroscopy. Additionally, the time resolved transmission of the unfocussed laser beam through each polymer has been determined to investigate laser interaction with the materials.

4.2 Polymers

The polyimide (PI) polypyromellitic dianhydrideoxydianiline (PMDA-ODA) is commercially known as Kapton and is one of the most commonly used polyimides in the electronics industry, particularly for flexible printed circuits boards. Other uses include sleeve bearings and valve seatings in the aerospace industry [51]. Laser

ablation offers an attractive method of drilling, cutting and marking this material, having applications in the micro-electronics industry. For example, laser removal of the film in certain locations permits electrical conduction through a circuit [7].

There are a number of available Kapton films, the two most common being Kapton H and Kapton HN. The two types possess the same (PMDA-ODA) chemistry and have the same physical and chemical properties. The difference between them is that Kapton HN contains a slip additive based on dicalcium phosphate while Kapton H does not [52]. The structural formula of a Kapton monomer is shown in figure 4.1 [19, 51].

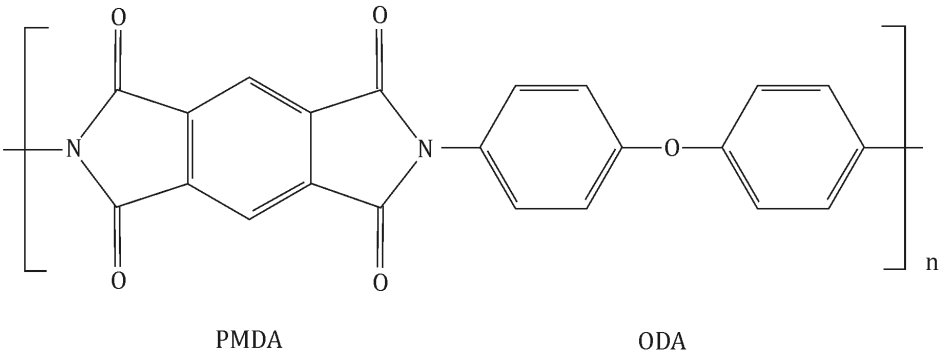

FIGURE 4.1: The structural formula of a Kapton PI monomer [19]. The parts labelled PMDA (pyromellitic dianhydride) and ODA (oxy dianiline) refer to the components from which the polymer is synthesized.

In figure 4.1, the sections labelled PMDA and ODA refer to the components from which PI is synthesised; pyromellitic dianhydride and oxy dianiline respectively.

Polyether ether ketone (PEEK) is a physically strong polymer with high temperature resistance, good chemical resistance and inherently low flammability, water absorption and smoke emission [51]. Industrial applications include flexible printed circuit boards, injection moulded engineering components and items used

in aerospace and radiation environments [51, 53]. The high solvent resistance, good impact-strength and good thermal stability make it a good candidate as a thermoplastic matrix for graphite composites [51].

The structural formula of a PEEK monomer is shown in figure 4.2 [54].

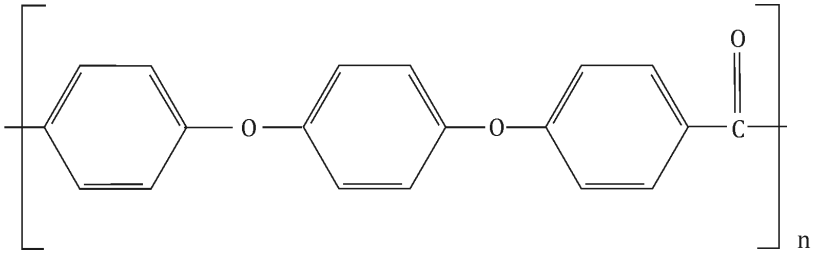

FIGURE 4.2: The structural formula of a PEEK monomer [54].

Polyethylene terephthalate (PET) is a thermoplastic polymer used extensively in the manufacture of high-strength textile fibres, photographic films, cable coatings and bottles [55, 56]. PET has a very low gas and water-vapour permeability due to its high crystallinity, making it particularly applicable as a barrier film in food packaging (especially plastic bottles for carbonated drinks) [51]. The chemical structure of PET is shown in figure 4.3 [56].

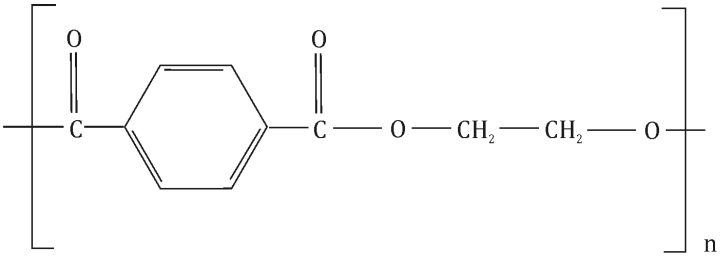

FIGURE 4.3: The structural formula of a PET monomer [56]

The light weight thermoplastic polymer polypropylene (PP) is used widely for the manufacture of pipe, sheet, blow moulded containers, textile fibre (carpeting, webbing, rope, cordage) and in the toy industries [51, 56, 57]. The structural formula of PP is shown in figure 4.4 [51].

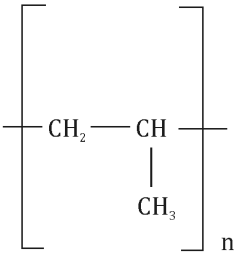

FIGURE 4.4: The structural formula of a PP monomer [51]

Polymers are broadly classified into two categories: thermoplastic and thermoset. Thermoplastics are polymers which can be melted upon the application of heat. Thermosets are intractable once formed and degrade rather than melt upon heating [51, 58]. PI is classified as thermoset, decomposing rather than melting. PEEK, PET and PP, on the other hand, are thermoplastic, having a melting temperature.

All the polymers used in this work were obtained from Goodfellow Cambridge Ltd, UK.

4.3 Thermo-gravimetric Analysis of PI, PEEK, PET and PP

It was expected that, due to the wavelength of the laser being used in this work, the dominant mechanism for laser induced change in the polymers would be a

result of their thermal response. Thermal degradation would therefore be the most likely route for laser induced damage, as has been discussed briefly in the literature review in Chapter 2. The decomposition temperature of each of the polymers was measured using thermo-gravimetric analysis (TGA). This technique involves heating a known weight of a sample and measuring the weight loss as a function of temperature. The instrument used was a Mettler Toledo TGA with STARe System Software v. 9.10.

The results for the sample weight remaining as a function of polymer temperature are shown in figure 4.5 for PI. The TGA was performed in an air atmosphere with a gas flow rate of 100mL/min and a heating rate of 20K/min.

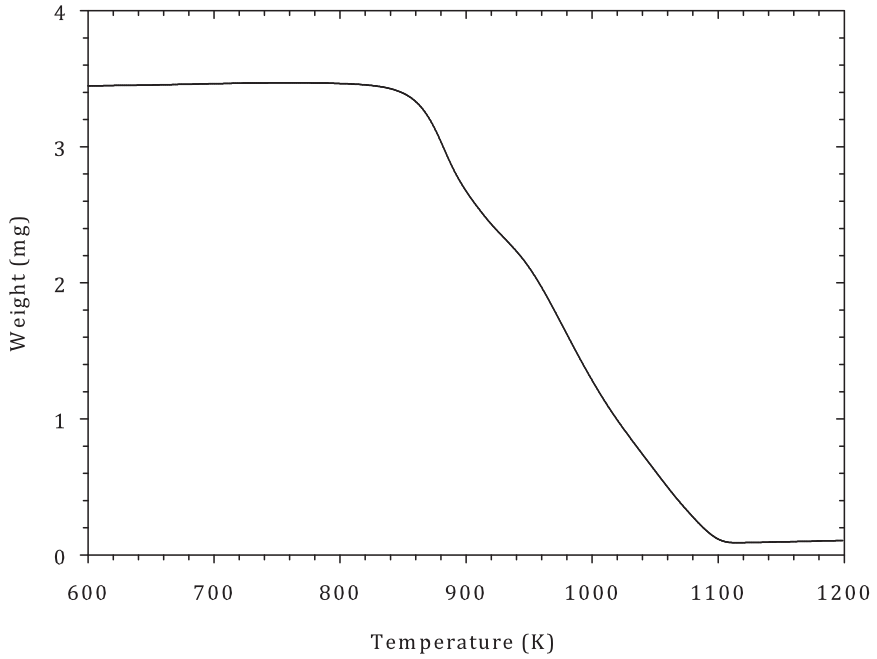

FIGURE 4.5: The weight of a PI sample as a function of temperature. The TGA was performed in an air atmosphere with a gas flow rate of 100mL/min and a heating rate of 20K/min.

The rate of weight change of PI was then plotted as a function of temperature

to determine the inflexion point of the graph shown in figure 4.5 and therefore determine the temperature of decomposition more accurately. This is shown in figure 4.6.

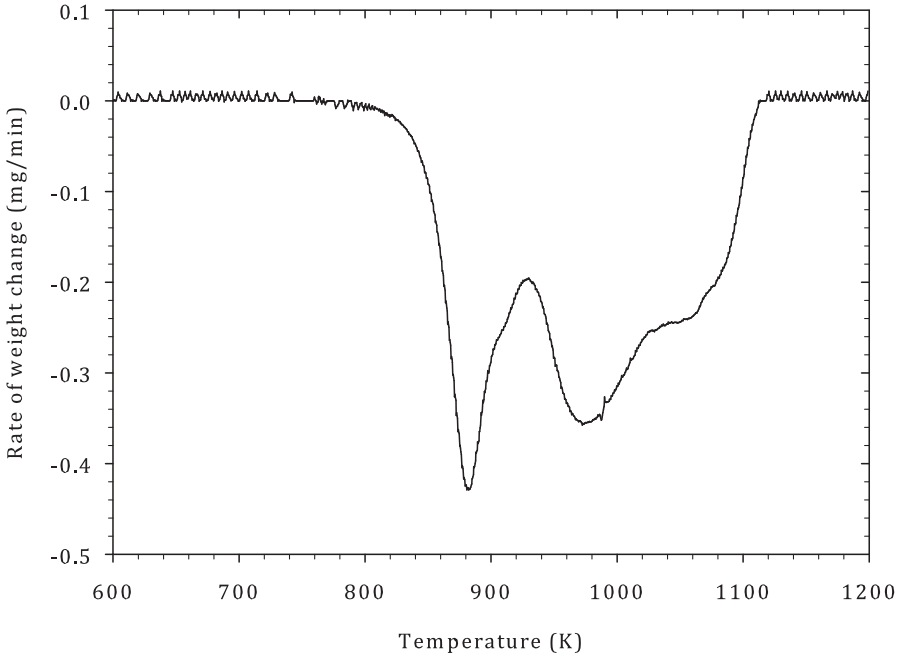

FIGURE 4.6: The rate of weight change of a PI sample as a function of temperature. The TGA was performed in an air atmosphere with a gas flow rate of 100mL/min and the heating rate was 20K/min.

It is clear from figure 4.6 that there was significant decomposition at a temperature of 880K. Values for the temperature of decomposition of PI in the literature were found to be in the range of 823-877K [59–61] which is broadly consistent with the value found here. The small difference was attributed to the atmosphere in which the TGA was performed and slight differences in the PI sample sources. The decomposition temperature of 877K in reference [59] was determined in a nitrogen atmosphere at a heating rate of 10K/min. In reference [60] the PI sample was sandwiched between two aluminium plates and heated in an argon atmosphere at

a rate of 7K/min, yielding a decomposition temperature of 823K. Finally, in reference [61] a decomposition temperature of 845K was obtained in an air atmosphere at heating rates in the range 5–40K/min. Reference [61] also shows a two stage decomposition as was observed in the experiments performed here. In the reference the second stage decomposition occurred at a temperature of approximately 1100K, whereas the experimental data obtained in this work indicated that the second stage of decomposition occurred at 970K. The second stage was thought to be oxidative in nature, as it was not observed in a nitrogen atmosphere [61].

Similarly, the rate of weight change of PEEK, PET and PP samples are shown in figure 4.7 as a function of temperature. The results were taken in an air environment with a gas flow rate of 100mL/min and the rate of heating was 20K/min, as with the PI sample.

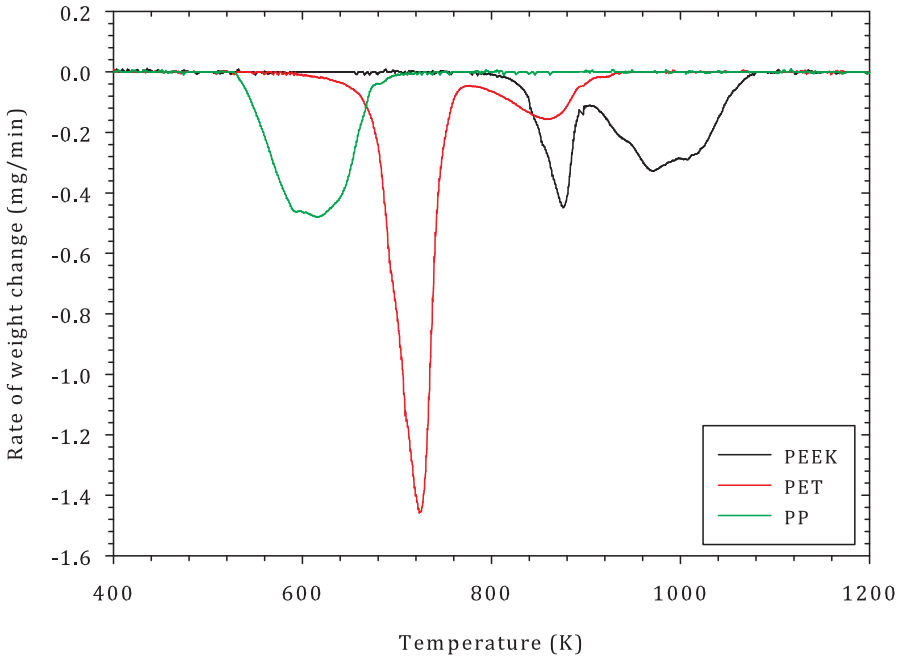

FIGURE 4.7: The rate of weight change of PEEK, PET and PP samples as a function of temperature. The TGA was performed in air with a gas flow rate of 100mL/min and a heating rate of 20K/min.

From the results shown in figure 4.7 it is clear that significant decomposition of PEEK occurred in two stages, the first at 875K and the second at 970K. Results for the decomposition temperature of PEEK in air in the literature range from 833–853K for the first stage of decomposition and 863–923K for the second [62–64]. In reference [62] the rate of heating was 10K/min and the air flow rate was 50mL/min, resulting in a decomposition temperature of approximately 853K and 923K for the first and second stages respectively. In reference [63] the rate of heating was also 10K/min, however the air flow rate was 10mL/min. Two pyrolysis steps at temperatures of 833K and 863K were observed. The parameters used for TGA were not specified in reference [64] except that the analysis was performed in air, yielding temperatures of 848K and 923K for the first and second stages of decomposition respectively. The results obtained in this work are within the range of those quoted in the literature.

A two stage decomposition process was observed for PET where the first stage occurred at 725K and the second at 850K. The literature values for the temperatures of the first and second stage decomposition in air were in the range 699–703K and 797–823K respectively [65, 66]. The heating rate in both references were 10K/min. The gas flow rate was not indicated in either publication except that the analysis was performed in air. The results obtained in this work were slightly higher than those in the literature. This was assumed to be due to the slightly different heating rates and the material sources.

It is clear from figure 4.7, that the temperature of the maximum rate of decomposition of PP was 620K. In the literature a range of 611–614K was found for the

maximum rate of decomposition in air [67, 68]. In reference [67] the temperature of decomposition of PP was found to be 614K in an air environment at a heating rate of 20K/min. In reference [68] a heating rate of 20K/min was also used and a decomposition temperature of 611K was obtained. Neither reference stated the flow rate of the gas.

Results obtained for the decomposition temperatures of all the polymers in this work were consistently higher than those found in the literature. Repeat measurements indicated that this was likely to be a systematic effect as there was little change between experimental runs. The difference in experimental details such as the heating rate and gas flow rate could explain this and the materials used in the literature were obtained from different manufacturers than those in this work. Also, any uncertainty in the temperature calibration of the instrument used in this work could account for the inconsistency between results found in the literature and those measured here.

4.4 Fourier Transform Infrared Spectroscopy

An FTIR spectrometer (Thermo-Scientific Nicolet 380 FTIR Spectrometer and Omnic software) was used to determine the IR optical properties of the polymer samples at room temperature and as a function of elevated temperature. This was to allow quantification of laser absorption and the effect of laser heating on optical coupling to be investigated. Detailed operating principles of an FTIR spectrometer can be found in reference [69].

The polymers were mounted on a frame in the instrument and multiple spectra were taken to ensure consistency. The thickness of the PI used for the FTIR analysis was 125μm. The PEEK, PET and PP samples were 75μm thick.

The results obtained for PI are shown in figure 4.8, where apparent absorbance is plotted as a function of wavenumber.

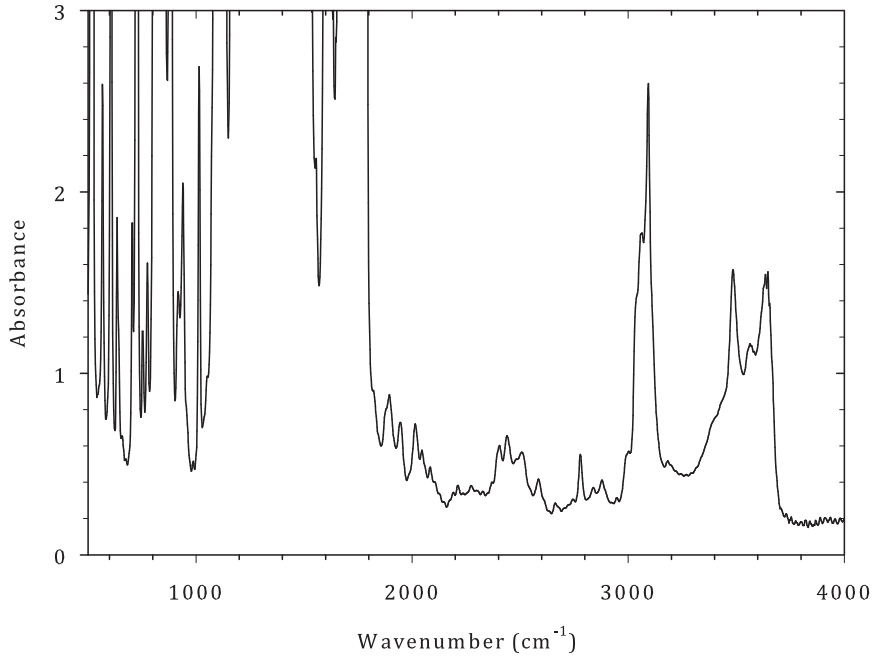

FIGURE 4.8: FTIR spectrum of PI (125μm thick sample) showing apparent absorbance as a function of wavenumber.

The wavelength measurements taken earlier indicated that the laser was operating on several emission lines between wavelengths of 10.53μm and 10.63μm, with a most prevalent wavelength of 10.59μm. The FTIR spectrum around this range is shown in figure 4.9, where wavenumber has been converted to wavelength. Also, the absorbance (A) has been converted into percentage transmission (T) using equation 4.1.

$$T = 100 \times 10^{-A} \tag{4.1}$$

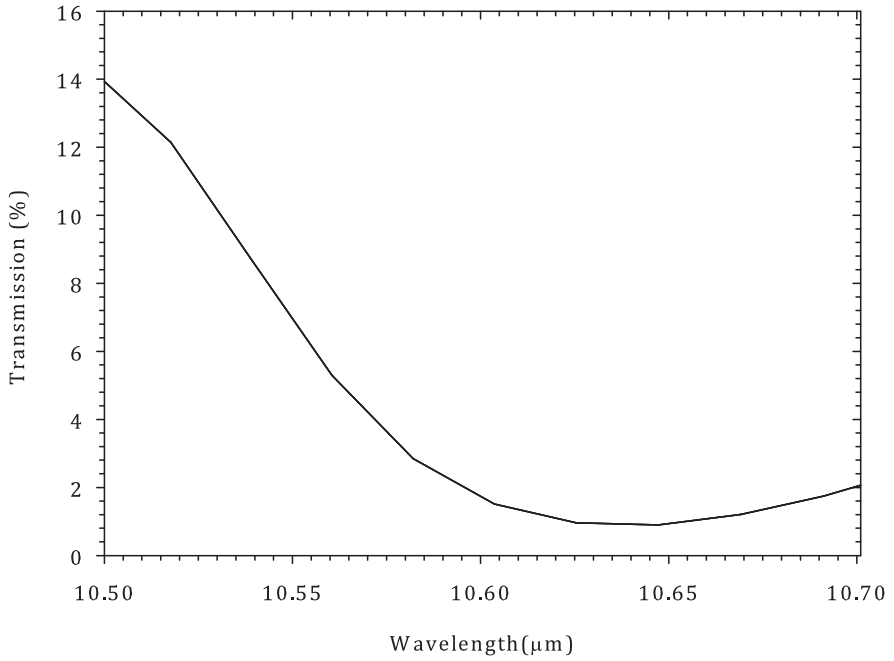

FIGURE 4.9: FTIR spectrum of PI (125μm thick sample) showing the percentage transmission (not corrected for reflective losses) as a function of wavelength.

The reduction in intensity (I) of a transmitted beam due to absorption can be calculated from the following well known Beer-Lambert law equation. In equation 4.2, I_0 is the initial intensity, z is the distance within the sample (which is the sample thickness when calculating transmission) and α is the absorption coefficient.

$$I = I_0 e^{-\alpha z} \tag{4.2}$$

The distance (or depth) at which z is equal to the reciprocal of the absorption coefficient is known as the optical absorption depth and is the characteristic depth

at which the intensity drops to $\frac{1}{e}$ of the initial value. This depth was calculated for each polymer and gives some indication of the irradiated volume within the sample. This will be discussed in more detail later.

Equation 4.2 was rearranged to include the transmission. The ratio of the two intensities multiplied by 100 was the percentage transmission. The equation used is shown below.

$$\alpha = -\frac{1}{\mathrm{z}}\ln\left[\frac{\mathrm{T}}{100}\right] \tag{4.3}$$

The transmission (T) was used to calculate the absorption coefficient (α) using equation 4.3. The distance (z) was the film thickness (125µm for PI).

The transmission shown in the graph in figure 4.9 does not take into account the reflection from both surfaces of the PI sheet. The transmission data shown are known as external transmission values, whereas the transmission taking into account the reflection is known as the internal transmission (i.e. assuming no interfaces). The refractive index of PI is 1.73 [70] at 10.60µm and the reflectivity (R) was calculated from equation 4.4. Here, n_0 is the refractive index of air and n_1 is the refractive index of PI. The extinction coefficient is not included, as in reference [70] it is very small and does not have a significant effect on the reflectivity when used in the calculation.

$$\mathrm{R} = \left[\frac{n_0 - n_1}{n_0 + n_1}\right]^2 \tag{4.4}$$

Using equation 4.4, a reflectivity of 7.2% was calculated for the front surface. However, the reflection from the back surface will have a smaller contribution to the total reflected light due to absorption through the sample thickness. This front surface reflectivity is in agreement with reference [7], which quotes reflectivity values between 6% and 9% from transmission and reflection experiments performed using a TEA-CO_2 laser at a wavenumber of 944cm^{-1}.

The absorption coefficients with and without the reflectivity are shown in equations 4.5 and 4.6 respectively. Here, the transmission has been modified to include reflection at the interfaces as well as absorption through the material. In the equations α_{R} is the absorption coefficient corrected for reflectivity, α is the absorption coefficient not corrected for reflectivity, R is the reflectivity based on the refractive index and z is the sample thickness.

$$\alpha_{\mathrm{R}} = -\frac{1}{\mathrm{z}}\ln\left[\frac{(1-\mathrm{R})^2 e^{-\alpha \mathrm{z}}}{100}\right] \tag{4.5}$$

$$\alpha = -\frac{1}{\mathrm{z}}\ln\left[\frac{e^{-\alpha \mathrm{z}}}{100}\right] \tag{4.6}$$

The difference between the absorption coefficients is therefore given by equation 4.7.

$$\Delta\alpha = \frac{2}{\mathrm{z}}\ln(1-\mathrm{R}) \tag{4.7}$$

Using the reflectivity for PI, the reduction in absorption coefficient caused by accounting for the reflectivity was calculated to be $\Delta\alpha$=12cm^{-1}. This was the internal absorption coefficient. All corrected results shall be referred to as simply the absorption coefficient henceforth, unless otherwise indicated.

The results for PI are shown in figure 4.10.

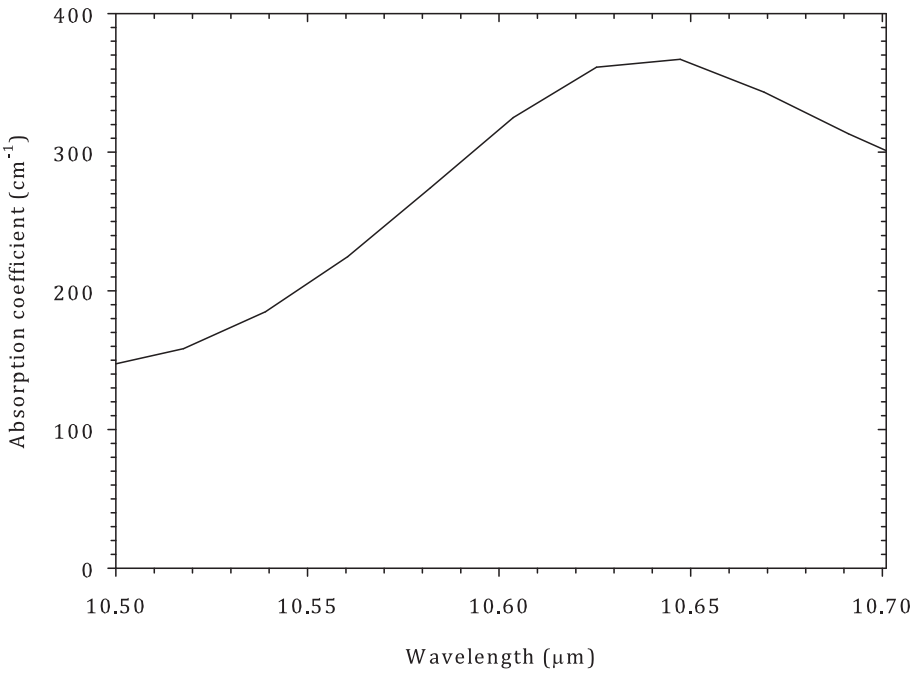

FIGURE 4.10: The absorption coefficient of PI as a function of wavelength, calculated from the transmission spectrum.

An absorption coefficient of 270cm^{-1} at 10.59μm is reported in reference [7] for a polyimide (Kapton type H). The absorption coefficient in reference [7] was obtained by determining the transmission of polyimide (type H) films of 75μm thickness using the 10.59μm line of a grating tuned pulsed CO_2 laser. The value for the absorption coefficient at 10.59μm obtained in this work is 295cm^{-1}. The difference between the two values may be attributed to the slightly different materials being

used for the study and the methods used to determine the transmission, however the values are the same order of magnitude. The percentage difference between the two results was calculated as approximately 8.5%, which is acceptable considering the usual experimental uncertainties.

The method detailed above was also used to determine the FTIR spectra and therefore the absorption coefficients of PEEK, PET and PP. All results were corrected for reflectivity, using the method detailed above.

Based on a refractive index of 1.65 [71], the reflectivity of PEEK was calculated to be 6%. The corrected absorption coefficient is shown as a function of wavelength in figure 4.11.

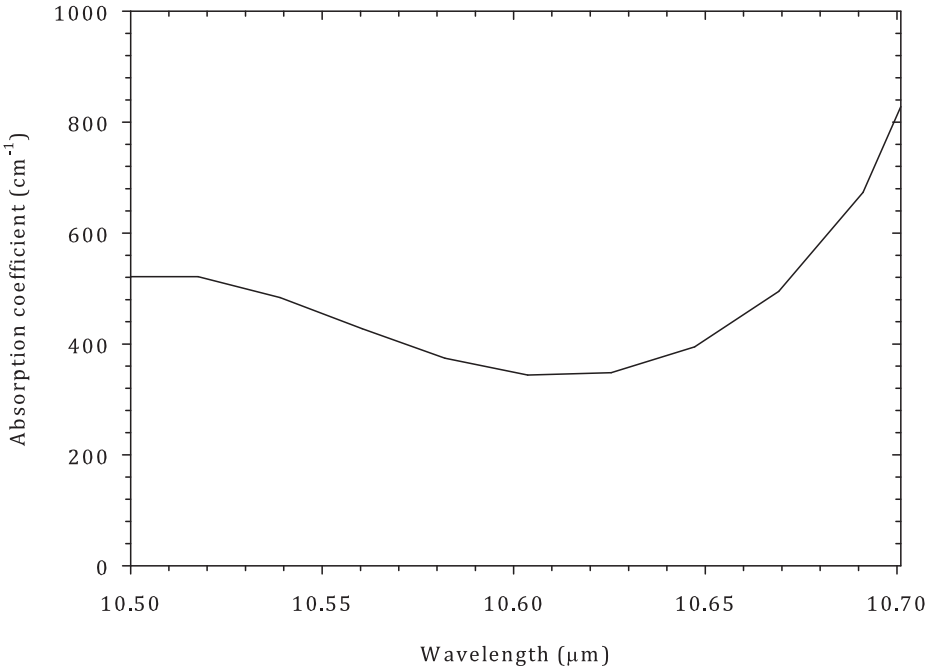

FIGURE 4.11: The absorption coefficient of PEEK as a function of wavelength.

As can be seen from figure 4.11, the absorption coefficient for a laser wavelength of 10.59μm was found to be 361cm^{-1}. In reference [6] the transmission spectrum for

a 25μm thick PEEK film was measured. The transmission at a laser wavelength of 10.59μm was inferred from the graph in the reference as being in the range of 40–50%. Using equation 4.3, this corresponds to an absorption coefficient range of 277–366cm^{-1}. The results found here are consistent with this.

The refractive index of PET has been reported to be 1.73 in reference [72]. In the reference, the refractive index was determined by placing a film of known thickness (in the reference this was 49μm) as a beam splitter in an interferometer. Due to interference effects in the film, intensity minima and maxima were observed, allowing the refractive index to be calculated [72]. The experiment was performed over a range of wavenumbers, up to 1200cm^{-1}.

The reflectivity (R) of PET was calculated to be 7.2%. The corrected absorption coefficient of PET is shown in figure 4.12 as a function of wavelength.

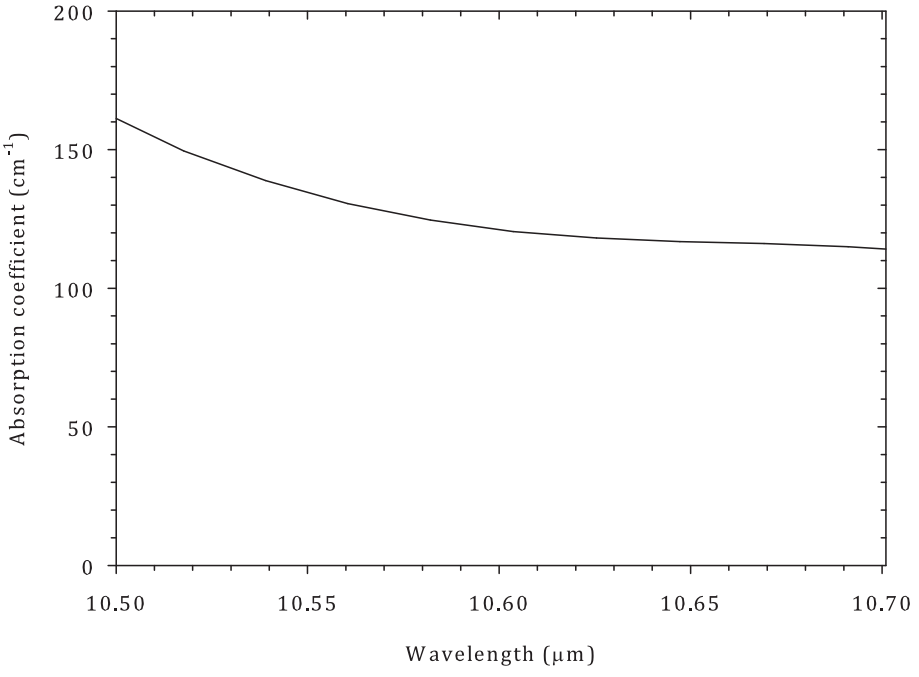

FIGURE 4.12: The absorption coefficient of PET as a function of wavelength.

The value obtained for the absorption coefficient of PET at 10.59μm was 123cm^{-1}. In reference [72] the transmission spectrum of PET as a function of wavenumber is presented. It is possible to estimate the absorption coefficient from the results in the reference for comparison to results presented here. At a wavenumber of 944cm^{-1} (corresponding to a laser wavelength of 10.59μm) the transmission was inferred from the data in the reference as being approximately 35-45%. Using a film thickness of 49μm, the absorption coefficient was calculated to be in the range 163-214cm^{-1}. Although the values are close, the absorption coefficients in the range calculated from the reference are larger than those measured experimentally here. This could be due to a difference in the manufacturing process of the polymers used or the method used to determine the transmission spectrum.

The absorption coefficient as a function of wavelength of PP is shown in figure 4.13. The reflectivity was calculated as being 4% from a refractive index of 1.5 [71, 72]. The absorption coefficient was reduced by 11cm^{-1} to account for this.

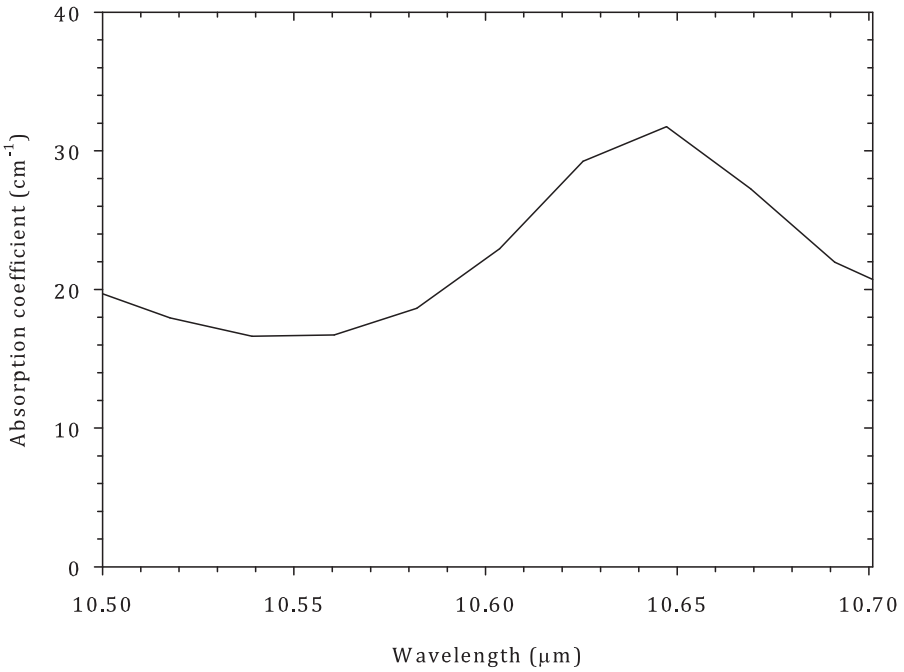

FIGURE 4.13: The absorption coefficient of PP as a function of wavelength.

The absorption coefficient of PP at 10.59μm was found to be 20cm^{-1}. From the transmission spectrum of PP given in [72] the absorption coefficient was calculated. At a wavenumber of 944cm^{-1} the transmission was estimated from the data in the reference as being approximately 85-90%. Using a film thickness of 15μm, the absorption coefficient was calculated as 70-108cm^{-1}. In two papers by Bormashenko et al [41, 73], the transmission of PP was also measured. The transmission was estimated from the spectrum given in the paper to be 85–90% with a film thickness of 20μm. This gave an absorption coefficient in the range 53–81cm^{-1}.

The optical parameters of PP were measured more directly in reference [74], for a laser wavelength of 10.6μm. The absorption coefficient was found to be 38cm^{-1} from measurements of transmission and use of the Beer-Lambert law. However,

whereas FTIR spectroscopy allowed the transmission to be determined for a range of wavelengths in this work, the experiment in reference [74] used only a laser beam with a wavelength of 10.6µm and does not specify the nature of the laser used.

Again the results found in the literature are larger than the results found experimentally and is assumed to be due to the different FTIR spectroscopy equipment and difference in manufacturer of the polymer.

Shown in figure 4.14 are the absorption coefficients as a function of laser wavelength at room temperature for all the polymers studied, for comparison.

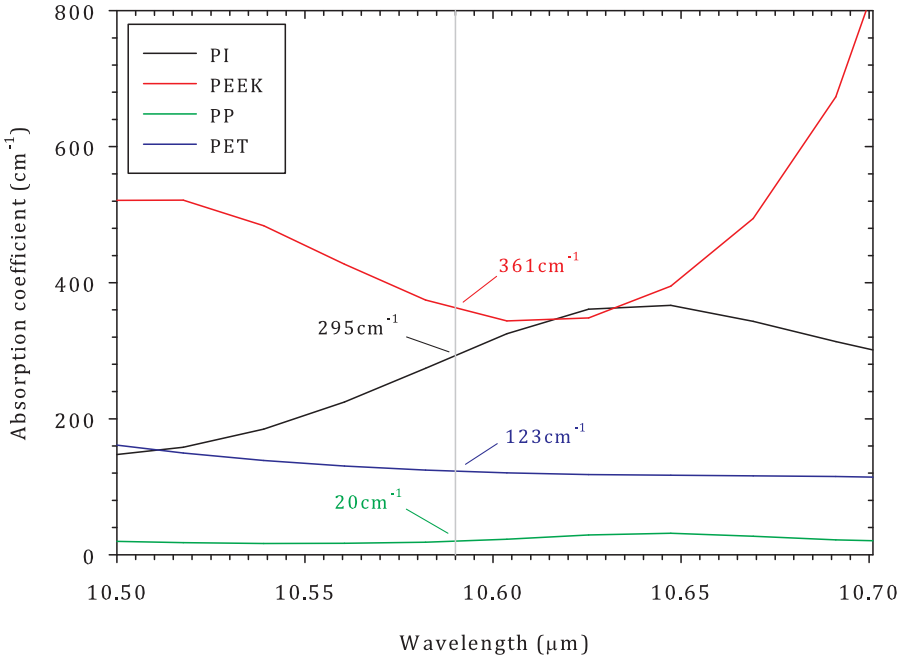

FIGURE 4.14: The absorption coefficient as a function of wavelength for PI, PEEK, PET and PP at room temperature. The absorption coefficients were calculated from the transmission of each polymer and were corrected for reflectivity. The vertical line on the graph indicates the laser operating wavelength of 10.59µm.

The results found in this section are summarised in table 4.1 for the laser wavelengths measured in Chapter 3.

TABLE 4.1: Room temperature optical absorption coefficient of PI, PEEK, PET and PP for different laser wavelengths

Wavelength (μm)	PI	PEEK	PET	PP
		α (cm^{-1})		
10.53	172	503	143	17
10.55	204	455	134	17
10.57	246	403	128	17
10.59	295	361	123	20
10.61	337	341	120	25
10.63	365	355	118	30

4.5 The Effect of Polymer Temperature on the Absorption Coefficient

It has been shown previously that the absorption coefficient of polymers changes as a function of temperature in the IR region [8]. In this reference, the effect of temperature on the absorption coefficient of Upilex polyimide R film at the strongly absorbed wavelength of 9.21μm (TEA CO_2 laser) was measured. Room temperature measurements yielded an absorption coefficient of 1900cm^{-1} at 9.21μm. It was seen that the absorption coefficient reached a peak of almost 2000cm^{-1} at a temperature of approximately 450K, before falling to 1500cm^{-1} at 900K.

In order to extend the work by Dyer et al [8] and examine how the whole IR spectrum changes upon heating, the temperature dependence of the absorption

coefficient of the polymers was measured using an in house fabricated heated sample holder. A schematic of the heater is shown in figure 4.15.

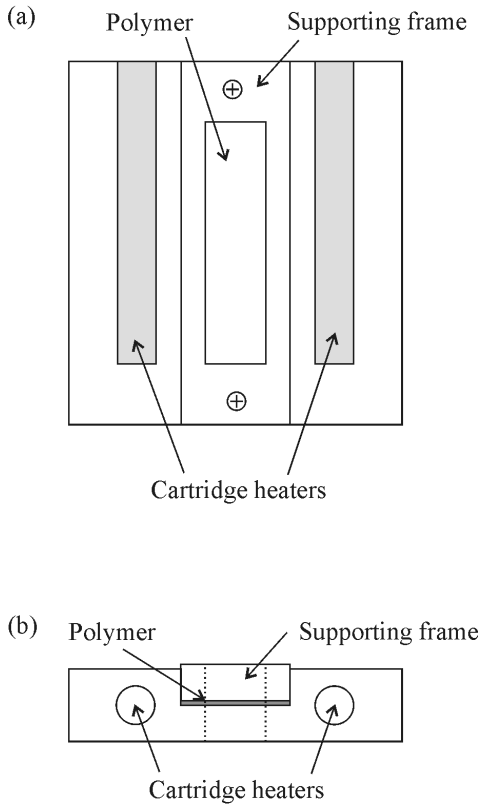

FIGURE 4.15: The heater fabricated to study the change in absorption coefficient of the polymer samples as a function of temperature. (a) is the front view of the heater and (b) is the top view. The sample holder was made from copper and the heaters used were 100W rated cartridge heaters housed in the copper vertically and parallel to the aperture. The polymer being studied was clamped tightly in place over the aperture by a supporting frame to ensure good heat flow between the copper and the test material.

Two electrical heaters were mounted in a copper block which included an aperture so that transmission measurements could be be made. The polymer was held tightly in place using a supporting frame which ensured good heat flow between the copper and polymer. The heaters were 100W rated cartridge heaters with a maximum working temperature of 750°C (from manufacturers data). A close milled interference fit was used to ensure minimal heat flow interruption between

the heaters and the copper. The voltage supplied to the heaters was controlled with a variac. The temperature of both the copper block and polymer was monitored throughout the experiment using a k-type, fibreglass coated, thermocouple and custom readout box.

The TGA data described earlier in this chapter gave the decomposition temperature of the polymers and these temperatures were not exceeded during the experiment. The melting temperatures of PEEK, PET and PP were also considered and the temperature of the copper block was monitored during the experiment to ensure that the melting point of each material was not exceeded, as the copper block was in close contact with the polymers. Individual melting temperatures will be discussed when detailing the results of each polymer. A heat mat was placed between the heating rig and the FTIR spectrometer base to protect the equipment. A schematic of the experimental set-up is shown in figure 4.16.

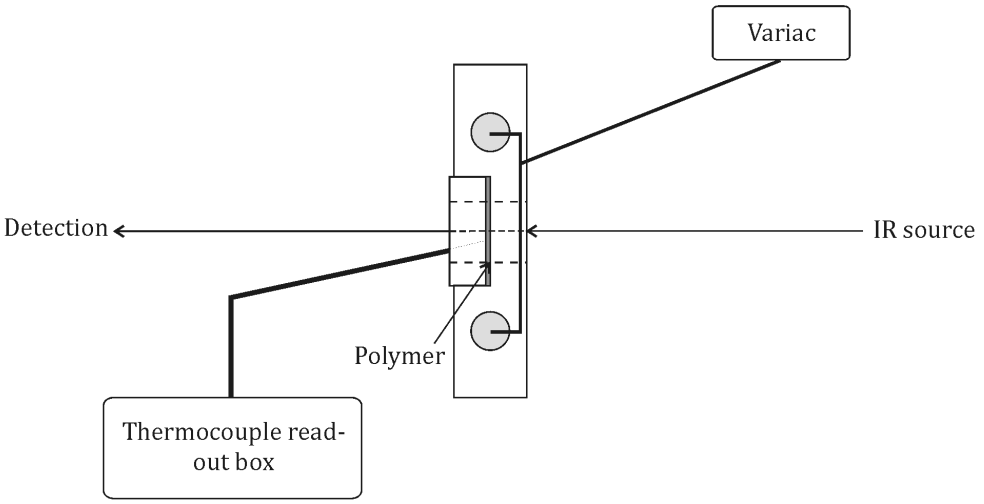

FIGURE 4.16: The experimental set-up used to measure the FTIR spectrum of the polymer samples as a function of temperature. The heating rig was placed in the FTIR spectrometer such that the beam passed through the aperture and thus the polymer. The surface temperature of the polymer was measured using a k-type, fibre-glass coated thermocouple and readout box. The voltage supplied to the heaters (and thus temperature of the heaters) was controlled using a variac.

As stated before, the absorption coefficient refers to the internal absorption coefficient which was corrected for the reflective losses calculated in the previous section. Calculations for each polymer within the temperature range revealed that the reflectivity remained approximately constant.

Figures 4.17 and 4.18 show the absorption coefficient as a function of wavelength for PI at a number of different polymer temperatures ranging from room temperature (approximately 300K) to approximately 520K, for the heating and cooling cycles respectively. Measurements made by TGA earlier in this chapter indicated the decomposition temperature to be 880K (in an air atmosphere). This was not exceeded by the copper block during the experiment as this was the region of the

heater which was in closest contact with the sample. Although only 5 and 6 different temperatures are shown in figures 4.17 and 4.18 respectively (as an overview of the behaviour of the material), spectra were taken at 17 different temperatures for the heating cycle and 11 for the cooling. The room temperature measurement in figure 4.9 was taken after several hours had elapsed after the previous measurement.

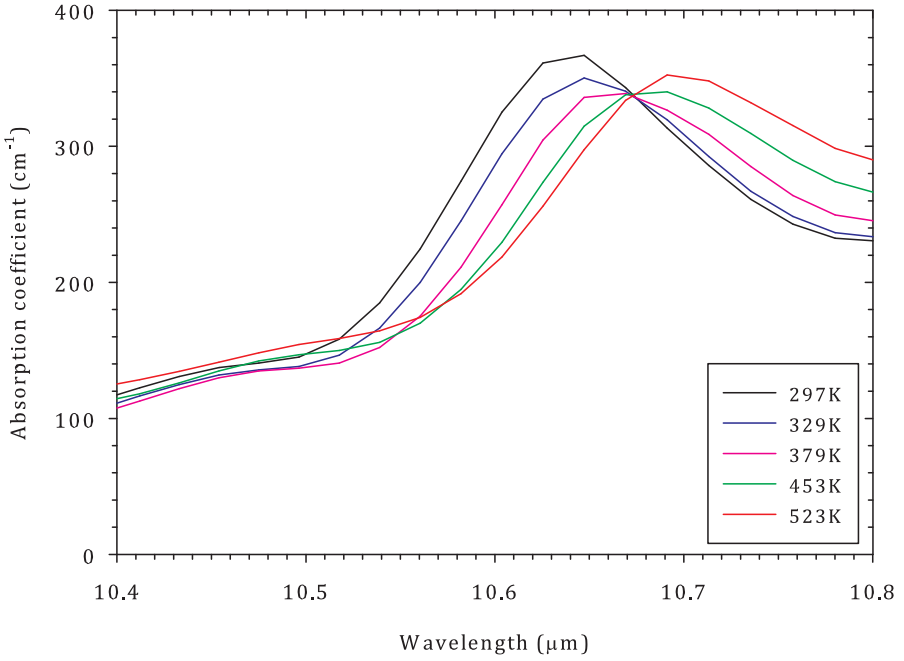

FIGURE 4.17: The absorption coefficient of PI as a function of wavelength at different temperatures during the heating cycle.

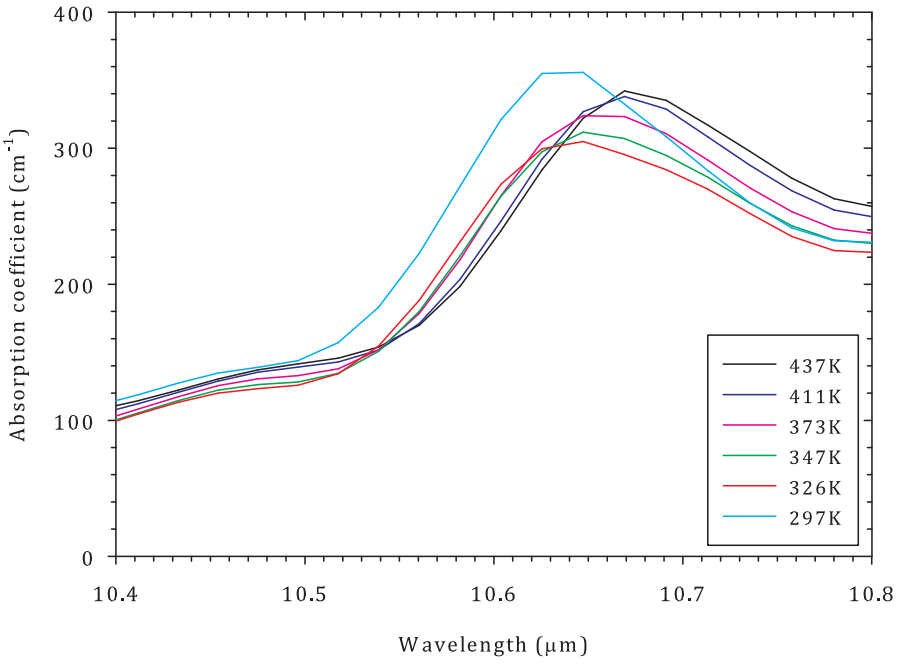

FIGURE 4.18: The absorption coefficient of PI as a function of wavelength at different temperatures during the cooling cycle. The room temperature measurement was taken a number of hours after the equipment was allowed to cool completely.

In reference [8], it was suggested that the change in absorption coefficient as a function of temperature observed in Upilex polyimide R could be attributed to the thermal population of higher vibrational states within the polymer. The optically driven oscillator would then become anharmonic, resulting in red-shift, and line broadening could also occur. It is clear from figures 4.17 and 4.18 that the temperature of the polymer had an appreciable effect on the absorption coefficient for certain wavelengths and almost no effect for others, within the range shown. It was noted that the peak which occurred at a wavelength of approximately 10.64μm at room temperature underwent a degree of red-shift, moving from the initial position to a wavelength of around 10.69μm. Therefore, significant changes in the absorption coefficient of PI at wavelengths on the edge of this peak were expected.

As has been previously discussed, a laser wavelength of 10.59μm was found to be the most prevalent emission line. Thus, the absorption coefficient as a function of temperature for the heating and cooling cycle for this wavelength is shown in figure 4.19.

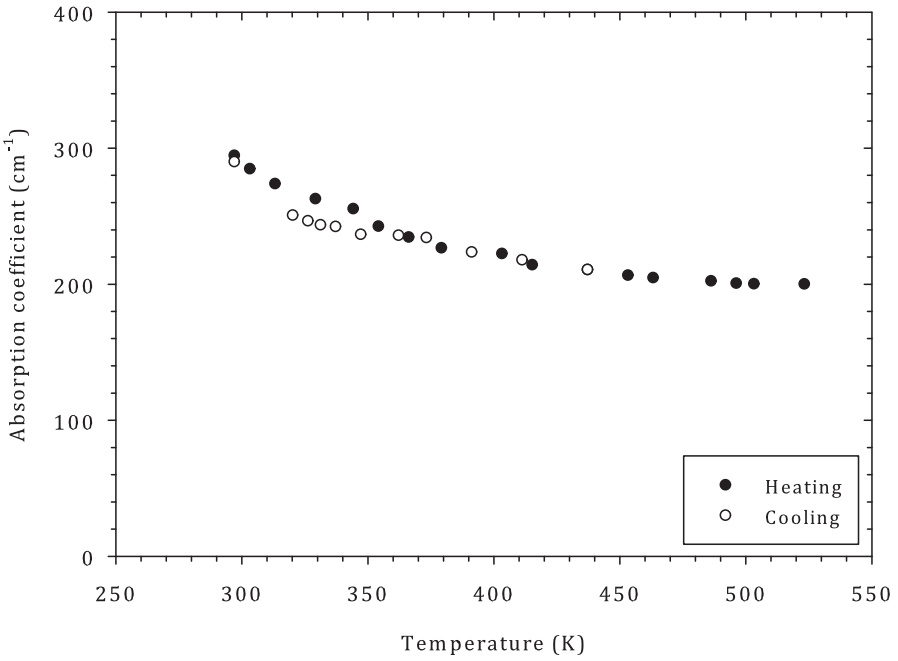

FIGURE 4.19: The absorption coefficient of PI as a function of polymer temperature at a wavelength of 10.59μm. Both the heating and cooling cycles are shown and are indicated in the legend. The room temperature absorption on the cooling cycle was measured a number of hours after the 318K measurement.

Figure 4.19 shows a decrease in the absorption coefficient of PI of approximately 30% over the temperature range measured. The effect was reversible, as can be seen in the figure, but demonstrated a small inconsistency on the cooling curve between approximately 350K and room temperature. As this path dependence occurred at temperatures below 100 °C, the apparent hysteresis was thought to be caused by temperature induced moisture loss from the PI, followed by slow re-absorption or adsorption. Water (with an extrapolated absorption coefficient

of 850cm^{-1} at 10.59μm [75]) can be absorbed in PI at a level of approximately 3% by weight over a 24 hour period [76]. As previously mentioned, a number of hours elapsed between measurements at 318K and 293K (room temperature) during the cooling cycle, allowing re-absorption of water from the surrounding environment and thus giving a possible explanation for the hysteresis observed.

The laser was also shown to operate at wavelengths of 10.53μm, 10.55μm, 10.57μm, 10.61μm and 10.63μm. The absorption coefficient of PI as a function of temperature during heating is shown in figure 4.20 for all the wavelengths for comparison, including 10.59μm. The wavelengths are indicated in the legend on the graph.

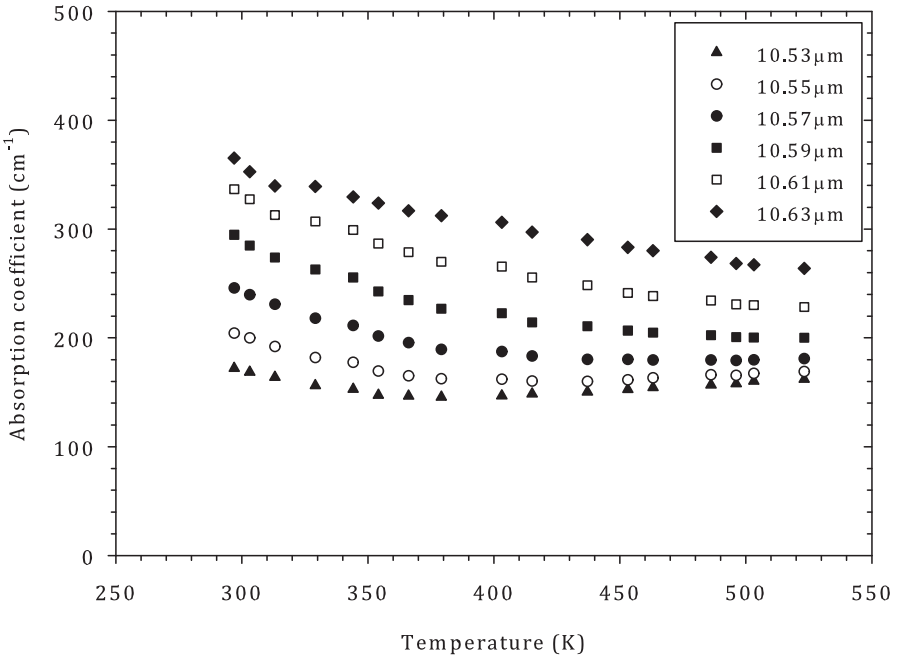

FIGURE 4.20: The absorption coefficient of PI as a function of temperature for all the laser wavelengths for the heating cycle. The laser wavelengths are indicated in the legend on the graph.

The results shown in figure 4.20 indicate that at every wavelength there was a steady decrease in the absorption coefficient as the temperature was increased,

with the exception of 10.53μm, which showed an initial decrease in the absorption coefficient up to a temperature of approximately 350K, followed by a steady increase.

The absorption coefficient as a function of temperature was measured for PEEK using the method detailed for PI above. In references [62, 63], the melting temperature of PEEK was determined by differential scanning calorimetry (DSC). Briefly, DSC is a thermal analysis technique that measures the change in energy provided to a sample and a reference material. Any phase change in the sample material (for example melting) results in more or less energy being supplied to the sample to keep it and the reference at the same temperature. The resulting curve allows the phase change temperatures to be determined from peaks or troughs in the energy being supplied [77].

The DSC results found in the literature were for semi-crystalline PEEK [62, 63]. Two melting temperatures were observed, the lower being in the range 486–551K and the higher being in the range 606–615K. The reason for the double melting temperatures is thought to be due to the semi-crystalline nature of the PEEK being studied in the references and from four contributions: melting of the original crystalline part of the material, recrystallisation, remelting of this crystalline structure and melting of the core crystalline regions [63]. It follows that the temperature at which melting occurs would depend on the initial amount of crystalline material in the PEEK sample and the thermal history of the sample. The manufacturers information states that thin films of PEEK are usually amorphous in nature [53]. Therefore it is likely that the initial peak of melting would not occur

due to there being no crystalline states present in the sample before heating. The melting temperature was therefore assumed to be in the higher range and the copper block was not allowed to exceed this temperature.

Figures 4.21 and 4.22 show the absorption coefficient as a function of wavelength for PEEK at a number of different polymer temperatures ranging from room temperature (approximately 300K) to approximately 370K, for the heating and cooling cycles respectively. Although only 5 different temperatures are shown in figures 4.21 and 4.22 as an overview of the behaviour of the material, 9 different temperatures within the range were recorded for the heating and 12 for the cooling.

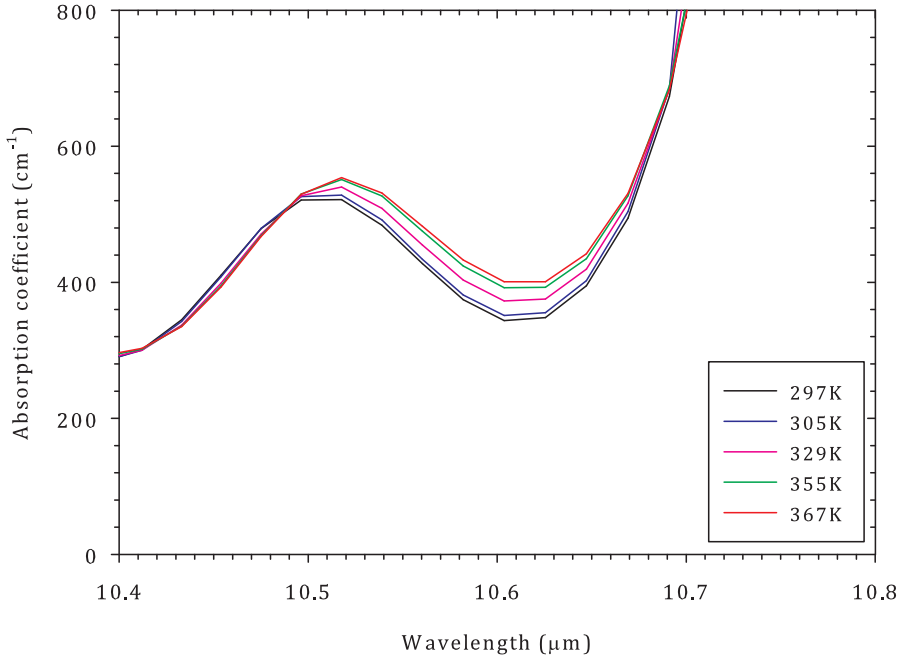

FIGURE 4.21: The absorption coefficient of PEEK as a function of wavelength at different temperatures during the heating cycle.

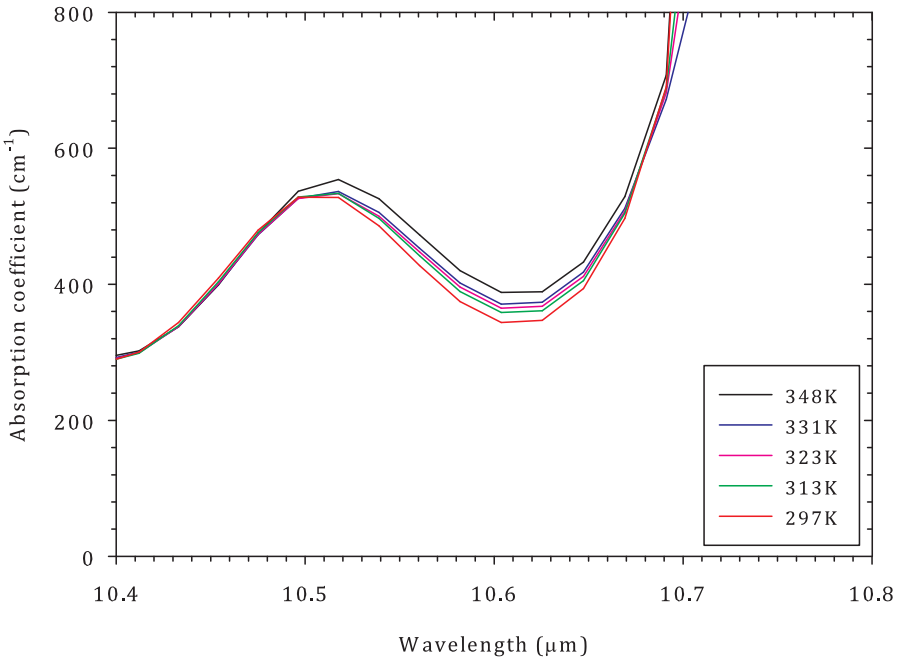

FIGURE 4.22: The absorption coefficient of PEEK as a function of wavelength at different temperatures during the cooling cycle.

It is clear from figures 4.21 and 4.22 that a change in polymer temperature had a modest effect on the absorption coefficient, particularly around the wavelength of 10.59μm. The peak which occurred at a wavelength of approximately 10.50μm at room temperature was seen to red-shift slightly as the temperature was increased. A degree of broadening of this peak was also observed.

In figure 4.23, the absorption coefficient of PEEK as a function of temperature for a wavelength of 10.59μm is shown. It is important to note that the absorption coefficient measurements at room temperature and 323K for both the heating and cooling cycle are so similar that they do not appear as separate points on the graph, although two data points are plotted for both these temperatures.

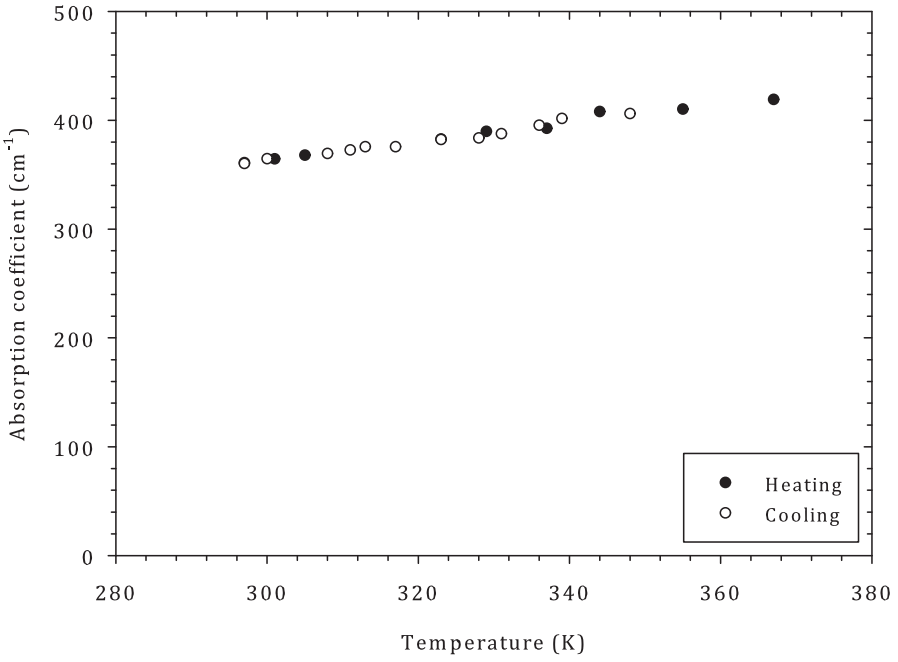

FIGURE 4.23: The absorption coefficient of PEEK as a function of polymer temperature at a wavelength of 10.59μm for both the heating and cooling cycle (indicated in the legend). Note that the absorption coefficient measurements at room temperature and 323K for both the heating and cooling cycle are so similar that they do not appear as separate points on the graph, although two data points are plotted for each temperature.

The results shown in figure 4.23 show an increase in the absorption coefficient of approximately 16% over the temperature range measured at a wavelength of 10.59μm. The effect was reversible, as can be seen in the figure, and did not appear to demonstrate the same hysteresis as was observed in the PI. This was attributed to the fact that the water absorption by weight in PEEK is much lower than that in the PI sample investigated earlier, at a maximum of approximately 0.4% by weight over 24 hours [53, 78]. The implication was that during the experiment there was not sufficient water content in the material to change the absorption coefficient due to evaporation during heating. Thus, no re-absorption was observed in the cooling cycle.

Figure 4.24 shows the absorption coefficient as a function of temperature for the laser wavelengths measured in this work.

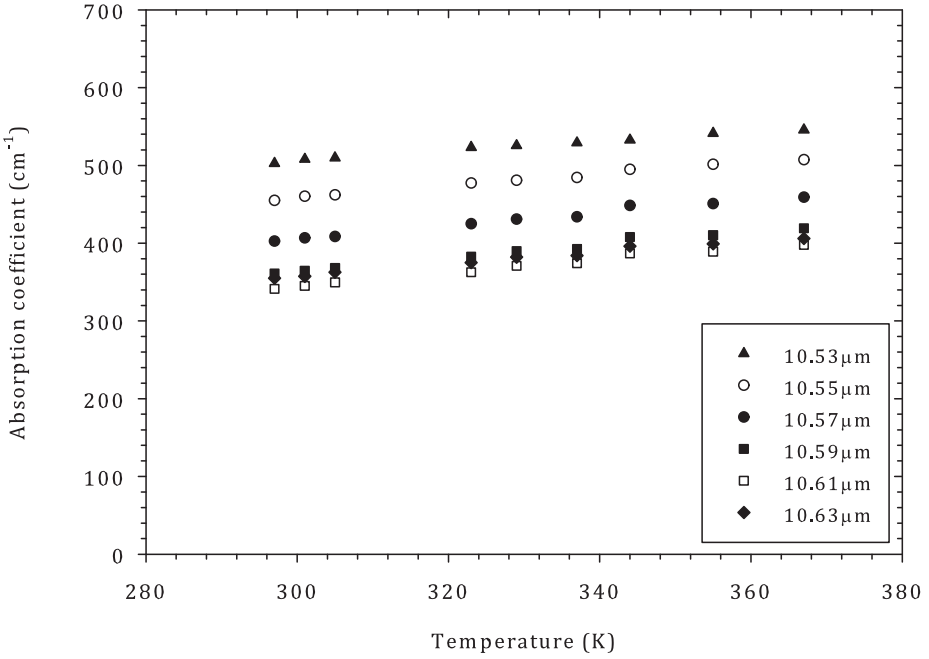

FIGURE 4.24: The absorption coefficient of PEEK as a function of temperature for the laser wavelengths for the heating cycle only. The laser wavelengths are indicated in the legend on the graph.

Clearly, all the wavelengths show the same behaviour in terms of the change in absorption coefficient as a function of temperature. The absorption coefficients increased by approximately 18% of the initial value at room temperature.

The same process was used to measure the FTIR spectrum of PET as a function of temperature. The melting temperature of PET is in the range 416–538K [51, 79]. This temperature was not exceeded by the copper block during the experiment for the reasons explained before.

The results are shown in figures 4.25 and 4.26 for the heating and cooling cycles respectively. Although only 5 different temperatures are shown in figures 4.25 and

4.26 as an overview of the behaviour of the material, 9 and 11 different temperatures within the range were used for the heating and cooling cycles respectively. It should be noted that on the cooling cycle the room temperature measurement was taken a number of hours after the equipment was allowed to cool completely.

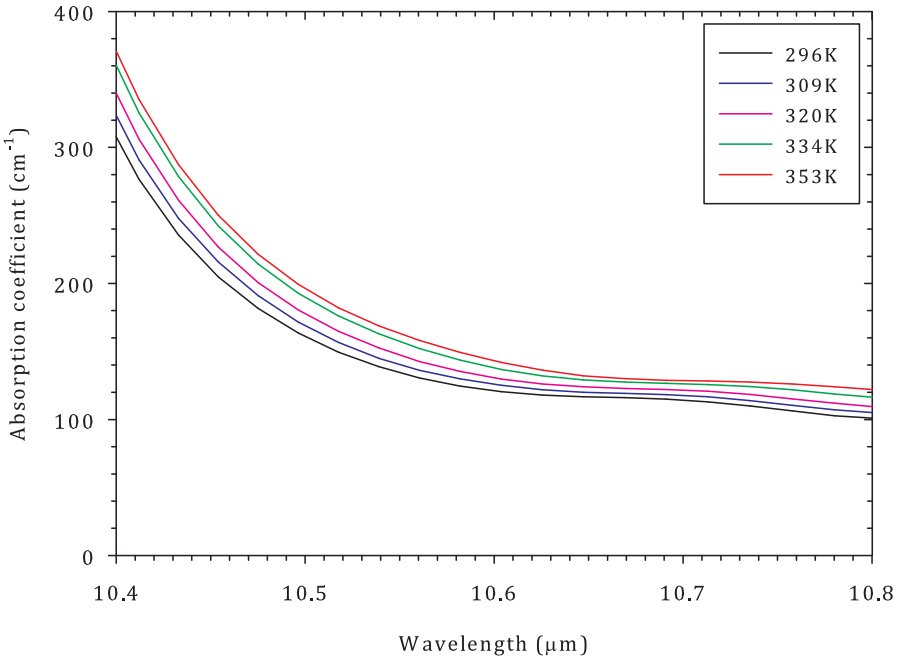

FIGURE 4.25: The absorption coefficient of PET as a function of wavelength at different temperatures during the heating cycle.

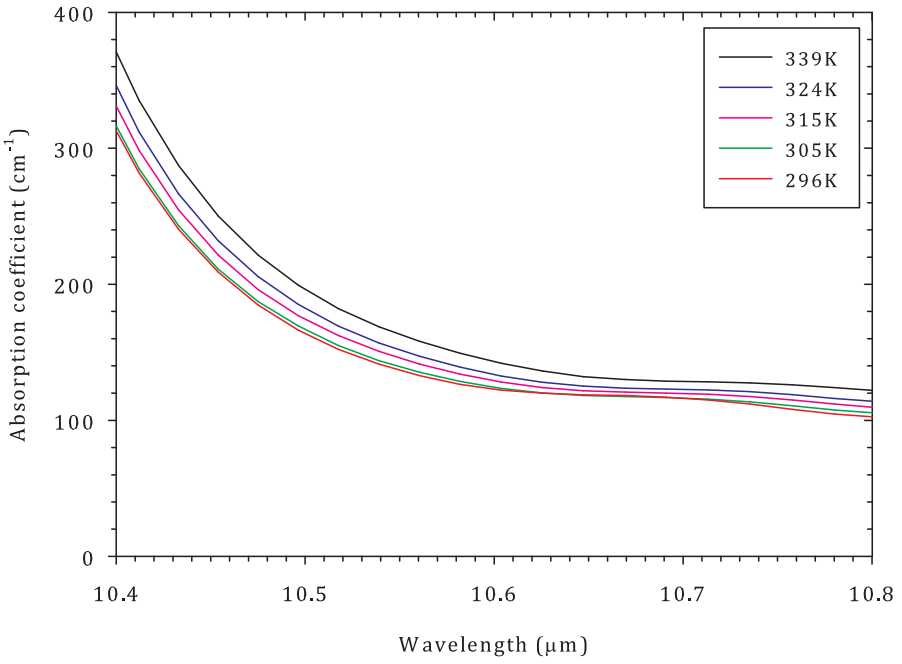

FIGURE 4.26: The absorption coefficient of PET as a function of wavelength at different temperatures during the cooling cycle. The room temperature measurement was taken a number of hours after the equipment was allowed to cool completely.

It is clear from figures 4.25 and 4.26 that the change in temperature of PET had an effect on the absorption coefficient which was fairly independent of the wavelength in terms of percentage change. For the most common laser operating wavelength (10.59μm) the absorption coefficient of PET as a function of temperature is shown in figure 4.27 for the heating and cooling part of the experiment.

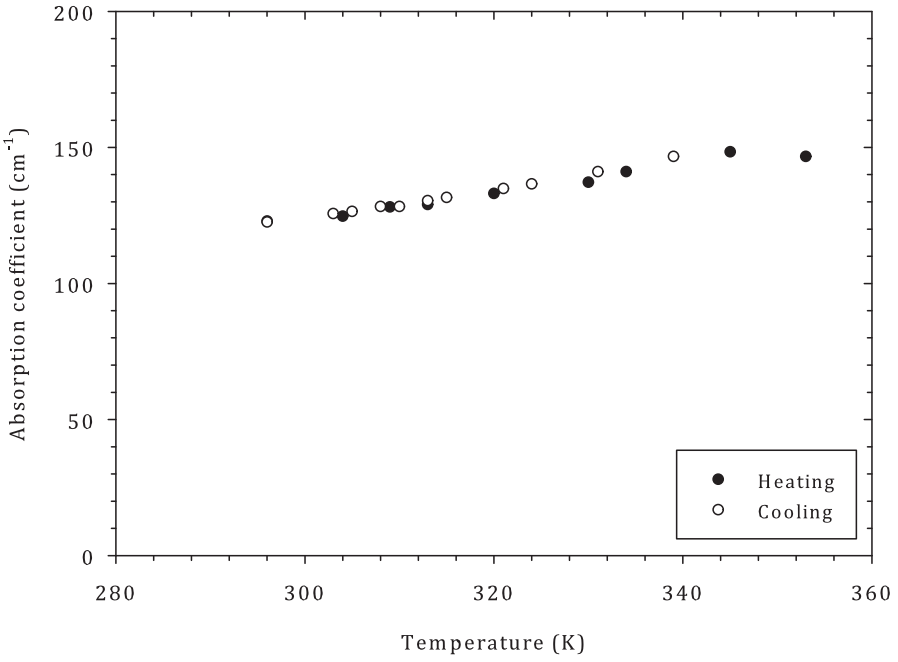

FIGURE 4.27: The absorption coefficient of PET at 10.59μm as a function of polymer temperature for both the heating and cooling cycle. The room temperature result for the cooling cycle was taken a number of hours after the equipment was allowed to cool completely.

It is clear from figure 4.27 that the temperature rise caused the absorption coefficient of the polymer to increase. At the last temperature on the heating cycle, it appeared that the absorption coefficient would have started to fall again, but it was not possible to heat the sample any further due to the copper approaching the melting temperature of the PET sample. The cooling cycle demonstrated no hysteresis. This is to be expected as (similarly to PEEK) the water absorption of PET is less than 0.1% over a 24 hour period [79]. This implies that the water content of PET was sufficiently low that no water loss (or re-absorption) was measured in the experiment.

The absorption coefficient of PET as a function of temperature for the laser wavelengths measured in this work is shown in figure 4.28.

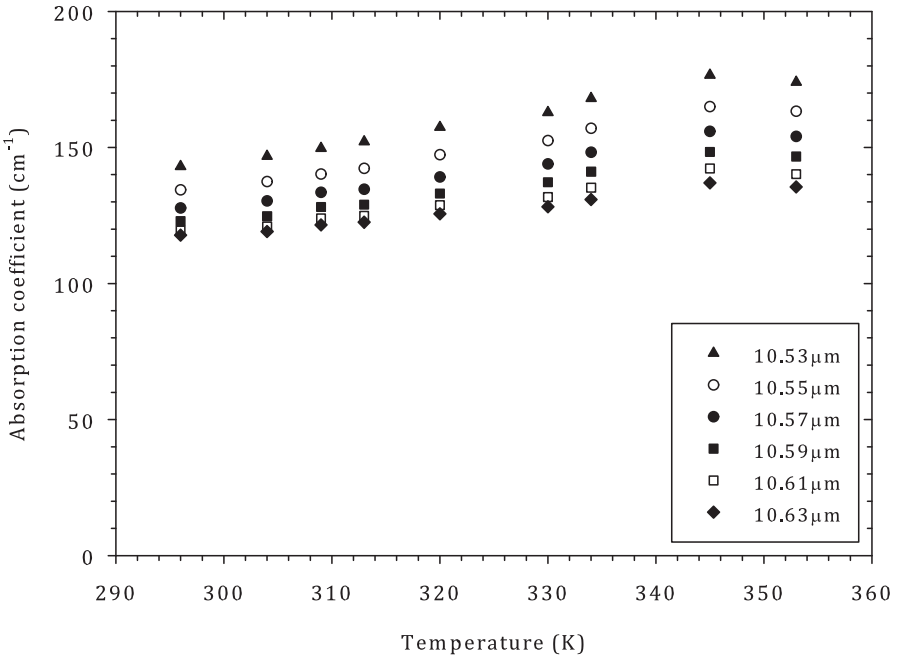

FIGURE 4.28: The absorption coefficient of PET as a function of temperature for the laser operating wavelengths for the heating cycle only. The laser wavelengths are indicated in the legend on the graph.

Figure 4.28 indicates that for each wavelength shown, the increase in polymer temperature resulted in the absorption coefficients increasing by approximately 17% of the initial value. At the maximum temperature studied, however, the absorption coefficient was seen to reduce slightly as was observed at a wavelength of 10.59μm.

Finally, the temperature dependent absorption coefficient of PP was determined. The melting temperature of PP is in the range 393–449K [51, 80]. It was ensured that this temperature was not exceeded by the copper block in the experiment, as has been explained before.

Figures 4.29 and 4.30 show the absorption coefficient as a function of wavelength for PP at a number of different polymer temperatures ranging from room temperature (approximately 300K) to 343K, for the heating and cooling cycles respectively. Although only 4 and 3 different temperatures are shown in figures 4.29 and 4.30 respectively as an overview of the behaviour of the material, 9 different temperatures within the range were used for both the heating and cooling cycles.

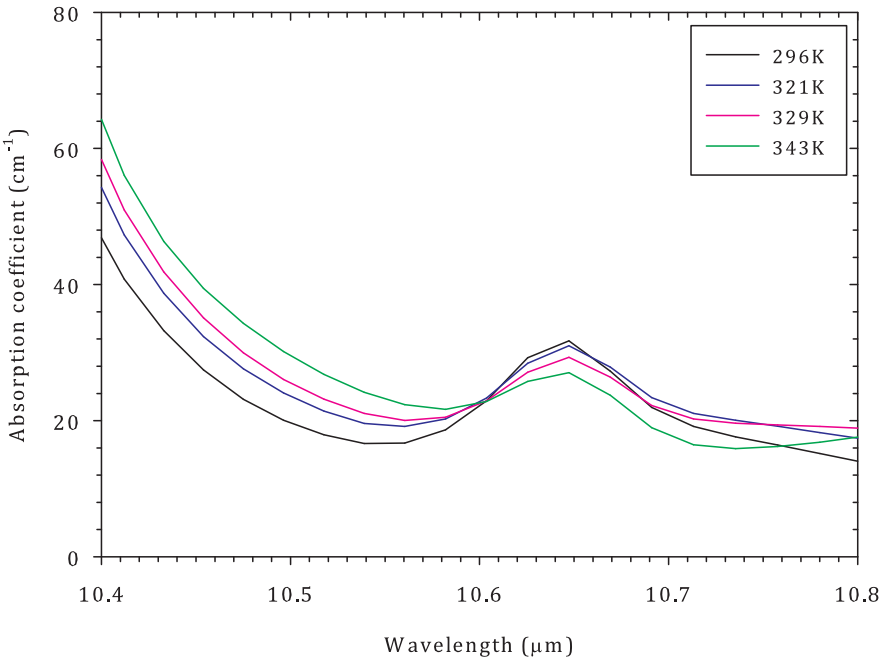

FIGURE 4.29: The absorption coefficient of PP as a function of wavelength at different temperatures during the heating cycle.

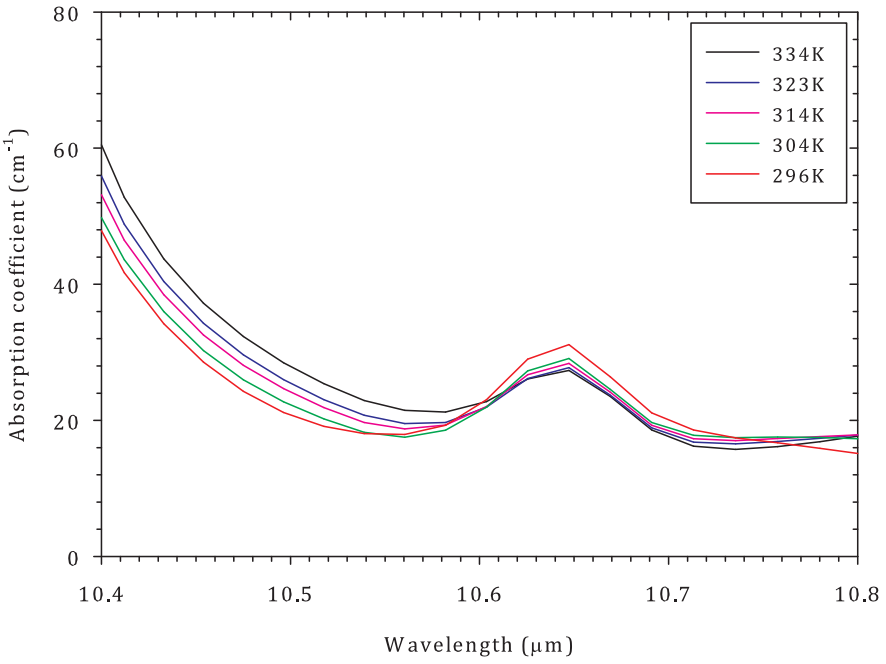

FIGURE 4.30: The absorption coefficient of PP as a function of wavelength at different temperatures during the cooling cycle. The room temperature measurement was taken a number of hours after the equipment was allowed to cool completely.

In figures 4.29 and 4.30 it is clear that there was some effect on the absorption coefficient with a change in polymer temperature, at some wavelengths. However, it is interesting to note that at a wavelength of approximately 10.59μm, the absorption coefficient did not appear to change significantly. The absorption coefficient of PP as a function of temperature is shown in figure 4.31 for this wavelength.

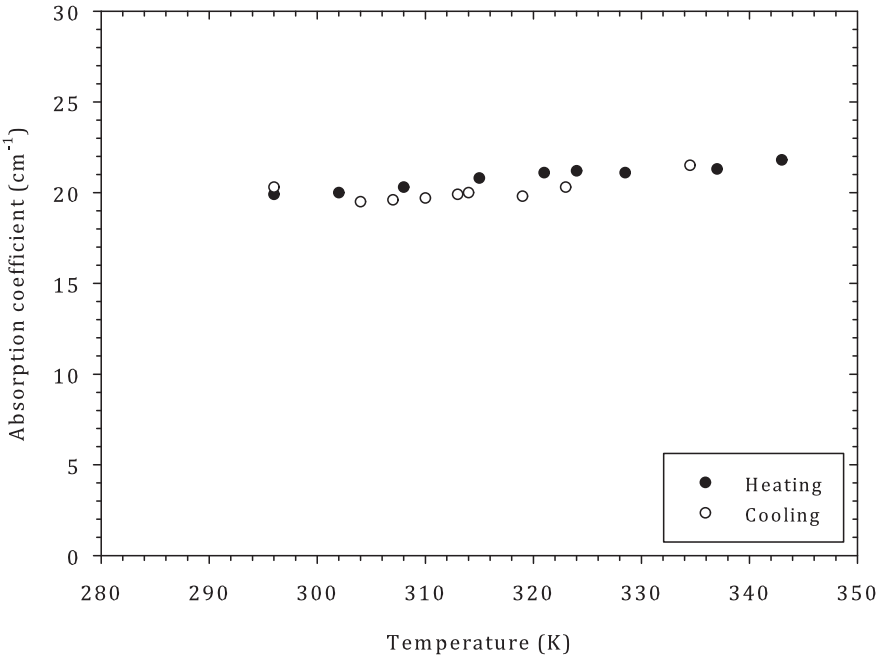

FIGURE 4.31: The absorption coefficient of PP as a function of temperature for both the heating and cooling cycle for a wavelength of 10.59μm. The room temperature result for the cooling cycle was taken after the equipment was allowed to cool completely.

From figure 4.31 it is clear that the absorption coefficient of PP did not change appreciably with temperature over the range measured at a wavelength of 10.59μm. Some change was observed on the cooling cycle, as with PI. This may have been due to slight changes in the polymer orientation to the instrument. During the heating cycle it was noted that the material softened (unlike PI) and there was a small degree of movement of the polymer surface. This may have resulted in a change in the amount of light reaching the detector in the FTIR instrument, causing an apparent change in absorption in the material. In this case, more light reaching the detector would have resulted in the apparent decrease in the absorption coefficient. Additionally, the reflectance of the surface would change if the orientation of the material to the beam was altered. The water absorption

of PP over a 24 hour period is 0.03% by weight [80] and is sufficiently small to discount the possibility of water evaporation and re-absorption being the cause of the hysteresis.

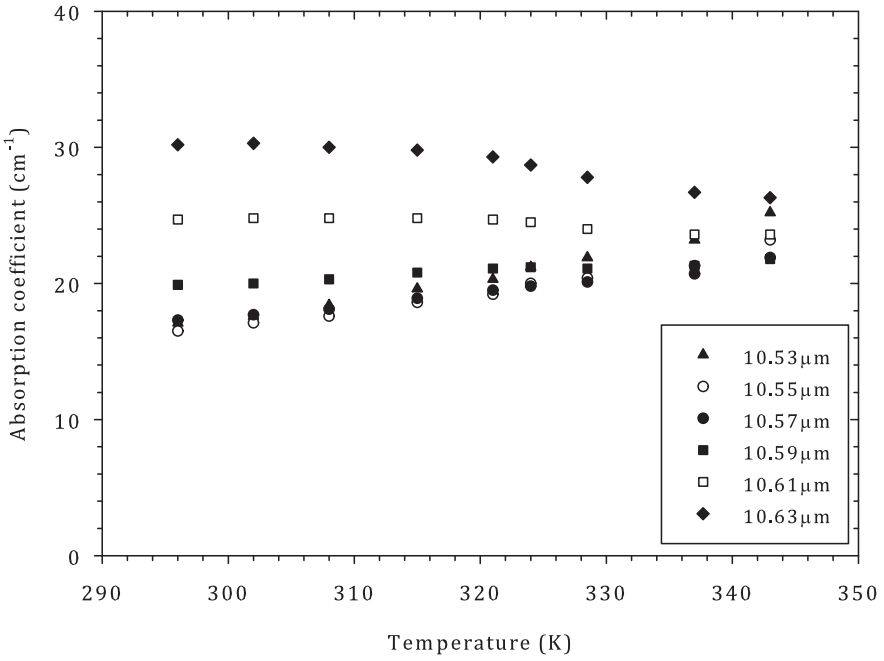

FIGURE 4.32: The absorption coefficient of PP as a function of temperature for the laser operating wavelengths for the heating cycle only. The laser wavelengths are indicated in the legend on the graph.

From figure 4.32 the relationship between the absorption coefficient and temperature clearly changed with wavelength for PP. This differed from the other materials as, although the initial absorption coefficients were different for each wavelength, the trend was consistent in terms of the % change in absorption coefficient with increasing temperature for all the other materials. For PP however, the absorption coefficient reduced as a function of temperature for wavelengths of 10.61µm and 10.63µm. As described before, the change at a wavelength of 10.59µm was

not significant. The absorption coefficient was seen to increase with increasing polymer temperature for wavelengths of 10.53μm and 10.55μm.

4.6 Time resolved polymer transmission of a laser pulse

To further understand the optical absorption and transmission characteristics of the polymers in the wavelength range of interest, an experiment was performed to determine the effective absorption coefficient of each polymer as a function of time during a laser pulse. A schematic of the experimental set-up is shown in figure 4.33.

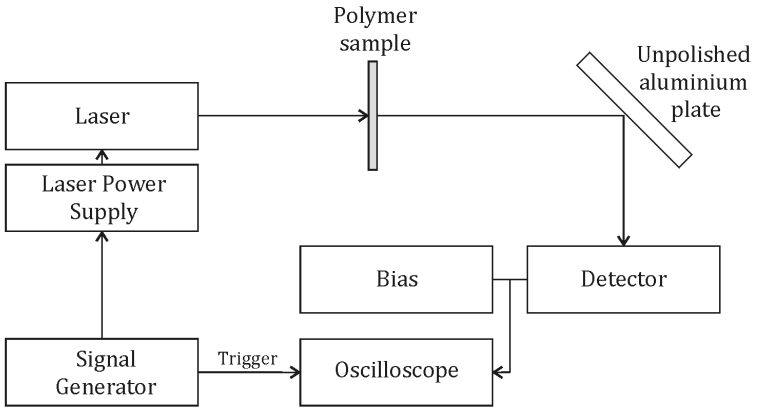

FIGURE 4.33: Schematic of the experimental set-up used to determine the time resolved transmission of the polymers. The Ge:Au detector was used in the same manner as that described in chapter 2 (figure 3.2). The polymer sample was placed in the path of the beam in front of the aluminium plate.

The experimental set-up is essentially the same as that described in figure 3.2 in Chapter 3 and the experiment was performed in the same way. Initially, the laser

pulse shape was recorded without the polymer sample in place (using the setup shown in figure 3.2). The laser repetition rate was approximately 2Hz and the TTL signal duration was 200μs (meaning a laser pulse duration of 189μs from the calibration described in chapter 2). The oscilloscope was set to average the Ge:Au detector signal (32 averages) in order to obtain an accurate representation of the pulse shape that would be incident on the sample. The laser pulse shape was checked between each new polymer sample to ensure the shape did not change significantly. The fluence was approximately $0.3 J/cm^2$

The polymer sample was then placed in the path of the beam, in front of the aluminium plate, as shown in figure 4.33. No visible damage to the polymers occurred during the experiment. This was confirmed by optical microscopy which showed no change to the irradiated region. Again, averaging was used to obtain an average transmitted signal (32 averages were used as before). Figures 4.34, 4.35, 4.36 and 4.37 show the results for PI, PEEK, PET and PP respectively. The detector signal of the laser pulse shape as a function of time is shown, both before (labelled 'Laser' on the graph) and after the sample was placed in the beam path. The thickness of the polymers was 75μm.

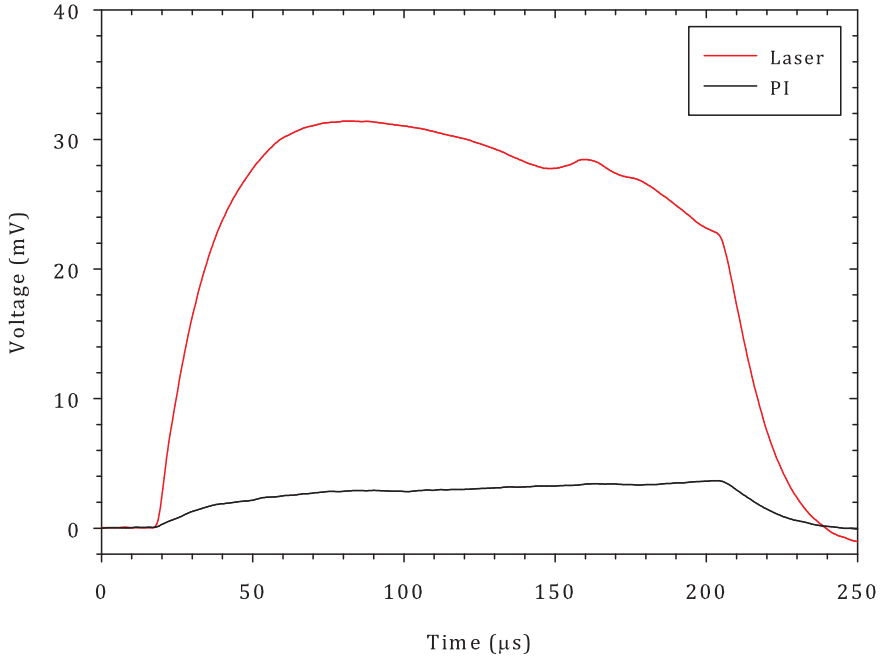

FIGURE 4.34: Ge:Au detector signal as a function of time for an average laser pulse with and without the PI sample (labelled 'PI' and 'Laser' respectively). The PI thickness was 75μm. Both results were taken with 32 averages on the oscilloscope.

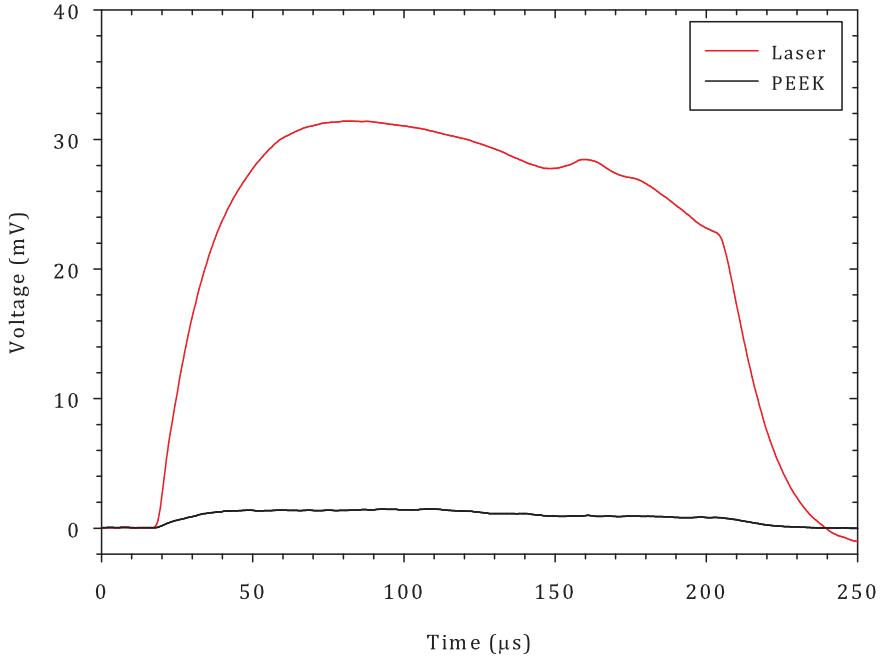

FIGURE 4.35: Ge:Au detector signal as a function of time for an average laser pulse with and without the PEEK sample (labelled 'PEEK' and 'Laser' respectively). The PEEK thickness was 75μm. Both results were taken with 32 averages on the oscilloscope.

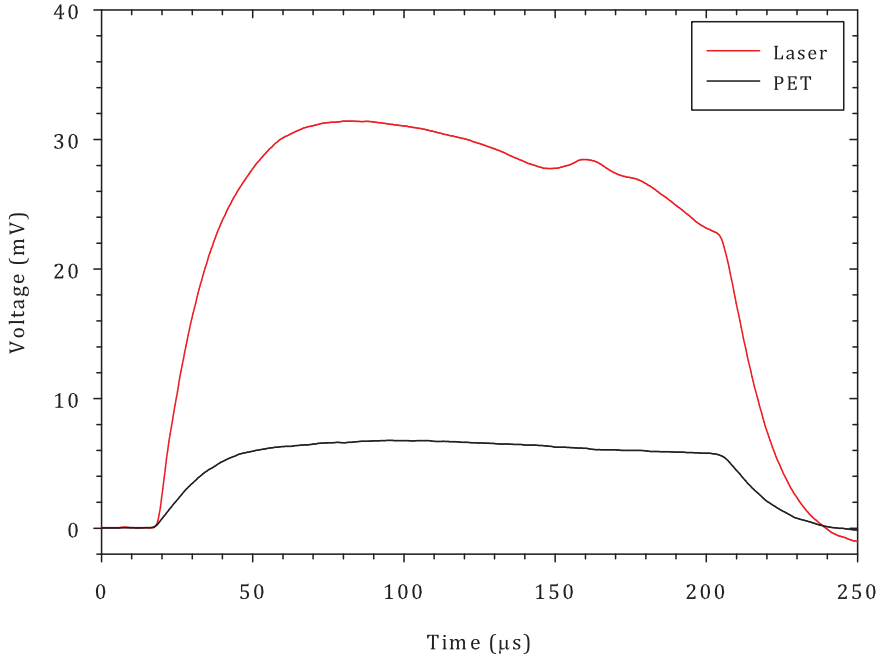

FIGURE 4.36: Ge:Au detector signal as a function of time for an average laser pulse with and without the PET sample (labelled 'PET' and 'Laser' respectively). The PET thickness was 75μm. Both results were taken with 32 averages on the oscilloscope.

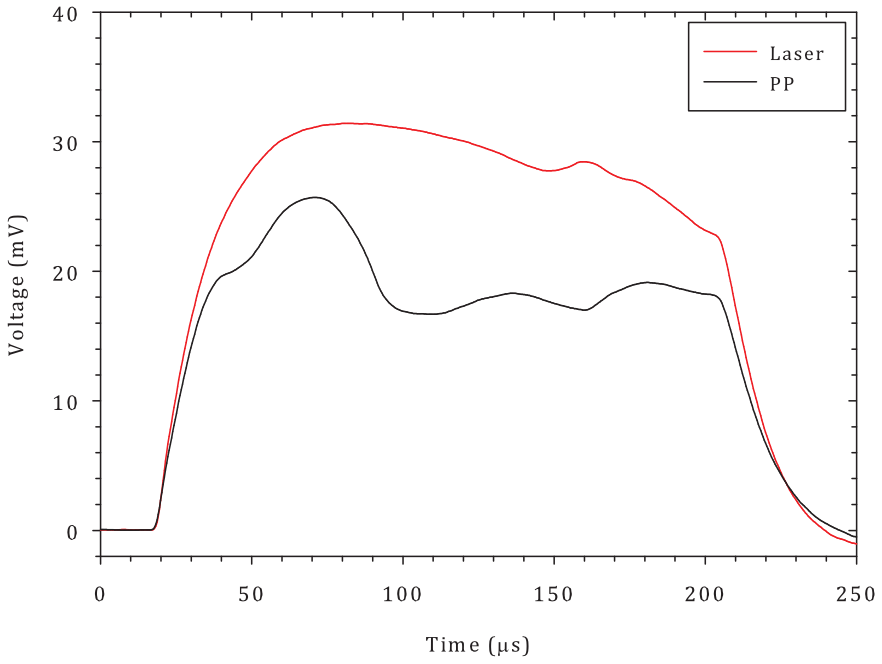

FIGURE 4.37: Ge:Au detector signal as a function of time for an average laser pulse with and without the PP sample (labelled 'PP' and 'Laser' respectively). The PP thickness was 75µm. Both results were taken with 32 averages on the oscilloscope.

The transmission was calculated by dividing the polymer signal by the laser signal. This was used to calculate the apparent absorption coefficient as a function of time during the laser pulse for each polymer. The reflectivity of the polymers was the same as that discussed earlier in this chapter and the results were corrected for this. The various effects of the laser interaction with the polymer during the laser pulse become important at this point, as some of the results from previous sections can be brought together. Changes in the absorption coefficient of the polymers observed in this experiment could be a result of:

- Chemical changes in the material due to the laser irradiation.

- Changes in the shape or deformation in the polymer due to heating. This is particularly relevant for polymers with a low melting or softening point, such as PET and PP.

- Laser heating causing the absorption coefficient of a polymer to shift due to relationships measured earlier in this chapter.

- Hopping of the laser wavelength during the pulse resulting in changes in the the absorption.

The possibility of changes in the material chemistry was rejected and was not considered in this case as no permanent alteration of the samples was observed. Changes in the shape of the polymers due to heat deformation were not quantified but were observed during the laser pulse for irradiation of PET and PP. This will be discussed in more detail later.

The laser wavelength and change in optical absorption coefficient as a function of temperature have been measured experimentally. Therefore, on the following graphs, the absorption coefficient at room temperature of each polymer was plotted for all the laser wavelengths that had been observed (see table 4.1). The temperature dependence of the absorption coefficient was also included. To avoid complicating the figures, only the maximum and minimum absorption coefficient for all observed laser wavelengths and temperatures within the measured range were plotted in the figure for each polymer. The range is indicated by the arrow on the right of the graph.

The results for the apparent absorption coefficient of PI, PEEK, PET and PP determined from laser light transmission are shown in figures 4.38, 4.39, 4.40 and 4.41 respectively. Also shown is the laser pulse shape which was scaled to indicate the time frame of the signal, but does not correspond to the units on the y-axis.

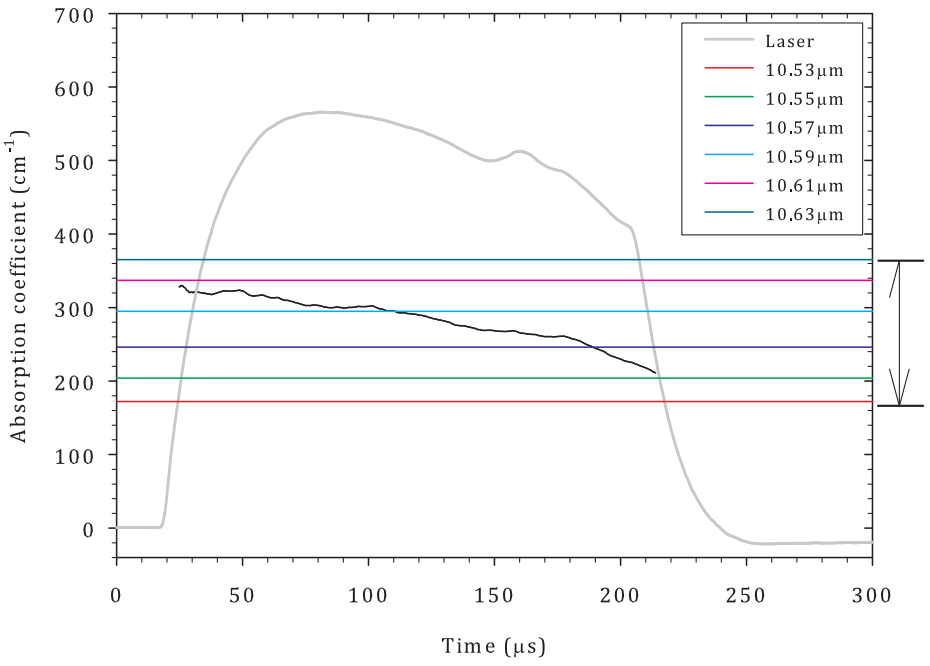

FIGURE 4.38: Absorption coefficient of PI as a function of time, calculated from the transmission of a 189µs laser pulse. The wavelengths corresponding to the absorption coefficients of PI measured by FTIR earlier in the chapter are also shown. The maximum absorption coefficient (365cm^{-1}) occurred at a wavelength of 10.63µm and a polymer temperature of 297K. The minimum absorption coefficient (162cm^{-1}) occurred at a wavelength of 10.53µm and a polymer temperature of 523K. The laser pulse shape shown was scaled to give a representation of the time frame of the results but does not correspond to the y-axis.

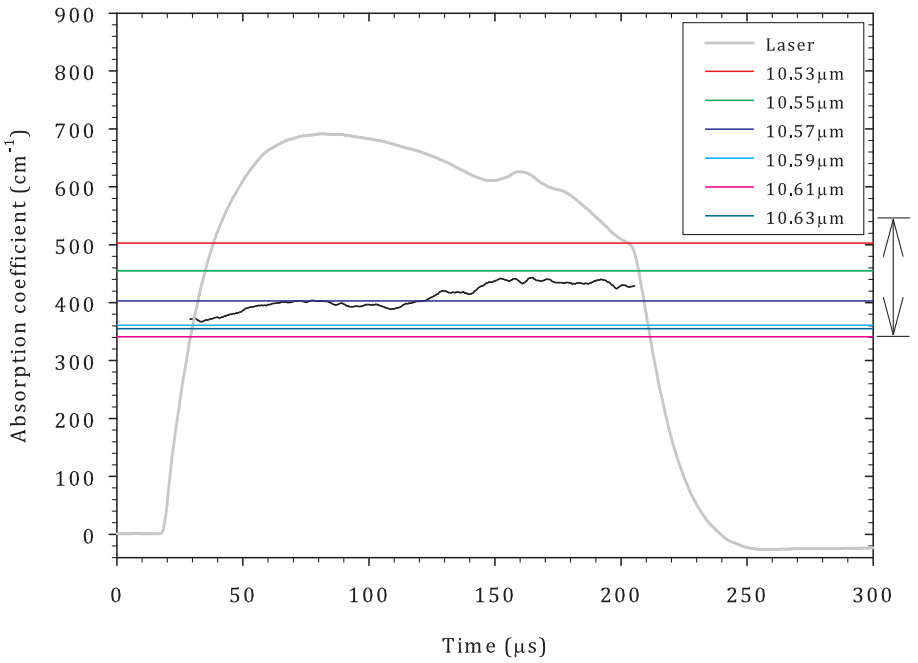

FIGURE 4.39: Absorption coefficient of PEEK as a function of time, calculated from the transmission of a 189µs laser pulse. The wavelengths corresponding to the absorption coefficients of PEEK measured by FTIR earlier in the chapter are also shown. The maximum absorption coefficient (546cm^{-1}) occurred at a wavelength of 10.53µm and a polymer temperature of 367K. The minimum absorption (341cm^{-1}) coefficient occurred at a wavelength of 10.61µm and a polymer temperature of 297K. The laser pulse shape shown was scaled to give a representation of the time frame of the results but does not correspond to the y-axis.

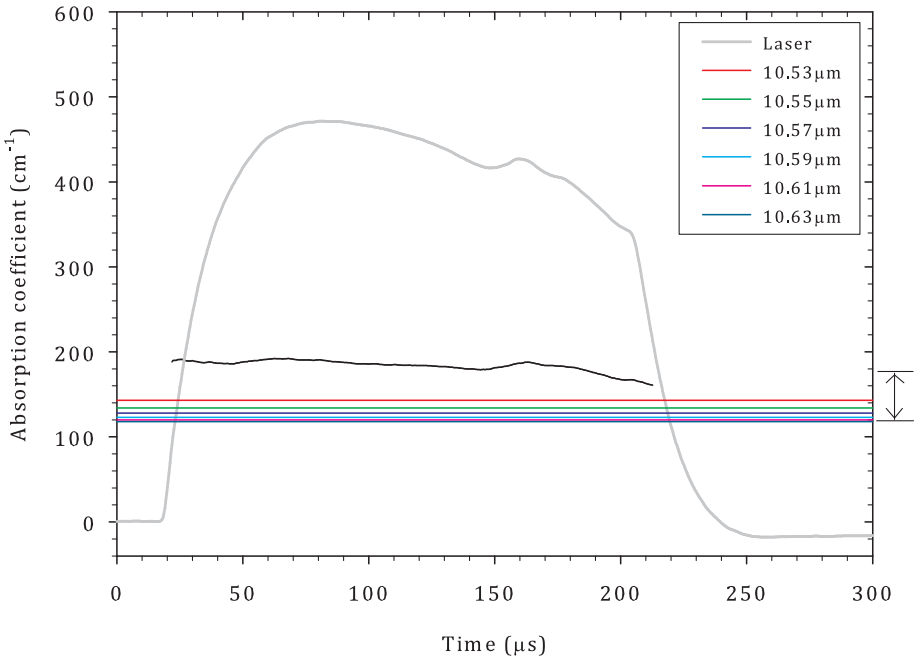

FIGURE 4.40: Absorption coefficient of PET as a function of time, calculated from the transmission of a 189µs laser pulse. The wavelengths corresponding to the absorption coefficients of PET measured by FTIR earlier in the chapter are also shown. The maximum absorption coefficient (177cm^{-1}) occurred at a wavelength of 10.53µm and a polymer temperature of 345K. The minimum absorption coefficient (118cm^{-1}) occurred at a wavelength of 10.63µm and a polymer temperature of 296K. The laser pulse shape shown was scaled to give a representation of the time frame of the results but does not correspond to the y-axis.

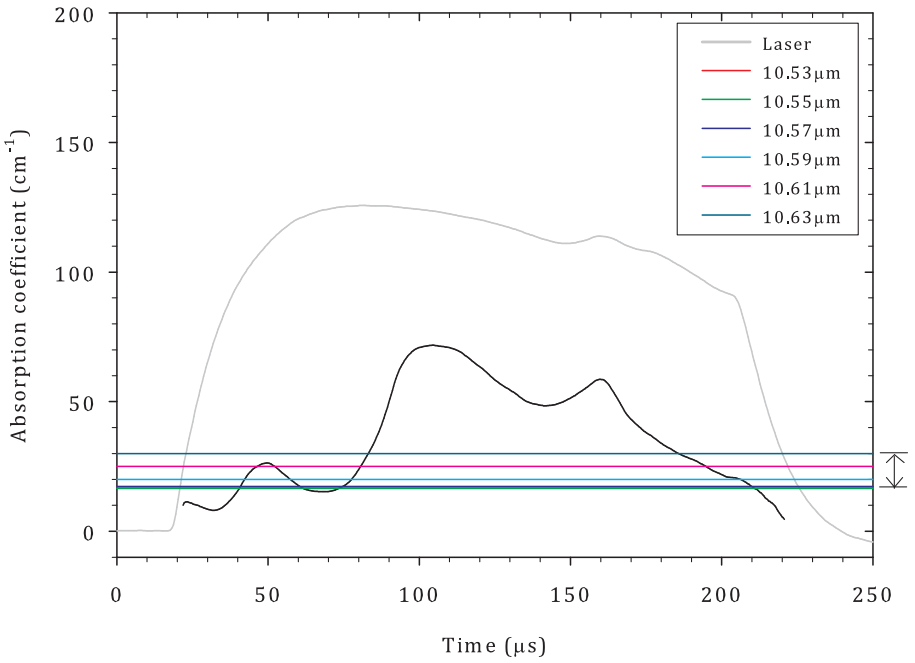

FIGURE 4.41: Absorption coefficient of PP as a function of time, calculated from the transmission of a 189µs laser pulse. The wavelengths corresponding to the absorption coefficients of PP measured by FTIR earlier in the chapter are also shown. The maximum absorption coefficient ($30cm^{-1}$) occurred at a wavelength of 10.63µm and a polymer temperature of 302K. The minimum absorption coefficient ($17cm^{-1}$) occurred at a wavelength of 10.55µm and a polymer temperature of 296K. The laser pulse shape shown was scaled to give a representation of the time frame of the results but does not correspond to the y-axis on the graph. It should be noted that the lines corresponding to absorption coefficients at wavelengths of 10.53µm , 10.55µm and 10.57µm are not distinguishable on the graph, all having a value of approximately $17cm^{-1}$, but all three are plotted.

The results for PI in figure 4.38 indicate that the laser was operating within the wavelength range of 10.53–10.63µm, as expected. It is important to note that the detector showed the same decrease in signal as the irradiation proceeded (as described in chapter 3). It is possible that this fall in signal, due to heating of the detector, resulted in a change in the apparent absorption coefficient. Additionally, when the PI sample was in the path of the laser beam, the laser light transmitted was reduced due to absorption. This would have resulted in less laser heating of the

detector and therefore less reduction in signal. It is clear from figure 4.34 that the results with the PI sample in the beam path did not show the same drop in voltage after the laser pulse ceased as with the free-space laser pulse. The voltage of the laser pulse signal shown in figure 4.34 was seen to decrease by approximately 1mV after the laser pulse ceased, compared to the initial detector voltage before the laser pulse began. If this voltage was corrected for in the calculated transmission, the result would be a decrease in the apparent absorption coefficient at the end of the pulse.

The results in figure 4.39 also indicate that the laser was operating in the wavelength range of 10.53–10.63μm when compared to the results shown in figure 4.14 of the absorption coefficient as a function of wavelength.

Unlike PI and PEEK, the absorption coefficient of PET did not indicate that the laser was operating in the wavelength range measured previously. The difference in the absorption coefficient from the range expected from figure 4.14 was attributed to a number of possible effects during irradiation by the laser. The absorption coefficient (approximately 180–190cm^{-1}) indicates a laser wavelength of 10.47μm from the room temperature FTIR results shown in 4.25. Figure 3.13 in the previous chapter shows that this wavelength occurs in the 001–100 transition in the P branch, as with the other laser wavelengths measured in Chapter 3. It is possible that the laser was operating at this wavelength for the duration of the experiment, though this was unlikely based on the time resolved wavelength measurements.

Another possibility is that some heating of the polymer occurred during the experiment which acted to increase the absorption coefficient, as was seen for all laser

wavelengths in figure 4.28. However, in order to increase the absorption coefficient to the level seen in figure 4.40, the polymer would require heating almost to the melting point, which obviously did not occur as no damage was observed. At an elevated polymer temperature of 345K the maximum absorption coefficient measured in this work was 177cm^{-1} and occurred at 10.53μm. This was not sufficiently high to explain the effect observed.

The effect thought to best explain the rise in absorption coefficient was deformation of the sample during the laser pulse due to a laser induced temperature rise (but below the melting point of the material). Deformation of the sample would lead to changes in the reflection properties of the sample if the beam was no longer at normal incidence to the surface. However, at close to normal incidence, the reflectivity is not a strong function of the incident angle. Another effect which could explain the behaviour is refraction through the distorted surface. This could lead to changes in the laser light reaching the detector and would appear as a change in the absorption coefficient, as was observed here. This is consistent with the classification of PET as a thermoplastic, which can deform upon heating. It is likely that the higher softening or melting point of PEEK compared to PET meant this effect was not observed for that particular material.

The apparent absorption coefficient of PP demonstrated that the laser was not operating in the range measured in the previous chapter. In order to reach the maximum absorption coefficient shown in figure 4.41 of approximately 70cm^{-1}, the laser would need to be operating at a wavelength of 10.35μm (extended data from figure 4.14). There was little evidence for this explanation and considering

the relative gain of the laser lines shown in figure 3.13, it was unlikely that the wavelength had shifted to the R branch in the 011–100 transition, as this had not been observed experimentally in the previous chapter. Again, the possibility of some heat rise causing the absorption coefficient to change was considered. However, the results shown in figure 4.13 and the maximum absorption coefficient indicated in figure 4.41 implied that this was not the case as the temperature would have to exceed the melting point of the polymer. The behaviour was therefore attributed to deformation of the material during the laser pulse, as with PET.

The thermal deformation of the polymers was limited somewhat during the temperature dependent FTIR measurements as the polymer samples were clamped tightly in the heating rig. In the laser transmission experiment the polymers were free-standing on a simple frame.

4.7 Discussion and conclusion

In this chapter, the thermal properties of the polymers PI, PEEK, PET and PP have been investigated using TGA. The infra-red optical coupling to the materials has also been studied, both at room temperature and as a function of temperature using FTIR. The transmission of the laser beam through each polymer was used to determine the apparent absorption coefficient for conditions which better represent those typically used experimentally. The wavelength measurements made in the previous chapter and the temperature dependent absorption coefficients were used to explain the effects observed.

TGA was used to determine the decomposition temperature of each of the polymers in air to inform both further experiments, where heating of the polymers was required, and modelling which will be discussed later. The temperatures of the maximum rate of material loss were determined by calculating the rate of change of weight of the sample as a function of temperature. The results obtained here agreed favourably with those found in the literature and discrepancies could be explained by the differing experimental conditions and the manufacturer source of the materials, as well as a small calibration offset which may have been present. To summarise, the decomposition temperatures of PI, PEEK, PET and PP were found to be 880K, 875K, 725K and 620K respectively.

The absorption coefficient of the polymers has been determined at room temperature. These were found to be 295cm^{-1}, 361cm^{-1}, 123cm^{-1} and 20cm^{-1} for PI, PEEK, PET and PP respectively for a laser wavelength of 10.59µm. This corresponds to an optical absorption depth of approximately 34µm for PI, 28µm for PEEK, 81µm for PET and 500µm for PP. The absorption coefficient was found to be dependent on the wavelength of the laser and using the wavelength range measured in Chapter 3 of 10.53–10.63µm the absorption coefficients of PI, PEEK, PET and PP were in the range 172–365cm^{-1}, 355–503cm^{-1}, 118–143cm^{-1} and 17–30cm^{-1} respectively. This leads to optical absorption depths within the ranges 27–53µm (PI), 20–28µm (PEEK), 53–70µm (PET) and 333–589µm (PP).

In order to determine if there was a relationship between optical coupling and the temperature of the polymers, the absorption coefficient has been measured as a function of temperature using a heated sample holder. The measurements were

made for both the heating and cooling cycles to determine whether the relationship observed was reversible. It was found that the temperature had a significant effect on the absorption coefficient at some of the laser wavelengths measured in Chapter 3. The following table summarises the results. The gradient of the absorption coefficient as a function of temperature for each polymer was calculated. This allows direct comparison of the temperature response of the polymers. Gradients were taken for all data in the temperature ranges.

TABLE 4.2: Change in absorption coefficient of PI with polymer temperature as a function of wavelength.

Wavelength (μm)	$d\alpha/dT$ ($cm^{-1}K^{-1}$)			
	PI	PEEK	PET	PP
10.53	-0.02	0.61	0.62	0.17
10.55	-0.13	0.76	0.58	0.14
10.57	-0.27	0.83	0.53	0.09
10.59	-0.40	0.86	0.48	0.04
10.61	-0.47	0.83	0.42	-0.03
10.63	-0.42	0.76	0.36	-0.09

The change in absorption coefficient with temperature measured for all the polymers was similar to the behaviour reported by Dyer et al [8]. In the paper, the absorption coefficient of Upilex polyimide was determined as a function of temperature using the transmission of laser light at wavelengths of 9.21μm and 10.3μm. The effect was attributed to an anharmonic effect which resulted in the broadening and red-shifting of absorption peaks when the system was driven by the laser field

as well as the temperature of the environment. In this thesis, the work presented in reference [8] was built upon by measuring the change in absorption coefficient over the entire range of relevant laser wavelengths. All the polymers demonstrated broadening of the absorption peaks in the proximity of the laser wavelengths of interest (see figures 4.17, 4.21, 4.25 and 4.29), with some degree of red-shift also noted for PI, PEEK and PET. This resulted in a range of values for the change in absorption coefficient with temperature for each polymer, depending on the position of the laser emission lines on the absorption peaks.

At room temperature, the absorption peak of PI in the region of interest occurred at a wavelength of 10.65μm. Over a temperature range of approximately 220K, this peak was seen to shift to a wavelength of 10.69μm. Some broadening of the peak also occurred. The overall effect at the laser wavelengths was a decrease in the absorption coefficient with increasing temperature. Due to the position of the laser emission lines on the edge of the peak, the effect was larger for some wavelengths than for others. Laser wavelengths of 10.53μm and 10.55μm showed the least effect and a wavelength of 10.61μm showed the most significant change, it being situated on the steep edge of the absorption peak. It is interesting to note that if the laser could be tuned to a wavelength of approximately 10.67μm (i.e the P28 rotational line in the 001 to 100 vibrational transition), no change in absorption coefficient would occur for the entire heating range (see figure 4.17).

For PEEK and PP absorption peaks were seen to occur at wavelengths of 10.50μm and 10.65μm respectively with the red-shift resulting in the peak of PEEK moving to 10.51μm. The effect was again dependent on the position of the laser emission

lines with respect to the peaks. The most significant change in absorption coefficient with increasing temperature was observed for PEEK at a wavelength of 10.59μm. If the laser could be tuned to a wavelength of 10.49μm (i.e the P10 rotational line in the 001 to 100 vibrational transition), no change in the absorption coefficient would result from heating the polymer.

The absorption peak of PET in the laser wavelength range of interest occurred at a wavelength of approximately 10.29μm with a small shoulder at 10.67μm. The large peak shifted to 10.31μm with an increase in temperature of approximately 57K and was seen to broaden with increasing temperature, as expected. This shift in the absorption peak resulted in a change in the absorption coefficient which was similar for all laser emission wavelengths.

When considering the results for all polymers at all wavelengths and temperatures shown in table 4.2, the polymer least effected by temperature and laser wavelength was PP. The polymer with the most dependence on these parameters was PEEK.

Finally in this chapter the time resolved transmission of the polymers was measured using a laser pulse of 189μs duration. This allowed the time dependent absorption coefficient to be inferred from the transmission. The results obtained for the absorption coefficient of PI and PEEK as a function of time during the laser pulse were consistent with the wavelength dependent absorption coefficients measured earlier within the laser wavelength range measured in Chapter 3. The results for these polymers strengthened the evidence for the wavelength hopping that was observed earlier in Chapter 3.

The results obtained for PET and PP, however, were inconsistent with the previous observations, leading to absorption coefficients which were higher than those expected from the FTIR results. The maximum and minimum possible absorption coefficients at all wavelengths and polymer temperatures were taken into consideration, to ascertain if the behaviour was due to heating by the laser, together with changes in wavelength. However, the range did not include the experimental results. Excluding wavelength and temperature dependent absorption coefficient effects as the only reason for the results, it was hypothesised that some physical deformation of these polymers had occurred during the laser pulse due to the thermoplastic nature of the materials. A small amount of heating resulting in the refraction properties of the polymer surfaces changing and leading to less laser light reaching the detector, would result in an apparent increase in the absorption coefficient. This argument fits with the classification of these polymers as thermoplastic. PEEK is also a thermoplastic but with a higher softening and melting temperature, meaning this effect was only seen for PET and PP.

Chapter 5

Laser-induced surface and volume changes in PI, PEEK, PET and PP

5.1 Introduction

In this chapter the interaction of single RF CO_2 laser pulses with the polymers PI, PEEK, PET and PP has been investigated. The literature review in Chapter 2 focussed on the mechanisms of ablation. Ablation was defined as material removal by high-intensity laser irradation, however a more relaxed view of this definition is used in this chapter. The term damage has been used to describe any irreversible change of the polymer surface which could be detected and measured by optical microscopy. This damage could have resulted from laser induced thermal decomposition or melting or indeed the ablation described in the literature review. The details of ablation are still applicable in terms of absorption and subsequent heating of the sample, but removal of material was not always the case.

A threshold fluence for damage of the polymers has been determined as a function of the laser pulse duration using the laser studied in Chapter 3. Initially, optical microscopy was used to measure the damage size. This data, along with the laser pulse energy, has been used to determine the threshold energy for damage and the laser spot size at the sample, resulting in a threshold fluence.

Scanning electron microscopy (SEM) has been employed to study changes in the surface of the polymers. A discussion of the specific morphology of the damage

sites has been left until the SEM section, as these images give more detail. White light interferometry (WLI) has been used to profile an irradiated region of PP as the smooth structures produced using the laser were ideal for this type of measurement and allowed the volume change of the polymer to be more accurately visualised.

5.2 Threshold fluence for laser-induced damage of PI, PEEK, PET and PP

The effect of the laser pulse duration on the threshold fluence for surface damage of the polymers was investigated using single pulses from the laser described in Chapter 3. Such a threshold fluence for polymers is most often derived from the etch depth per pulse (etch rate) as discussed in the literature review in Chapter 2 [8, 17]. In this work, the threshold fluence was defined as the fluence that must be exceeded to cause visible damage to the surface of a polymer.

5.2.1 Variation of damage diameter with fluence for a Gaussian beam

A Gaussian beam is defined by the following equation for the electric field ($\bar{E}$) as a function of radial distance, r.

$$\bar{E}(r) = \bar{E}_0 \, e^{-\frac{r^2}{{\omega_0}^2}} \tag{5.1}$$

In the equation, $\bar{E}(r)$ is the electric field at a given value of r. $\bar{E}_0$ is the maximum electric field. The laser spot size in terms of electric field is then ω_0. The irradiance of the beam is found from the time average of the Poynting vector and given by the following equation.

$$I = \frac{1}{2}\varepsilon_0 c\bar{E}^2_{max} \tag{5.2}$$

If equation 5.2 is substituted into equation 5.1, the Gaussian profile is now in terms of the laser irradiance, which has units of W/cm^2. If the beam is time averaged we can further simplify to the laser fluence, which has units of J/cm^2. The equation of a Gaussian beam in terms of fluence is therefore:

$$F(r) = F_0 e^{-2\frac{r^2}{{\omega_0}^2}} \tag{5.3}$$

Shown in figure 5.1 is a representation of a Gaussian distribution representing an idealised lowest order beam profile in terms of laser fluence.

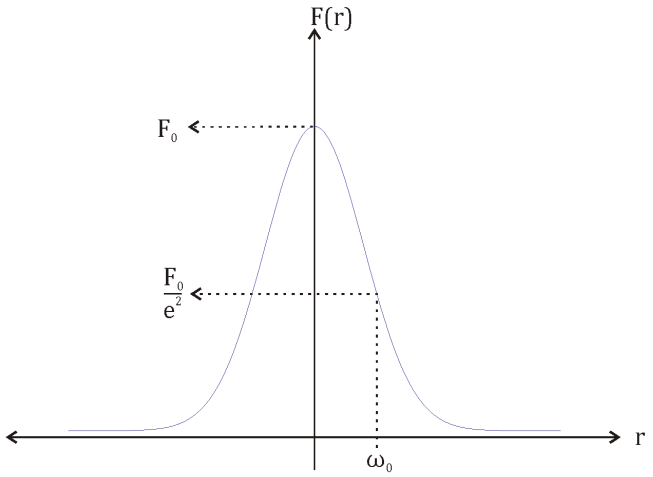

FIGURE 5.1: A Gaussian distribution cross-section representing an idealised lowest order beam profile from the laser. The laser fluence (F) is shown as a function of the radial distance (r).

F(r) is the fluence at a given value of r. F_0 is the maximum fluence. The laser spot radius in fluence is therefore ω_0 which represents the point at which the fluence is $\frac{1}{e^2}$ the initial value.

In order to determine the radial distance at which the threshold fluence for damage to a polymer (F_T) occurs, equation 5.3 is solved for r with $F(r)=F_T$ giving equation 5.4.

$$r^2 = \frac{1}{2}{\omega_0}^2 \ln \frac{F_0}{F_T} \tag{5.4}$$

Experimentally, it is easier to determine a diameter (d) rather than a radius. Therefore equation 5.4 becomes:

$$d^2 = 2{\omega_0}^2 \ln \frac{F_0}{F_T} \tag{5.5}$$

Equation 5.5 can therefore be expressed in terms of the threshold energy (E_T) and the pulse energy, E. The threshold energy can therefore be determined from plots of the polymer damage diameter squared as a function of the natural logarithm of the energy per pulse. It follows that the gradient is $2{\omega_0}^2$.

In cartesian coordinates, integration of equation 5.3 in 2D form will be the equivalent of the pulse energy. That is:

$$E = F_0 \iint_{-\infty}^{\infty} e^{\frac{x^2+y^2}{{\omega_0}^2}} dxdy = \frac{\pi {\omega_0}^2 F_0}{2} \tag{5.6}$$

Rearranging for fluence:

$$F_0 = \frac{2E}{\pi {\omega_0}^2} \tag{5.7}$$

Therefore, when the energy is equal to the threshold energy, that is, the intercept of a graph of damage diameter squared as a function of the natural logarithm of the pulse energy, the fluence in equation 5.7 is the threshold fluence. This is the fluence at which the damage diameter is 0.

The approach here is similar to that used in references [81–83]. In reference [81], a single-crystal silicon surface was irradiated with a Nd:YAG laser and the induced phase change was measured. The square of the damage radius was plotted as a function of the laser fluence on a log scale and used to determine the laser spot size and a threshold energy for changing the phase of the sample. In reference [82], the spot size of a TEA-CO_2 laser was measured by irradiating an aluminium

film deposited on a glass plate and measuring the area of removed material. The radius squared was plotted as a function of the natural logarithm of the energy and the spot size was extracted from the gradient, as with the work presented here. Similarly, the spot size of the CO_2 laser used in reference [83] was determined from the same data analysis method using laser induced damage sites on a high resolution holographic plate. The main difference between the method used in the references and that used here is the fact that the diameter is substituted for the radius.

A schematic of the experimental set-up used to determine the threshold fluence of the polymers as a function of laser pulse duration is shown in figure 5.2.

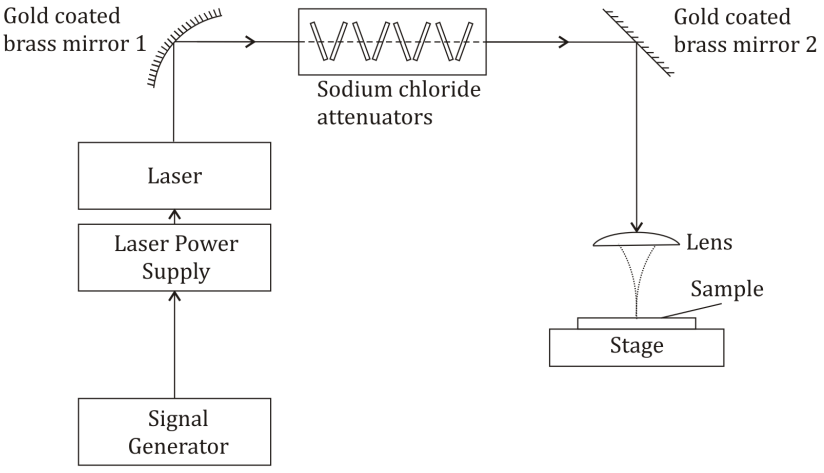

FIGURE 5.2: Schematic of the experimental set-up used to determine the threshold laser fluence for damage of the polymers as a function of laser pulse duration. The pulse energy of the laser was controlled by the NaCl attenuators. The laser light was focussed using a zinc selenide plano-convex lens with a focal length of 90mm. The sample was mounted on a frame (not shown in the figure) to avoid back surface effects that may occur from a support in the beam path. This was placed on the PC controlled motorised stage.

The laser repetition rate was 2Hz and the laser was left to run constantly during the experiment. The laser light was focussed using a zinc selenide (ZnSe) plano-convex

lens. The focal length of the lens was measured experimentally with the laser and was found to be 90mm. It was ensured that the laser beam went through the centre of the lens and that the lens was used in the optimum shape configuration (plane surface towards the focal point) to reduce aberrations.

The laser pulse duration was set, as has been described in chapter 3, with TTL pulses from the signal generator. The salt attenuators were used to control the average power and thus the energy per pulse for each pulse duration. The laser pulse duration and energy per pulse were determined using the calibration results in figures 3.6, 3.8 and 3.10. All pulse durations mentioned from this point are those corrected according to calibration.

The polymer sample being studied was placed a small distance beyond the focal point of the laser. Steps were taken to ensure the damage sites were as circular as possible. Two diameters were measured and an average taken. It was assumed that all the spots on the polymers were circular for all future calculations.

Single pulses were incident on each sample and between each pulse the motorized sample stage was used to move to a new site. This was achieved by running the laser at 2Hz and using a manually controlled shutter to allow single pulses through. It was ensured that the distance moved between sites on the sample was sufficiently large (between 1 and 2mm depending on the pulse duration and debris area) such that the new site was clear of debris from the previous interaction. In this way the initial sample surface remained constant. Experiments for each set of pulse durations and energies were performed multiple times to allow statistical analysis of the results. The diameter, d, of each damage site was measured using

an optical microscope (Leica DML microscope with Spot Advanced version 4.0.8 software).

The polymer samples were placed at a distance of approximately 95mm from the lens. This was adjusted where necessary to ensure the most circular damage sites, meaning the spot size was slightly different for each polymer. For PI, laser pulse durations in the ranges of 182–546μs and 71–189μs were used. For pulse durations of 71–189μs, the sample was moved slightly closer to the focal point as the laser fluence was not sufficient to damage the surface of the sample at the shorter pulse durations. It should be noted that there was some overlap of the data for the two sets of pulse durations. For PEEK, laser pulse durations of 95–378μs were used. The PEEK sample was positioned just beyond the focal point of the lens as this was found to yield the most circular damage sites. For PEEK it was particularly difficult to find the position in the focus which yielded the most circular damage sites. Laser pulse durations of 47–473μs were used to irradiate PET and PP was irradiated with pulses of 378–757μs duration.

Figures 5.3, 5.4, 5.5 and 5.6 show typical damage sites on the PI, PEEK and PET using 189μs duration laser pulses. PP damage site was made with a 378μs duration pulse. The images were taken with a total magnification of 100x. The samples were cleaned gently with isopropanol alcohol and a lens tissue before being measured. The sample thickness was 125μm, 75μm, 75μm and 300μm for PI, PEEK, PET and PP respectively.

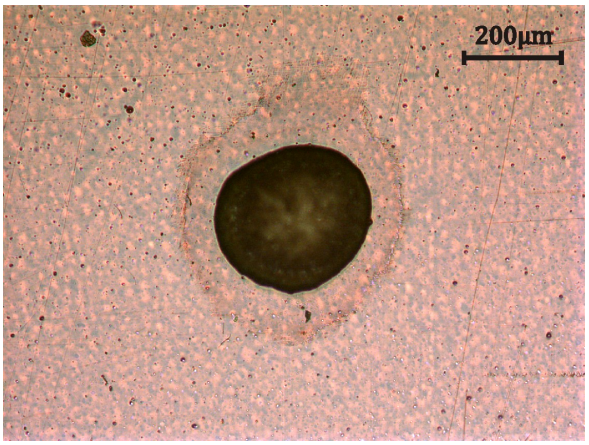

FIGURE 5.3: A typical damage site on a PI sample. The image was taken with 100x magnification and the laser pulse duration was 189µs.

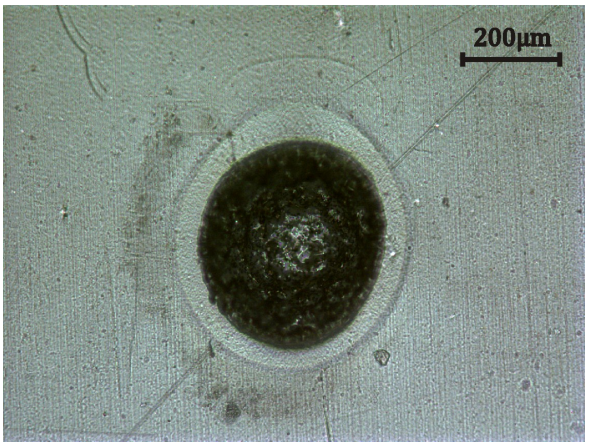

FIGURE 5.4: A typical damage site on a PEEK sample. The image was taken with 100x magnification and the laser pulse duration was 189µs.

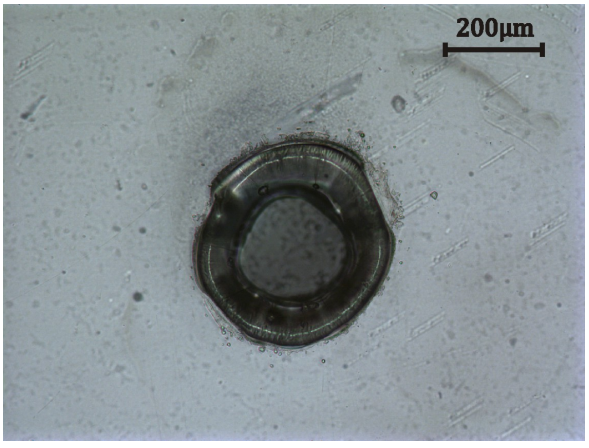

FIGURE 5.5: A typical damage site on a PET sample. The image was taken with 100x magnification and the laser pulse duration was 189µs.

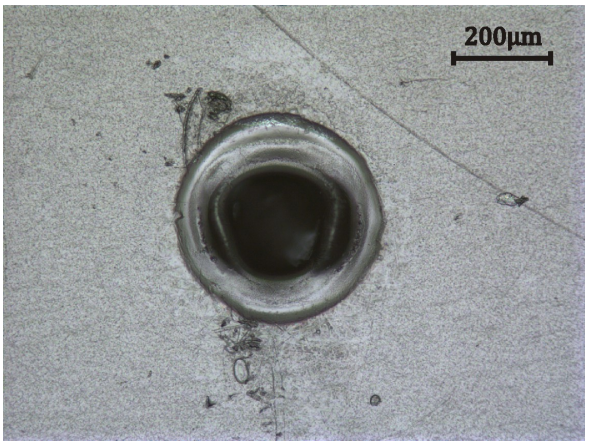

FIGURE 5.6: A typical damage site on a PET sample. The image was taken with 100x magnification and the laser pulse duration was 378µs.

The PI damage site was seen to be approximately circular with a well defined edge. The faint line around the damage site was debris remaining after cleaning. More vigorous cleaning removed this.

PEEK also demonstrated a well defined damage site. The region appeared to be decomposed rather than melted as there was no melt flow. A sub surface change to the PEEK was also observed. This can be seen as a ring around the main damage site shown in figure 5.4. Optical microscopy did not indicate whether this change was due to a refractive index change or a physical volume change. In reference [23], a CW CO_2 laser was used to irradiate PEEK samples at a range of sample feed-rates to control the intensity (or dose). The change in the amount of crystalline material was studied in the irradiated region. The PEEK samples in the paper were initially highly crystalline and the regions irradiated (but not decomposed) were shown to contain a larger amount of amorphous material. This could perhaps explain the behaviour seen here if the region which was not decomposed reached sufficient temperature to change the amount of crystalline material. Both PET

and PP showed melted regions around the edge of the damage sites. The edge of the melted region was well defined.

Figures 5.7 and 5.8 show the results for PI plotted as described earlier: d^2 as a function of the natural logarithm of the pulse energy. Figure 5.7 shows results for pulse durations in the range 71-189μs and figure 5.8 shows results for pulse durations between 182-546μs. The sample thickness was 125μm. Figures 5.9, 5.10 and 5.11 show the results for PEEK, PET and PP respectively. The pulse durations are indicated in the legends on each graph.

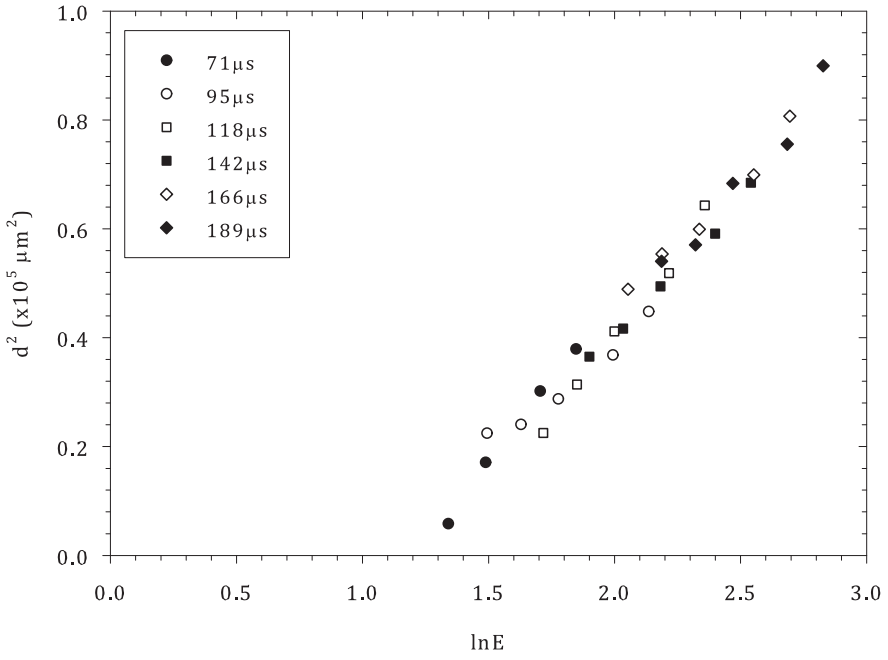

FIGURE 5.7: The diameter squared of the damage sites on PI as a function of the logarithm of the laser pulse energy for laser pulse durations ranging from 71μs to 189μs. The laser spot radius at the sample measured using this data was 161μm and the threshold energy using all the data was 3.3mJ.

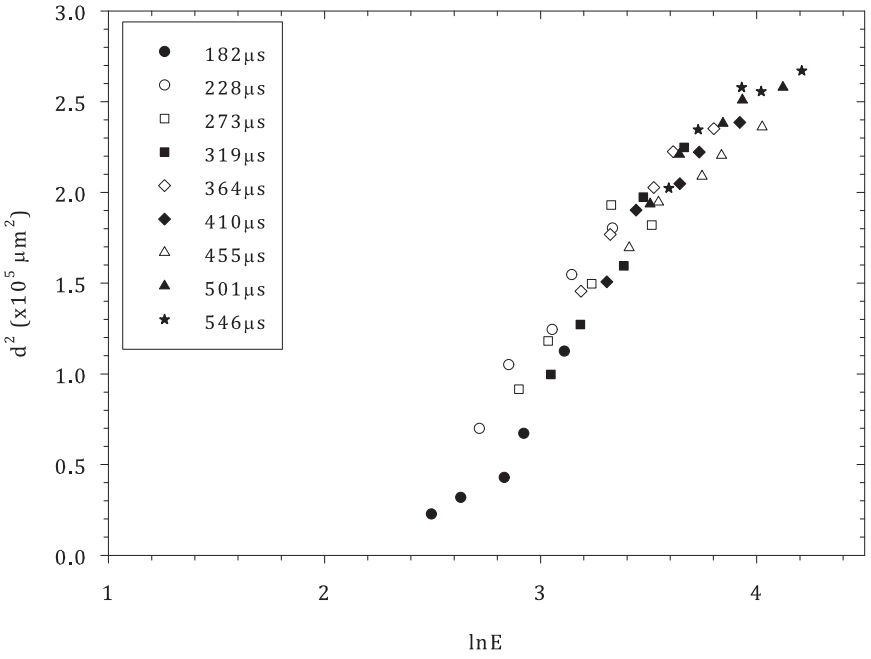

FIGURE 5.8: The diameter squared of the damage sites on PI as a function of the logarithm of the laser pulse energy for laser pulse durations ranging from 182µs to 546µs. The laser spot radius at the sample measured using this data was 275µm and the threshold energy using all the data was 9.8mJ.

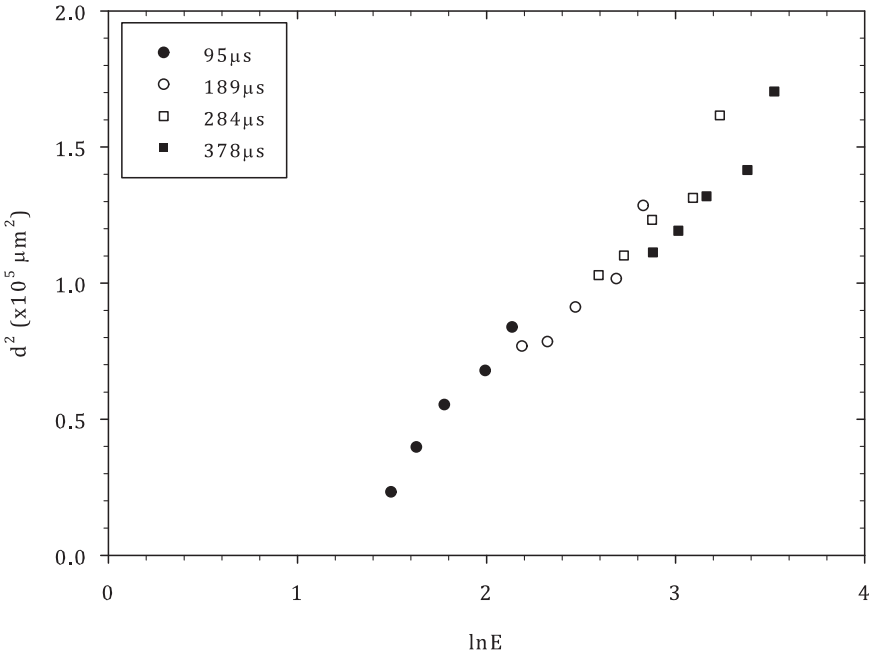

FIGURE 5.9: The diameter squared of the damage sites on PEEK as a function of the logarithm of the laser pulse energy for laser pulse durations ranging from 95µs to 378µs. The laser spot radius at the sample measured using this data was 179µm and the threshold energy using all the data was 2.7mJ.

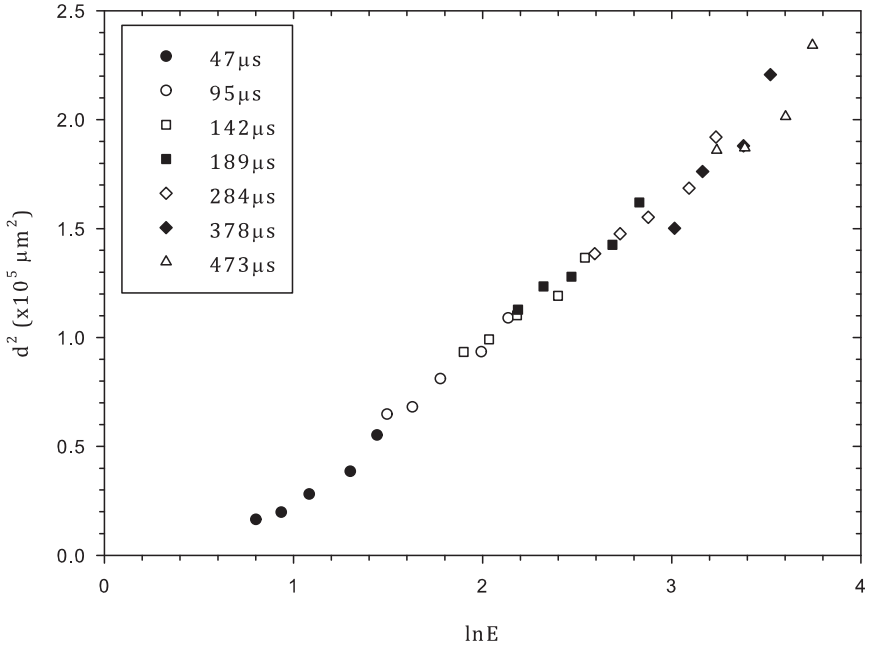

FIGURE 5.10: The diameter squared of the damage sites on PET as a function of the logarithm of the laser pulse energy for laser pulse durations ranging from 47µs to 473µs. The laser spot radius at the sample measured using this data was 189µm and the threshold energy using all the data was 1.9mJ.

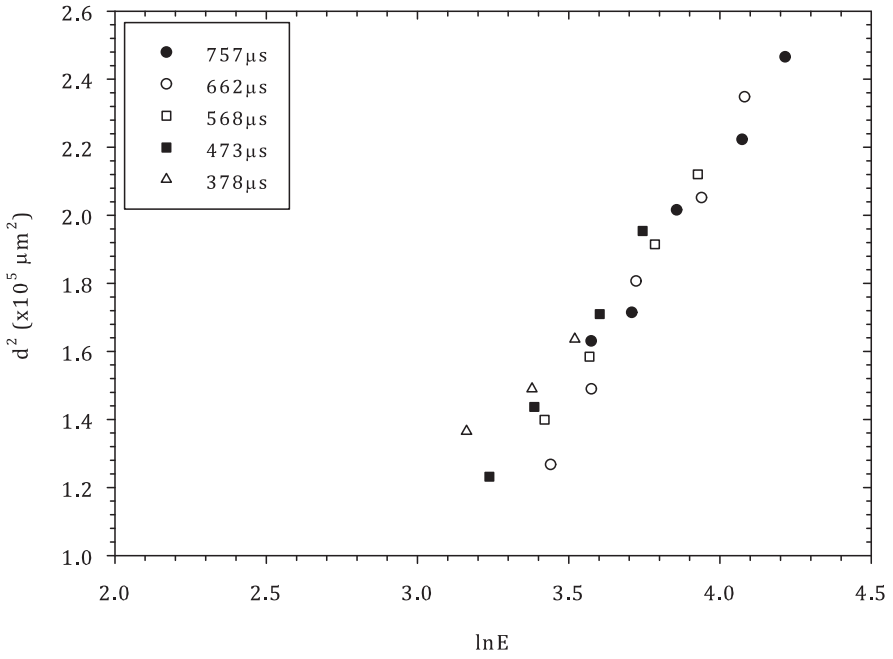

FIGURE 5.11: The diameter squared of the damage sites on PP as a function of the logarithm of the laser pulse energy for laser pulse durations ranging from 378µs to 757µs. The laser spot radius at the sample measured using this data was 237µm and the threshold energy using all the data was 8.5mJ.

The graphs show that the laser spot radius was constant for each set of data. For a constant lens to sample distance, this was expected. Also, there was a common threshold energy for each polymer irrespective of laser pulse duration.

For PI, laser spot radii of 161µm and 275µm were determined from the gradients of the graphs shown in figures 5.7 and 5.8. Threshold energies of 3.3mJ and 9.8mJ were determined from the intercepts of the graphs shown in figures 5.7 and 5.8 respectively. Using equation 5.7, the average threshold fluence was calculated as 8.1J/cm^2 for pulse durations between 71µs and 189µs and 8.2J/cm^2 for pulse durations between 182µs and 546µs.

A laser spot radius at the sample of 179μm was found for PEEK. The threshold energy was 2.7mJ. Using equation 5.7, the average threshold fluence for pulse durations between 95μs and 378μs was found to be 5.36J/cm^2. It should be noted at this point that for PEEK irradiated with laser pulse energies of 33.8mJ, 29.4mJ and 24.4mJ (that it, a laser pulse duration of 378μs with 0 and 2 attenuators and 284μs with 0 attenuators) there was a hole at the back of the material. It was decided that this would have little effect on the threshold fluence results as the measurement of the diameter was taken from the edge of the damaged site on the surface of the material and the threshold energy results were extrapolated to the point at which damage only just occurs. It was also noted that in figure 5.9, the energies at which a hole was present did not appear to affect the gradient of the graph.

The laser spot radius at the PET sample was found to be 189μm and the threshold energy was 1.9mJ. The average threshold fluence for pulse durations between 47μs and 473μs was therefore 3.39J/cm^2. All of the laser irradiated sites on PET showed holes such as that shown in figure 5.5. In the same way as for PEEK, the damage beyond the hole was measured for figure 5.10.

A laser spot radius at the PP sample surface of 237μm was found together with a threshold energy of 8.5mJ. The average threshold fluence for pulse durations between 378μs and 757μs was therefore found to be 9.58J/cm^2. It was not possible to damage the PP samples in a way that could be accurately measured at laser pulse durations shorter than 378μs. The reason for this was most likely due to the very small absorption coefficient resulting in a higher laser fluence being required.

It was not possible to position the polymer sample closer the focal point (thus increasing the laser fluence above the damage threshold) as the spots became messy, non-circular and difficult to measure.

It might be expected that due to heat flow out of the irradiated area during the pulse, more energy would be needed to cause damage if the pulse duration were to be increased while the energy was kept constant. This is, of course, assuming that the damage is thermal in origin (this will be explored in depth later). However the results indicated that the threshold energy, and therefore threshold fluence, were independent of the pulse duration for all values between 70µs and 550µs. In order to demonstrate this further, the threshold fluence for each individual pulse duration was calculated with a fixed laser spot size. The results for PI, PEEK, PET and PP are shown in figures 5.12, 5.13, 5.14 and 5.15.

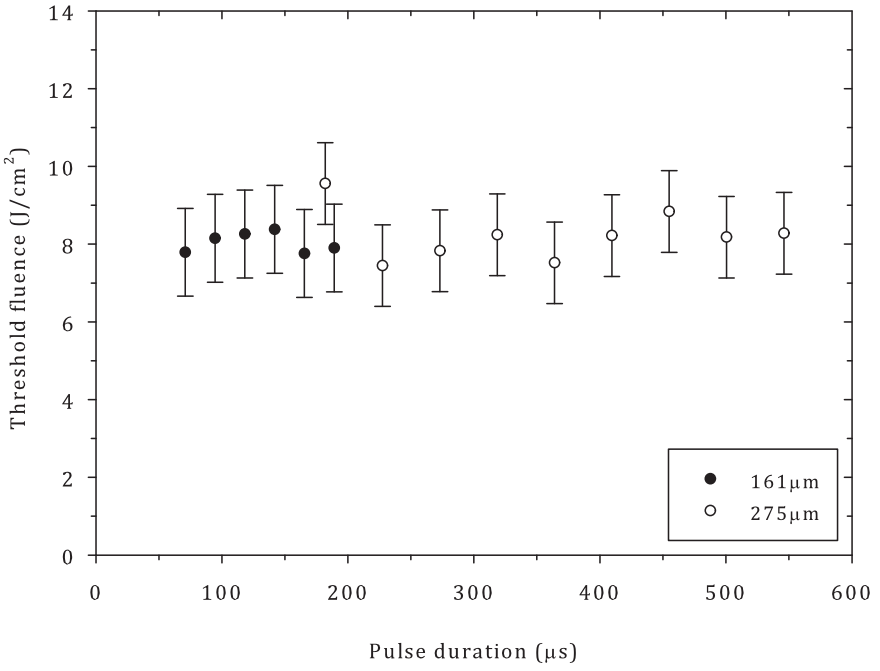

FIGURE 5.12: The threshold fluence of PI as a function laser pulse duration with fixed laser spot sizes of 161µm and 275µm as indicated in the legend.

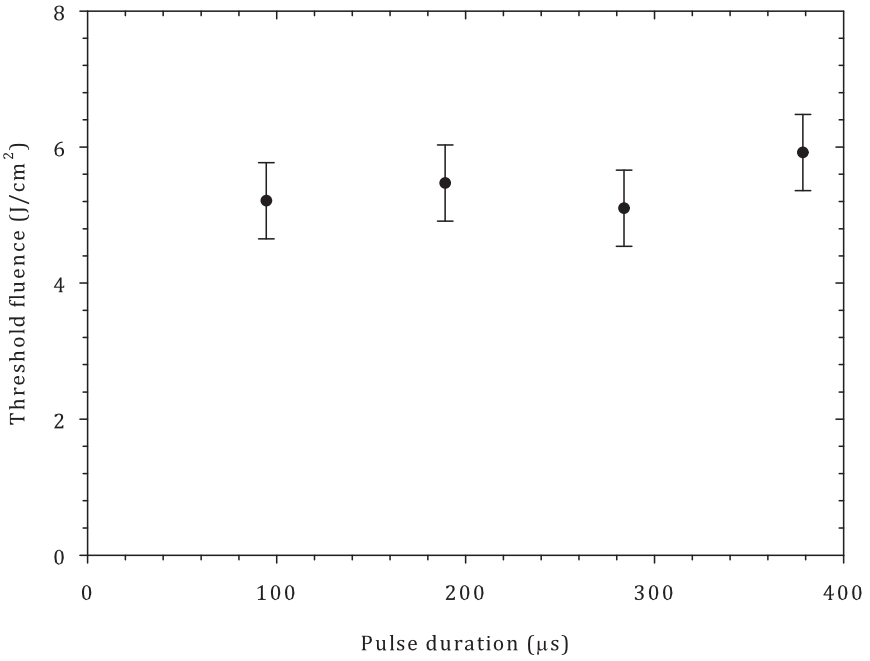

FIGURE 5.13: The threshold fluence of PEEK as a function laser pulse duration with a fixed laser spot radius of 179μm.

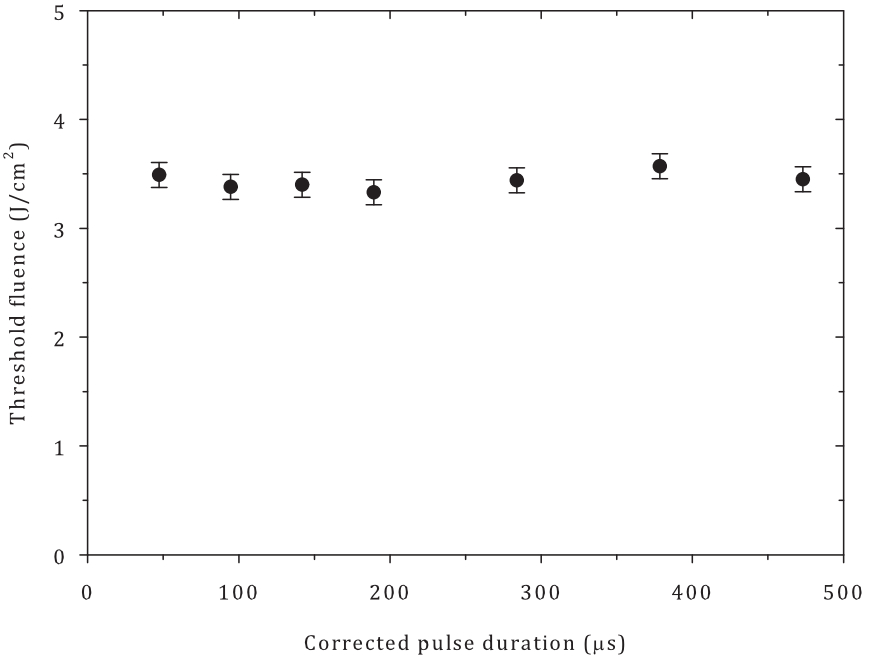

FIGURE 5.14: The threshold fluence of PET as a function laser pulse duration with a fixed laser spot radius of 189μm.

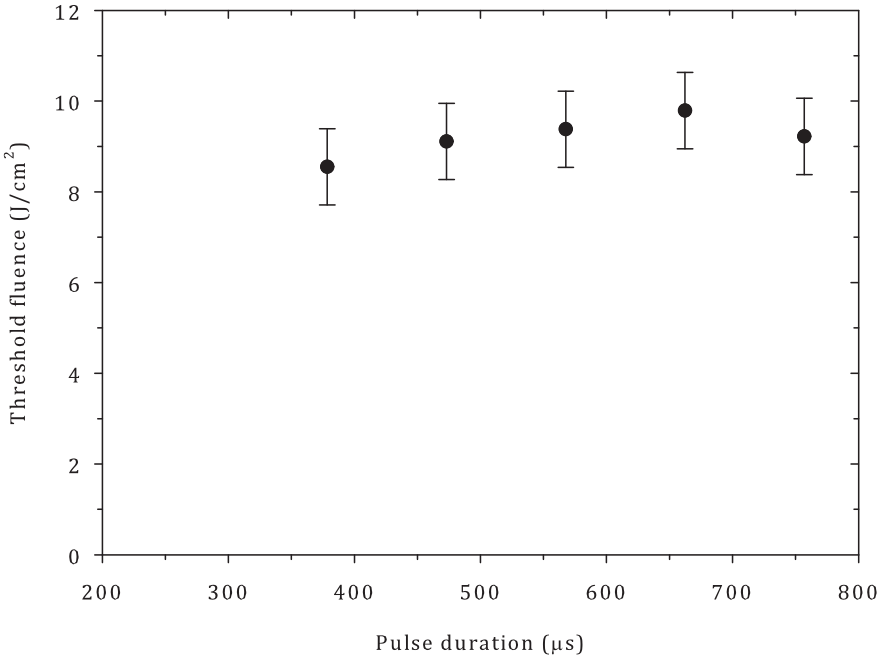

FIGURE 5.15: The threshold fluence of PP as a function laser pulse duration with a fixed laser spot radius of 237μm.

It is obvious from figures 5.12, 5.13, 5.14 and 5.15 that the pulse duration did not have an effect on the threshold fluence of any of the polymers. The reason for this behaviour was thought to lie with the relative sizes of the laser spot size, optical absorption depth and the thermal diffusion length.

The thermal diffusion length (δ) is defined as the distance at which the amplitude of the heat flux reduces to $\frac{1}{e}$ of the initial value [84] and for the heating geometry considered here, can be estimated from equation 5.8.

$$\delta = 2\sqrt{Dt} \tag{5.8}$$

In the equation, t is the time over which the heat flow is followed (which in in this case would be the laser pulse duration) and D is the thermal diffusivity which is

calculated from equation 5.9. Here, K is the thermal conductivity, ρ is the density and C is the specific heat capacity.

$$D = \frac{K}{\rho C} \tag{5.9}$$

The properties of the polymers are given in table 5.1 [53, 76, 79, 80]. The absorption coefficients at room temperature for a laser wavelength of 10.59μm are also given, with the corresponding optical absorption length found from the reciprocal, labelled a. The thermal diffusion length was calculated for the maximum and minimum pulse durations used in this section and is therefore given as a range of values.

TABLE 5.1: Thermal, optical and physical parameters of PI, PEEK, PET and PP. The range of δ values arises from the range of laser pulse durations used.

Property	Units	PI	PEEK	PET	PP
α	cm^{-1}	295	361	123	20
a	μm	34	28	81	500
C	$JK^{-1}kg^{-1}$	1090	1450	1275	1800
ρ	kgm^{-3}	1420	1260	1350	900
K	$Wm^{-1}K^{-1}$	0.16	0.25	0.14	0.16
D	$x10^{-7}$ m^2s^{-1}	1.03	1.37	0.80	0.99
δ	μm	5.4–15.0	7.3-14.5	3.9–12.4	12.2-17.3

Referring to the damage results for PEEK and PET which had holes in the sample, the possibility of a change in heat flow due to removal of material was discounted as

the heat diffusion length was not of sufficient size that there would be a difference between damage at the edge of the site with or without material at the centre being present. For example, for a pulse of duration 473μs, the damage site diameter used for the threshold fluence calculations of PET was 484μm and the hole diameter was approximately 300μm. The distance between the edge of the hole and the edge measured was therefore 92μm. The heat diffusion length at this pulse duration therefore accounts for less than 15% of the minimum distance between the hole edge and the damage edge.

A simplified representation of this system consists of a cylinder of absorbed laser light, found from the spot radius and the absorption depth. The laser heated volume of this is given by:

$$V = \pi\omega^2 a \tag{5.10}$$

At the end of a laser pulse, the volume calculated by equation 5.10 will have been extended to include the thermal diffusion length, and the new volume is:

$$V_\delta = \pi(\omega + \delta)^2(a + \delta) \tag{5.11}$$

It follows that if the laser spot radius and/or the optical absorption length are much larger than the thermal diffusion length, the heat flow has a negligible affect on the heated volume and therefore the final temperature. The final fractional change in volume caused by heat flow, Z, is given by equation 5.12.

$$Z = \frac{V_\delta - V}{V} \tag{5.12}$$

Using the results in table 5.1, Z was calculated for the polymers. In the case of PET and PP, where the optical absorption depth exceeds the thickness of the sample, the sample thickness was used. Obviously there would be no change in volume due to heat diffusion through the thickness of the polymer in this way, but the equation still gives an estimation of the effect. The fractional change is shown as a range in table 5.2. This range is due to the effect of pulse duration in equation 5.8. The average of the two spot sizes was used for PI.

TABLE 5.2: Fractional change to the heated volume due to heat diffusion during the laser pulse

Polymer	Fractional change
PI	0.22–0.65
PEEK	0.36–0.77
PET	0.10–0.32
PP	0.15–0.22

The results in table 5.2 explain the constant threshold fluence over pulse duration range measured for PET and PP as the contribution of heat diffusion is small. The largest fractional change in volume was seen for PEEK. This may explain the subsurface change observed for the single pulse. The heat flow in PI was thought to be unlikely to result in a sufficient temperature rise in the extended volume to decompose the material.

5.3 SEM study of polymer damage sites

In order to study the changes induced in the polymers in more detail, scanning electron microscopy was used. This allowed the physical changes in the polymers to be studied while excluding refractive index changes which were visible using optical microscopy. All samples shown were coated with gold before being imaged, unless otherwise indicated.

5.3.1 PI

It was noted earlier in this chapter that single pulse laser irradiation of PI resulted in some carbon formation on the polymer surface. This was fragile and easily cleaned with isopropanol for measurements of the damage diameters to be taken. Shown in figure 5.16 is an SEM micrograph of the carbon structure (before cleaning) on the PI surface made using a single 189µs duration laser pulse. The pulse energy was 16.9mJ. The sample stage was tilted by 60 ° to clearly show the structure.

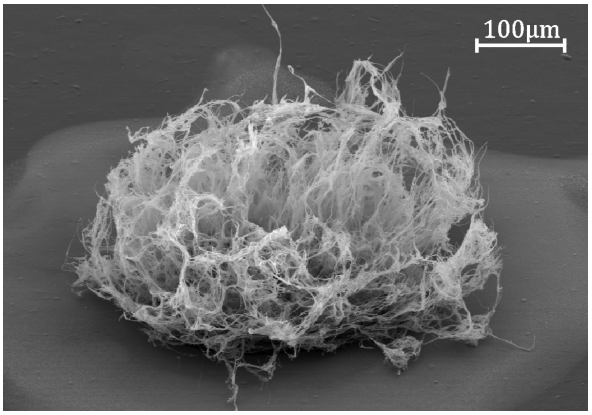

FIGURE 5.16: SEM micrograph of a single pulse damage site on PI. The laser pulse duration was 189µs. This corresponds to a pulse energy of 16.9mJ. The tilt of the sample stage was 60 °.

The structure observed here is similar to carbonisation of PI and materials similar to PI observed in the literature [5, 7, 16, 19, 85, 86]. The material being studied in reference [16] was the same as in this work. A focussed beam and 1000 pulses from a Nd:YVO_4 laser with a wavelength of 1064nm were used to irradiate the sample in the reference, resulting in highly textured micro-structure. When subjected to the vacuum required for preparation for SEM imaging the structure was more pronounced than that observed under optical microscopy, implying that trapped gas had been released by the conditions. Raman spectroscopy indicated that there was a presence of an amorphous form of carbon that had some degree of nano-crystallinity [16]. In the reference, the distribution of the carbonised material (a level of carbonisation was present over the entire width of the ablation crater, although the strength of the Raman signal fell off rapidly away from the centre) was different to that found here, where the structure was evenly distributed over the whole area of the irradiated spot. This was thought to be due to the large number of pulses used in [16] compared to single pulse irradiation in this work. More pulses could have removed the centre portion of the structures observed in the reference and further carbonised the material at the centre of the irradiated area.

In a paper by Brannon et al [7], TEA-CO_2 laser pulses incident on PI also produced a black, fibrous debris in and around the etched region for laser wavelengths of 9.2μm and 10.59μm. More of the structure was observed for the 10.59μm wavelength. Comparison between the ablation of PI with UV and IR lasers has been made by Srinivasan [19]. In the paper the plume resulting from IR irradiation

using a TEA-CO_2 laser was studied and it was noted that there was the same debris as that reported in [7]. TEA-CO_2 irradiation of Upliex PI was seen to result in fibrous carbonisation [5] and irradiation of PI with a continuous wave 50W CO_2 laser 'resulted in a low density, crusty char residue' [85]. This was thought to increase the threshold fluence for subsequent pulses by acting as a thermal and optical barrier to further irradiation.

The carbon formation was assumed not to effect the threshold energy as the gradient remained constant for spots where carbon was and was not present. The carbon did, however, affect the absorption coefficient during the laser pulse and this will be discussed further using the time resolved above threshold transmission measurements presented in the next chapter.

As has been mentioned earlier, the carbon was easily removed with isopropanol and a lens tissue. Figure 5.17 shows the cleaned equivalent of the sample in figure 5.16. The tilt of the SEM sample stage was, as before, 60 °.

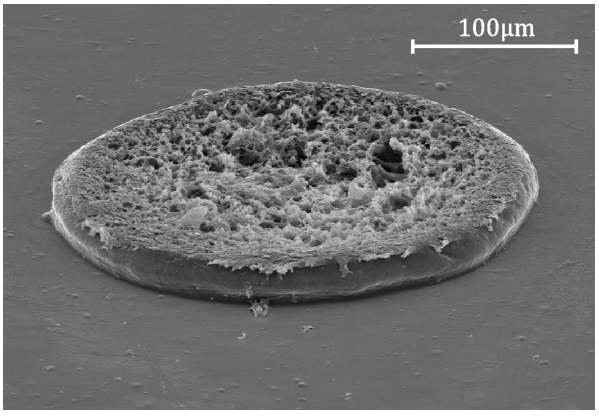

FIGURE 5.17: SEM micrograph of a single pulse damage site on PI after being cleaned with isopropanol and a lens tissue. The laser pulse duration was 189µs. This corresponds to a pulse energy of 16.9mJ. The tilt of the sample stage was 60 °.

The micrograph in figure 5.17 indicated that the structure observed in figure 5.16 was approximately uniformly distributed over the irradiated area for this pulse duration.

In contrast to the micrographs shown in figures 5.16 and 5.17, the result of a single laser pulse of duration 71µs (with a pulse energy of 6.4mJ being delivered to the sample) is shown in figure 5.18.

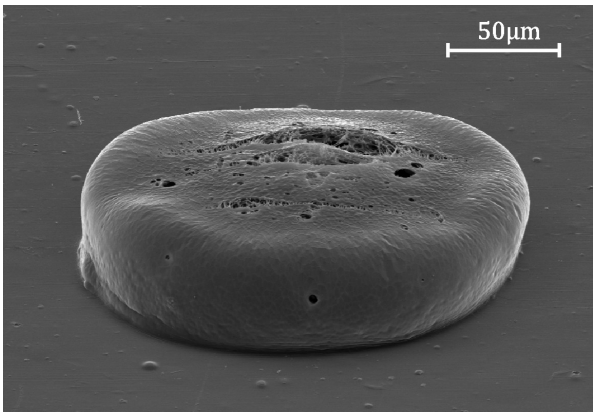

FIGURE 5.18: SEM micrograph of a single pulse damage site on PI. The laser pulse duration was 71µs. This corresponds to a pulse energy of 6.3mJ. The tilt of the sample stage was 60 °.

The shorter pulse duration resulted in no carbon formation on the polymer surface; optical microscopy showed no carbonised material. However the raised structure implied a volume (and therefore density) change. In order to study the structure within the volume change, a damage site made with the same laser parameters as those used to make the structure shown in figure 5.18 was approximately cut through the middle with a scalpel. A new scalpel blade was used and the sample was cut in half with one pass to avoid disrupting the site of interest. The sample was then mounted such that an SEM micrograph could be taken of the cross-section. The micrograph is shown in figure 5.19. The site in the figure is smaller

than that shown in figure 5.18 as the site was not cut exactly in half as would have been ideal. The dotted lines indicate the polymer edge and delineates between the exterior and interior of the original material.

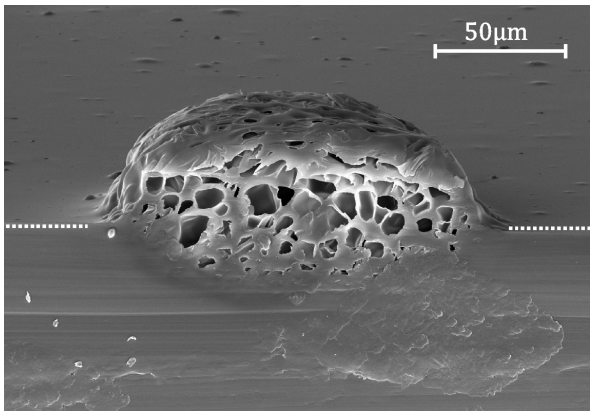

FIGURE 5.19: SEM micrograph of the cross-section of a single pulse damage site on PI. The laser pulse duration was 71µs. This corresponds to a pulse enery of 6.3mJ. The dotted line represents the edge of the polymer.

Clearly there was some change to the average material density which resulted in the raised region seen in figure 5.18. This swelling was thought to arise from trapped gas phase material in the polymer which stretched the original material into the filaments seen in the figure. It was thought unlikely that the structure was due to re-solidified molten material due to the fact that PI decomposes but does not melt.

5.3.2 PEEK

PEEK samples were also studied using SEM. The following figure 5.20 shows the result of applying a single laser pulse of duration 189µs. The pulse energy was therefore 16.9mJ. The sample stage was tilted by approximinately 20 °. The sample was not cleaned prior to being coated in gold for the SEM.

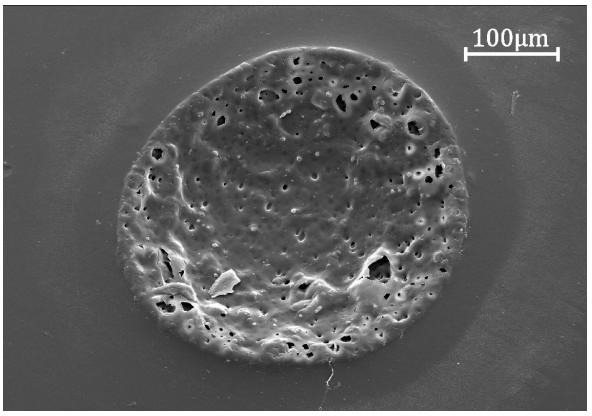

FIGURE 5.20: SEM micrograph of a single pulse damage site on PEEK. The laser pulse duration was 189µs. This corresponds to a pulse energy of 16.9mJ. The tilt of the sample stage was 20°. The sample was not cleaned.

Figure 5.20 shows a well defined damage site. The image also indicated that there was gas bubbles trapped in the irradiated sample and small holes where it appeared gas had vented. It was thought that the vacuum required for coating for SEM imaging burst the bubbles as these holes were not seen with optical microscopy. The results shown in figure 5.21 further supported this theory as there appeared to be regions where a thin membrane of material had ruptured, revealing further areas containing micro-holes. The same sample is shown in figure 5.21 and the regions of interest are highlighted in the figure. Again, it is important to note that the sample had not been cleaned.

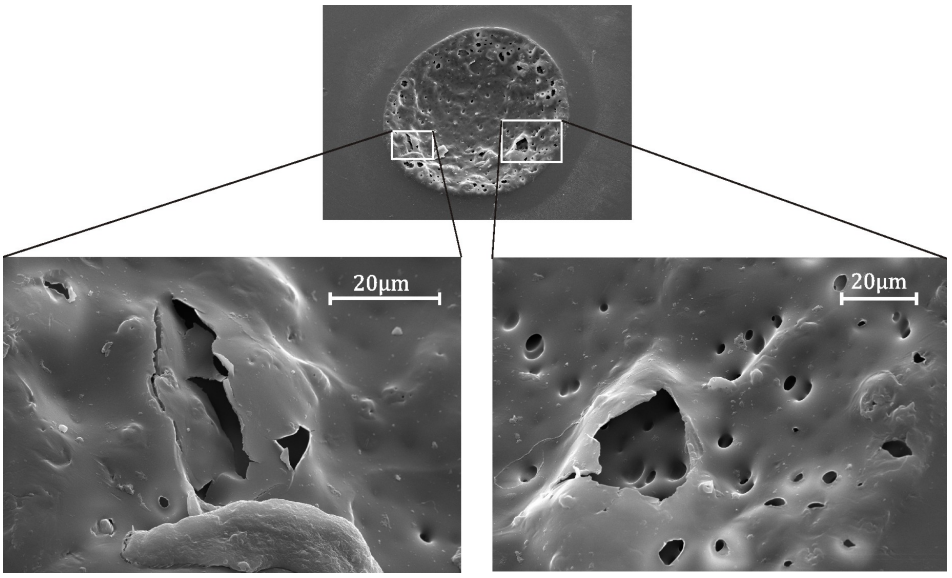

FIGURE 5.21: SEM micrograph of a single pulse damage site on PEEK. The laser pulse duration was 189μs. This corresponds to a pulse energy of 16.9mJ. The tilt of the sample stage was 20°. The sample was not cleaned.

Infrared laser interactions with PEEK have been studied in the literature [6, 23]. In [6], a TEA-CO_2 laser aligned to the strongly absorbed line in PEEK (9.32μm)was used. PEEK was seen to ablate with a well defined edge between the irradiated and non-irradiated regions, when using a contact mask in vacuum. When performed in air, micro-holes were noted in the paper, similar to those observed here.

In an attempt to determine the origin of the sub-surface changes noted for PEEK earlier in this chapter, a sample made using the same conditions as that shown in figure 5.4 was cut in half using as scalpel blade. The edge on damage site is shown in figure 5.22. The dotted lines shown in the figure indicate the top and bottom edges of the sample.

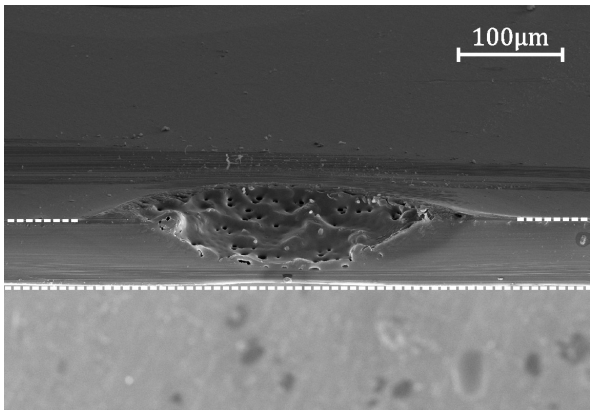

FIGURE 5.22: SEM micrograph of the cross-section of a single pulse damage site on PEEK. The laser pulse duration was 189µs. This corresponds to a pulse energy of 16.9mJ. The dotted lines represent the front and back surface of the polymer.

There was no indication of the extended sub-surface change observed using optical microscopy. This implied that a change in the amount of amorphous material or material crystallinity (as was observed in reference [23]) may have occurred, resulting in a refractive index change.

Shown in figure 5.23 is an example of some of the debris left behind after a single laser pulse of duration 189µs. Debris was observed leaving the surface of the polymer during the laser pulse as a white cloud of material which then redeposited on the surface of the polymer. There was no specific pattern to the distribution of the redeposited material and this seemed to depend on the air currents in the vicinity of the experimental site. The possibility of static charge attracting the debris back to the surface of the material was thought to the main contributing factor in the re-deposition observed. In the figure the pulse energy was, as before, 16.9mJ. An overview of the debris area and laser damage site is shown in the figure to put the image into context.

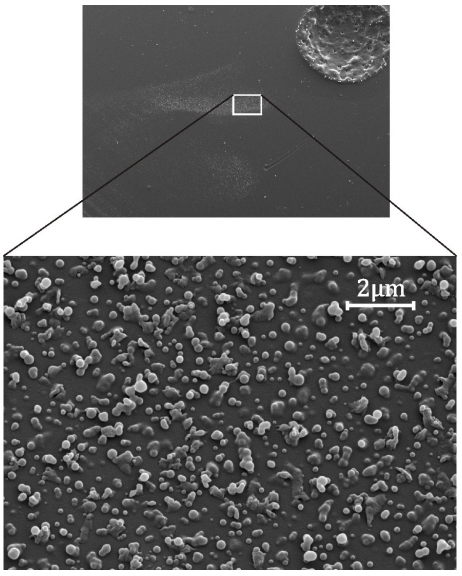

FIGURE 5.23: SEM micrograph of the debris resulting from a single pulse damage site on PEEK. The laser pulse duration was 189µs and the pulse energy was 16.9mJ. An overview of the debris area and damage site is shown to put the image in context. The tilt of the sample stage was 20°. The sample was not cleaned.

There was seen to be loose debris on the surface of the PEEK sample and also areas where the debris appeared to have become attached to the polymer surface due to either the temperature of the surface (or indeed the debris itself) being sufficiently high to recombine. The loose debris was easily removed using isopropanol and gentle cleaning with a lens tissue.

5.3.3 PET

Shown in figure 5.24 is a damage site on PET. The single pulse was of duration 189µs and the energy was 16.9mJ. The sample stage was at an angle of 20° to give a clear image and the sample was not cleaned prior to coating.

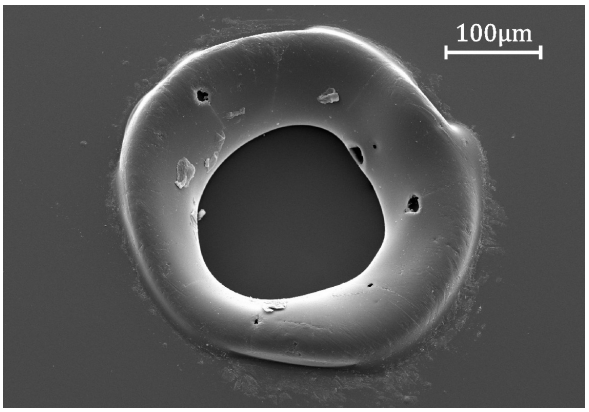

FIGURE 5.24: SEM micrograph of a single pulse damage site on PET. The laser pulse duration was 189µs. This corresponds to a pulse energy of 16.9mJ. The tilt of the sample stage was 20°. The sample was not cleaned.

It is clear from the micrograph that there was either a significant increase in the volume of the PET around the hole, redeposited molten material or melt flow away from the centre which resulted in a ridge around the edge of the hole. The outer edge of this ridge was measured for the threshold measurements described earlier. In reference [9] a similar effect was noted when pulses from a TEA-CO_2 laser were used to etch PET. The laser was tuned to the weakly absorbed 10R18 transition (10.26µm). There were seen to be holes in the wall of the etched hole in the paper (as in figure 5.24) and this was attributed to internal vapour production. The same ridge as shown in figure 5.24 was observed in the paper and was thought to be due to melt flow.

In order to investigate this effect further, a sample made using the same conditions as those used in figure 5.24 was cut in half. The same method as with the PI was used.

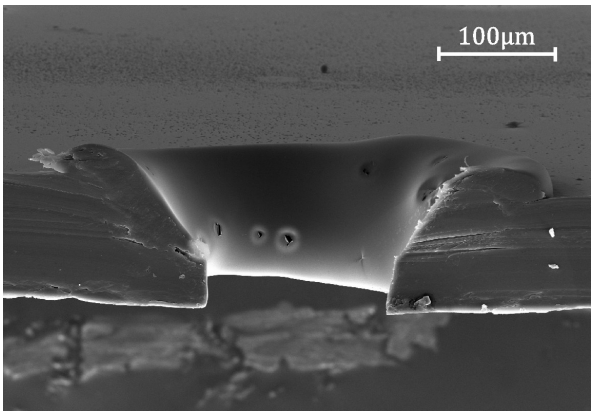

FIGURE 5.25: SEM micrograph of the cross-section of a single pulse damage site on PET. The laser pulse duration was 189µs. This corresponds to a pulse enery of 16.9mJ.

There did not appear to be any change in the material in the ridge region, implying that the volume had not changed due to the presence of gas products as in the PI sample shown earlier. This further supported the idea that the ridge had resulted from the flow of molten material. Unlike PI and PEEK, it was difficult to distinguish the laser induced damage due to the presence of this ridge. If caused by the molten material flowing out of the irradiated region onto the surrounding material, the laser damage site would be smaller than that measured for the threshold fluence. However, in this work the 'damage site' was defined as any change to the polymer surface that could be measured optically and in this way, it was appropriate to measure the edge of the ridge as the damage diameter. The good correlation of data shown in figure 5.10 indicated that the damage site was well defined regardless of it being due to melted material or not.

In reference [87] a raised area around a hole made with a CW argon ion laser was noted. The laser was chopped to produce pulses in the duration range 10–400µs. The raised region (or ridge) was attributed to molten products being ejected from

the hole and accumulating around the edge. It was also noted in the reference that the distance of the highest point on the ridge was at a larger distance from the edge of the hole than could be accounted for by the heat diffusion length during the laser pulse. This was also found to be the case here, with the heat diffusion length during a 189μs laser pulse being 7.8μm. Determining the highest point of the ridge depended on where the edge of the hole in figure 5.25 was defined. It was clear from the edge view of the damage site that this distance was larger than the heat diffusion length during the pulse.

Debris was also present on the polymer surface for the PET damage sites. The PET debris was seen to be very similar to that observed for PEEK. Two examples resulting from a 189μs duration pulse are shown in figure 5.26. An overview of the debris area is also shown for context.

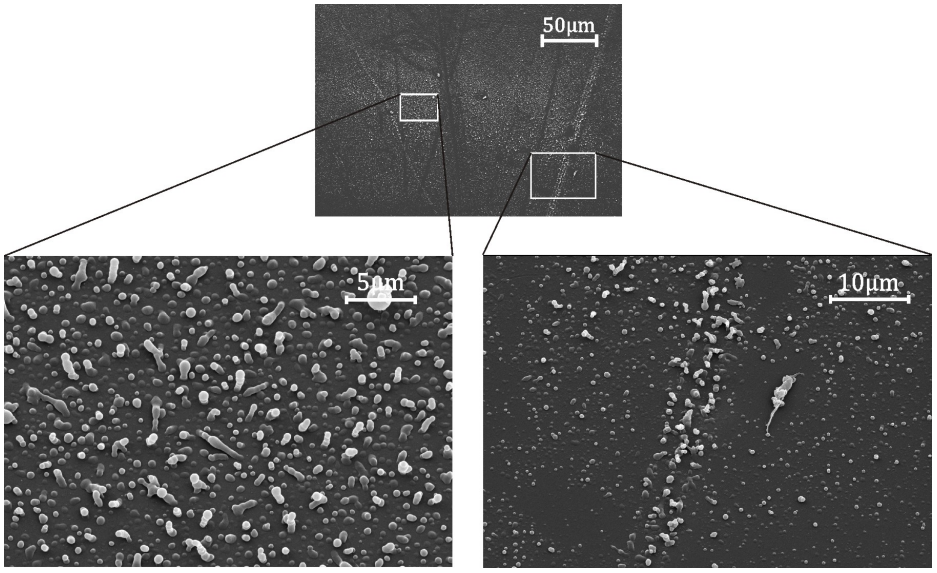

FIGURE 5.26: SEM micrograph of the debris resulting from a single pulse damage site on PET. The laser pulse duration was 189μs and the pulse energy was 16.9mJ. An overview of the debris area is shown to put the image in context. The tilt of the sample stage was 20°. The sample was not cleaned.

As seen with PEEK, the debris consisted of small particles of PET, assumed to

be ejected as molten material from the hole. No change in the debris material was though to have occurred as it appeared to be the same as the bulk material. During the experiment there were seen to be fibrous debris in the material cloud leaving the surface and these also redeposited onto the sample surface, as shown in the right image in figure 5.26.

5.3.4 PP

Finally, PP irradiated with single pulses from the laser was studied using SEM. Shown in figure 5.27 is an SEM image of a damage site on PP. The single pulse was of duration 378μs and the energy was 33.8mJ. The SEM sample stage was at an angle of 20° to give a clear image and the sample was not cleaned prior to coating. The sample thickness was 300μm.

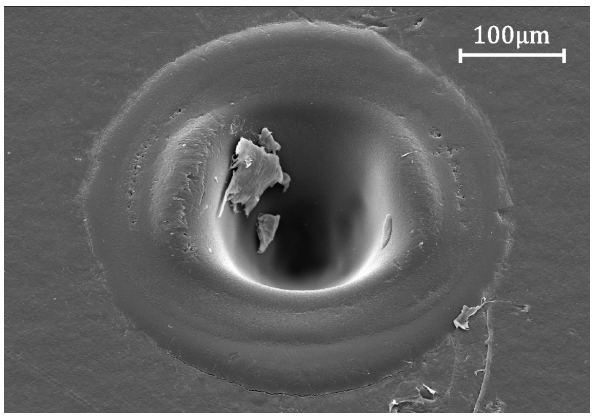

FIGURE 5.27: SEM micrograph of a single pulse damage site on PP. The laser pulse duration was 378μs. This corresponds to a pulse energy of 33.8mJ. The tilt of the SEM sample stage was 20°. The sample was not cleaned.

The PP sample showed a similar effect to PET when irradiated with a single pulse; a raised region around the central hole. The sample thickness in the case of PP was larger than that of the PET sample and therefore the hole did not break through

to the back of the material. Again, the possibility of the damage edge being due to molten material was not taken into account in the calculation of the threshold fluence but, as with PET, the data was well correlated.

In work by Bormashenko et al [41, 73] tunable and non-tunable CO_2 lasers (operating at 10.3μm and 10.6μm respectively) were used to irradiate PP samples. For the tunable laser, the wavelength was tuned for maximum absorption in PP. A thermal deformation was seen to take place when the PP was irradiated with this tuned laser radiation, resulting in craters on the polymer surface. When irradiated with the 10.6μm non–tunable laser, the same effect was noted but the threshold power density for this was higher, as would be expected. The features were similar to that shown in figure 5.27, that is, there was a ridge around the edge of the irradiated site. The ridge in the paper was smoother than that obtained in this work, however, and had a less well defined edge. This could have been due to the features in the paper resulting from a highly absorbed laser line rather than a very weakly absorbed wavelength as used here. Little information about the pulse durations of the lasers used were given in the references.

5.3.5 White light interferometry of PP damage sites

One of the PP damage sites was studied in more detail using white light interferometry (WLI). The SEM images gave more detail than optical microscopy, however WLI allowed the surface topology to be more accurately determined without the need to cut the sample in half. It also allowed the entire damage site to be studied without the need for multiple cross-sections to be taken.

An in depth description of the method of WLI can be found in the literature (see, for example, [88]). The working mode used in this work was the white light vertical scanning mode (VSI). White light reflected from a reference mirror is recombined with white light reflected from the sample being studied which produces interference fringes. The sample moves through the focus positions (which are very shallow due to the short coherence length of white light) and the camera in the system captures frames of interference at intervals during the scan. The system software then constructs a profile from these separate frames.

An SEM image of the damage site studied is shown in figure 5.28. The pulse duration was 568µs, which corresponded to a pulse energy of 50.8mJ.

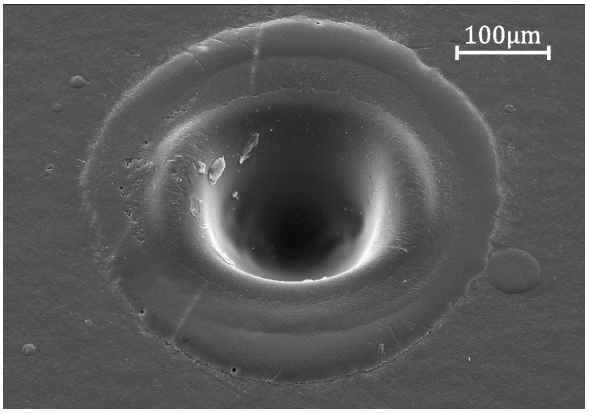

FIGURE 5.28: SEM micrograph of a single pulse damage site on PP. The laser pulse duration was 568µs. This corresponds to a pulse energy of 50.8mJ. The tilt of the SEM sample stage was 20 °. The sample was not cleaned.

VSI surface profiles of this spot were then taken using the white light interferometer (Veeco WYKO NT1100 with WYKO Vision32 software). It should be noted at this point that the sample had been coated in gold for the SEM images. This had the advantage of eliminating artefacts sometimes seen in transparent materials, due to multiple surfaces and refractive index changes, for example. Both surface profiles

shown in figures 5.29 and 5.30 were taken with a 50x objective and a 0.5x camera field of view. The modulation threshold was 4%. The profiles were constructed from 6 separate profiles taken across the sample surface. The experimental data is shown in red in both figures.

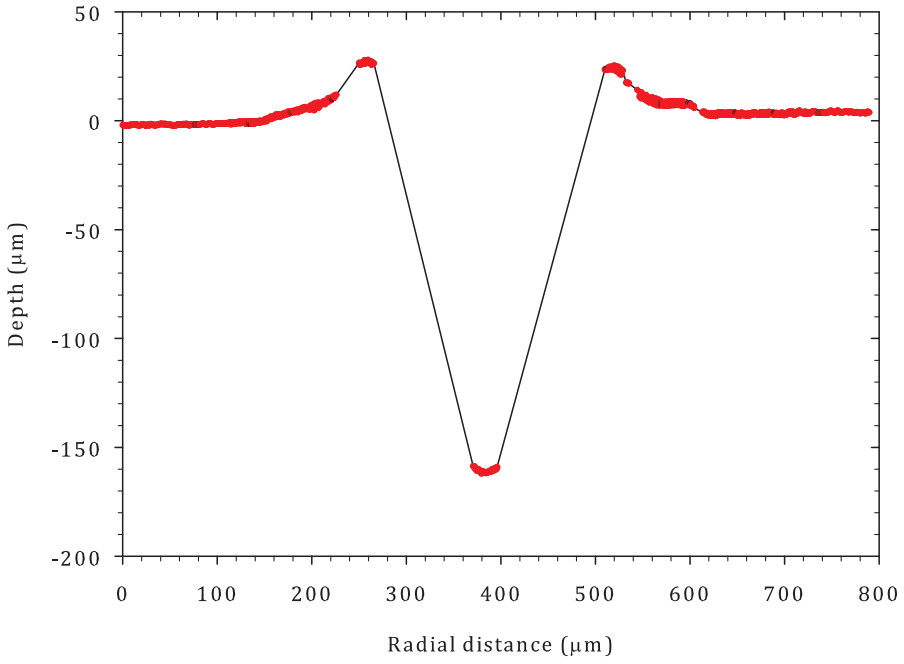

FIGURE 5.29: Left to right radial surface profile of a PP damage site made using a single laser pulse of duration 568µs (pulse energy 50.8mJ). The profile was constructed from 6 separate profiles taken with a 50x objective and a 0.5x camera field of view. The modulation threshold was 4%. The red data points are the experimental data.

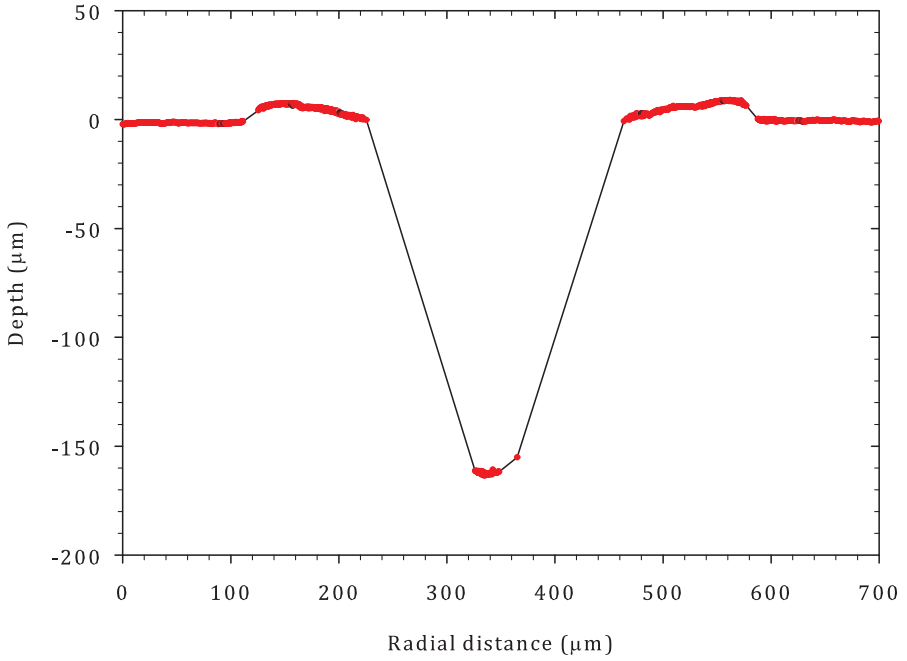

FIGURE 5.30: Top to bottom radial surface profile of a PP damage site made using a single laser pulse of duration 568µs (pulse energy 50.8mJ). The profile was constructed from 6 separate profiles taken with a 50x objective and a 0.5x camera field of view. The modulation threshold was 4%. The red data points are the experimental data.

A sample made using the same laser parameters as that shown in figure 5.28 was cut in half in the same way as described for PI. This cross-section is shown in figure 5.31.

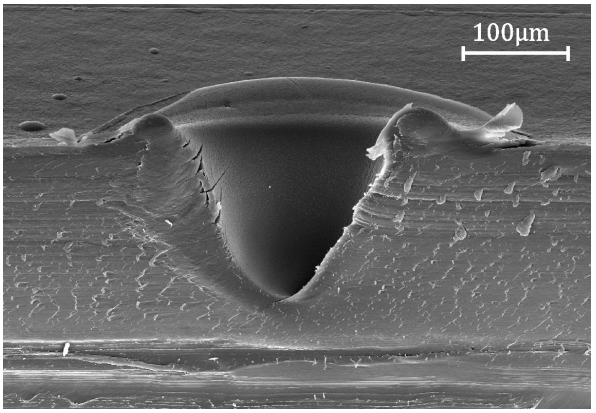

FIGURE 5.31: SEM micrograph of a single pulse damage site on PP. The laser pulse duration was 568µs. This corresponds to a pulse energy of 50.8mJ. The tilt of the SEM sample stage was 20°. The sample was not cleaned.

Clearly the result shown in the SEM micrograph was in good agreement with the WLI results obtained. However, the WLI allowed much more information to be obtained about the ridge around the edge of the hole, which was seen to be different horizontally and vertically. The volume of material around the edge of the hole clearly does not account for the material removed from the centre of the damage site. It was thought likely, therefore, that ablation and melt flow had occurred. However, the area of interest was the melted region, as this was measured as the damage diameter.

For smooth features (such as those obtained for PP) WLI allows characterisation of the laser damage sites without the need for cross-section measurements to be made. It would have suited the features obtained in references [73] and [41] as a method of profiling the 'micro-lenses' in the paper. In this case, the sample being studied was coated but another possibility would have been to make a contact relief mould of the features.

5.4 Discussion and conclusion

In this chapter, the single pulse irradiation of PI, PEEK, PET and PP has been studied. The threshold fluence for damage of the polymers has been determined as a function of the laser pulse duration from measurements of the damage diameter. The threshold fluences for PI, PEEK, PET and PP have been measured for pulse durations in the range 71–546μs, 95–378μs, 47–473μs and 378–757μs respectively.

The average threshold fluence and absorption coefficient of each polymer are shown in table 5.3. The absorption coefficient of each polymer is also shown for a wavelength of 10.59μm and at room temperature. The enthalpy (or energy density) was calculated for each polymer and is also included in the table.

TABLE 5.3: Average threshold fluence, room temperature absorption coefficient at 10.59μm and the resulting enthalpy for each polymer

Polymer	F_T (J/cm^2)	α (cm^{-1})	ΔH (kJ/cm^3)
PI	8.15	295	2.4
PEEK	5.36	361	1.9
PET	3.43	123	0.1
PP	9.58	20	0.2

The results for PI, PEEK and PET in table 5.3 can be directly compared to the results of the enthalpy found in the literature and shown in tables 2.1, 2.2 and 2.3 in Chapter 2. The enthalpy or energy density for damage of PI and PEEK is consistent with accepted values for PI and PEEK.

However, PET has a smaller enthalpy than those determined from the literature. This was attributed to the difference in the method used to determine the threshold fluence. As etch rate measurement are usually used to determine the threshold fluence, the energy density does not take into account melting as this is not considered an ablation mechanism (i.e. material is not removed). Therefore, for PET, the damage enthalpy is lower than the enthalpy of ablation. Although accepted values for the energy density were not available for PP, the energy density was seen to be small and this was thought to be again due to melting requiring less fluence than ablation.

The damage sites have been studied in detail using SEM imaging. Features resulting from laser irradiation of PI were seen to agree well with those described in the literature. Particularly the carbonisation of PI, which was seen to occur for pulse durations exceeding approximately 189μs. The carbon was fibrous and easily cleaned away. Damage caused by pulses of shorter duration have been shown to increase the volume of the irradiated sites. An image of the cross-section of one of these sites showed fibrous structure within the increased volume, which was thought to be due to gas phase products.

The irradiation of PEEK has been shown to result in well defined damage sites which had gas bubbles trapped in the irradiated volume, as shown in detail using SEM imaging. This effect had also been noted in the literature cited. An SEM image of the cross-section of an irradiated site showed no indication of the subsurface change seen using optical microscopy. This was therefore thought to be due to a change in the amount of crystalline or amorphous material in the polymer due to laser heating as was observed in a paper by Hartwig et al [23]. It was thought that decomposition, rather than melting had occurred due to the appearance of the damage sites.

The PET damage sites showed similar features as those cited in the literature for irradiation using a chopped CW argon ion laser [87]. A hole surrounded by a ridge of molten material ejected during the laser pulse was seen to result from singe pulse laser irradiation. The cross-section of this showed no physical change in the material density of the ridge (i.e. extensive gas phase bubbles such as those

seen in PI below pulse durations of 189μs), which implied that the material was frozen PET which had flowed during the laser pulse.

Similar features to those shown for PET were observed for PP, that is, a ridge of polymer surrounding a deep hole. Again, the ridge did not show signs of density change and was therefore assumed to have resulted from molten material flow during the laser pulse. WLI was used to measure the surface profile of a damage site and this has been shown to be an appropriate method to study the topology of the features without the need to cut the sample in half, if the features are smooth. The WLI also allowed the profile to be determined for any cross-section and here it was shown that the ridge around the hole was not the same in orthogonal directions.

The results obtained in this chapter imply that the mechanisms and material response involved in long pulse irradiation of PI, PEEK, PET and PP are favourably comparable to those observed in the literature for other IR wavelengths and shorted pulse durations. Longer time-scale irradiation and differences in the absorption coefficients were thought to have resulted in larger threshold fluences than the accepted values. The threshold enthalpy was consistent with the literature for PI and PEEK, meaning the scaling of the two parameters was as expected.

The features described in this chapter are similar to those observed in the literature, further indicating a common mechanism for polymer damage.

Chapter 6

Heat flow and decomposition model for the analysis of the behaviour of polymers under laser irradiation

6.1 Introduction

This chapter focuses on theoretical calculations and their application to the experimental observations presented in the preceding experimental chapters. A thermal process was assumed based on experimental evidence and existing literature. The heat diffusion equation has been used to examine the laser heating of the polymers and to determine the fluence required to reach the thermal decomposition or melting temperatures, thus causing the damage observed experimentally. The software used for the modelling was Mathematica (Wolfram Research Inc, version 7.0.0).

6.2 Photochemical or photothermal?

The photon energy of the laser used for the work presented in this thesis is approximately 0.1eV. It is known that the bond energies in most polymers are in the range of approximately 3-11eV. For example, to directly break the C–H bond in an organic polymer, a photon energy exceeding 3.5eV would be required i.e. XeCl (4eV) or XeF (3.5eV) [3]. It is therefore unlikely that polymer damage measured

here is due to a purely photochemical process and therefore a photothermal process was thought to be dominant. A photothermal process is further supported by data and theoretical modelling in existing literature, as was described in the literature review.

6.3 Heating model calculations for Polymers

A heat diffusion model following the approach given by reference [89] was developed to study the temperature excursion as a function of time and distance in the polymers.

The heat diffusion equation in one dimension is as follows.

$$\frac{\partial \mathrm{T}}{\partial \mathrm{t}} = \mathrm{D}\frac{\partial^2 \mathrm{T}}{\partial \mathrm{z}^2} + \frac{\alpha}{\rho \mathrm{C}}\mathrm{I(t)}e^{-\alpha \mathrm{z}} \tag{6.1}$$

In equation 6.1, T is the temperature, t is the time, z is the distance into the sample, α is the optical absorption coefficient, D is the thermal diffusivity (calculated from equation 5.9 in Chapter 5), I is the irradiance, ρ is the density and C is the specific heat capacity. The irradiance was included as a function of the laser fluence (F), laser pulse duration (τ) and the polymer reflectivity (R). This is shown in equation 6.2 below which assumes a square temporal profile.

$$\mathrm{I} = \frac{(1-\mathrm{R})\mathrm{F}}{\tau} \tag{6.2}$$

It should be noted that the reflectivity used here is for the top surface only. At this stage, all optical and thermo-physical parameters were assumed to be independent of temperature.

It is well documented [27, 89, 90] that equation 6.1 only has analytical solutions for a small number of special cases. More generally applicable solutions can be found which approximate to the geometry used in the experiments presented in this thesis, but these are semi-analytical in nature. One such approximation is given by equation 6.3 [89].

$$\mathrm{T}_{(\mathrm{z,t})} = \mathrm{T}_{\mathrm{Room}} + \frac{(1-\mathrm{R})\mathrm{I}}{\mathrm{K}}\Big\{\delta\ ierfc\left(\frac{\mathrm{z}}{\delta}\right) - \frac{1}{\alpha}e^{-\alpha \mathrm{z}} + \frac{1}{2\alpha}e^{(\alpha\delta/2)^2}\ \times \left[e^{-\alpha \mathrm{z}}erfc\left(\frac{\alpha\delta}{2} - \frac{\mathrm{z}}{\delta}\right) + e^{\alpha \mathrm{z}}erfc\left(\frac{\alpha\delta}{2} + \frac{\mathrm{z}}{\delta}\right)\right]\Big\} \tag{6.3}$$

This solution is for a semi-infinite solid (i.e. it has one surface at z=0) that is irradiated by a penetrating source of continuous power. The penetration means that the material has a finite absorption coefficient. It is possible to turn the semi-analytical solution into a pulsed laser model by subtracting a second solution displaced in time by a value equal to the laser pulse duration. This gives a fast calculation of the temperature distribution in one dimension as a function of time. The evaluation of the complimentary error function and the integral complimentary function, erfc and ierfc in equation 6.3, was handled by Mathematica.

In order to include finite sample thickness, variable irradiance profile in time and a temperature dependent absorption coefficient, a numerical solution to equation 6.1 was also used. In this case, Mathematica was used to solve the partial differential equation with the following boundary and initial conditions.

- Heat flow across the boundary from air to polymer was not allowed by setting $\partial T/\partial z$ to 0 for the polymer surface.
- At t=0, the initial temperature of the polymer was uniform for all z.
- The rear surface was considered to be sufficiently far away from the heat source that its temperature did not change in time.

The last point may not be physically correct for all conditions considered in the preceding chapters. For example, the small absorption coefficient of PET along with the long pulse durations will certainly lead to some temperature rise at the rear surface. However, in terms of the estimation of the threshold fluence for damage at the entrance surface, this was not thought to be problematic.

The output of the semi-analytical and numerical models were compared to check convergence of the solutions. For acceptable agreement the run time of the numerical model was several minutes as opposed to seconds for equation 6.3. Whilst it was not arduous to use the full numerical simulation, the speed and simplicity of the semi-analytical solution was preferred unless variable parameters were used.

Table 6.1 shows the thermal, optical and physical parameters of PI, PEEK, PET and PP required to determine the temperature rise [51, 53, 76, 79, 80, 91]. Also

shown is the decomposition temperature of PI and PEEK as measured in Chapter 4. It was found in the previous chapter that the edge of the damage site of PET and PP was melted rather than decomposed. Therefore, the melting temperature range is included for these polymers. The damage temperature, whether decomposed or melted, is labelled as T_D.

The optical absorption coefficient, α, is the room temperature value at a laser operating wavelength of 10.59μm. It was found that the absorption coefficient was dependent on the material temperature for all the polymers. Also, measurements of the laser wavelength as a function of time revealed that the laser operated at a number of different wavelengths during a typical pulse. For the initial temperature calculations, the laser was assumed to be operating at the most prevalent wavelength of 10.59μm and the absorption coefficient was assumed to be the value measured at room temperature. The temperature dependence will be revisited later in the chapter.

TABLE 6.1: Thermal, optical and physical parameters of PI, PEEK, PET and PP

Property	Units	PI	PEEK	PET	PP
R	%	7.2	6.0	7.2	4.0
α	cm^{-1}	295	361	123	20
C	$JK^{-1}kg^{-1}$	1090	1450	1275	1800
ρ	kgm^{-3}	1420	1260	1350	900
K	$Wm^{-1}K^{-1}$	0.16	0.25	0.14	0.16
D	$x10^{-7}$ m^2s^{-1}	1.03	1.37	0.80	0.99
T_D	K	880	875	416–538K	393–449K

The models were solved for PI for pulse durations of 200μs, 500μs and 1ms and a laser fluence of $2J/cm^2$. For the numerical solution, a sample thickness of 125μm

was used. The numerical solution is shown in figure 6.1 and the semi-analytical in figure 6.2. Temperature was plotted as a function of time for the top surface of the polymer, i.e. z=0. Although most of the experimental work was done at pulse durations shorter than 600μs, the 1ms data was included to give an indication of what would be expected at longer pulse durations.

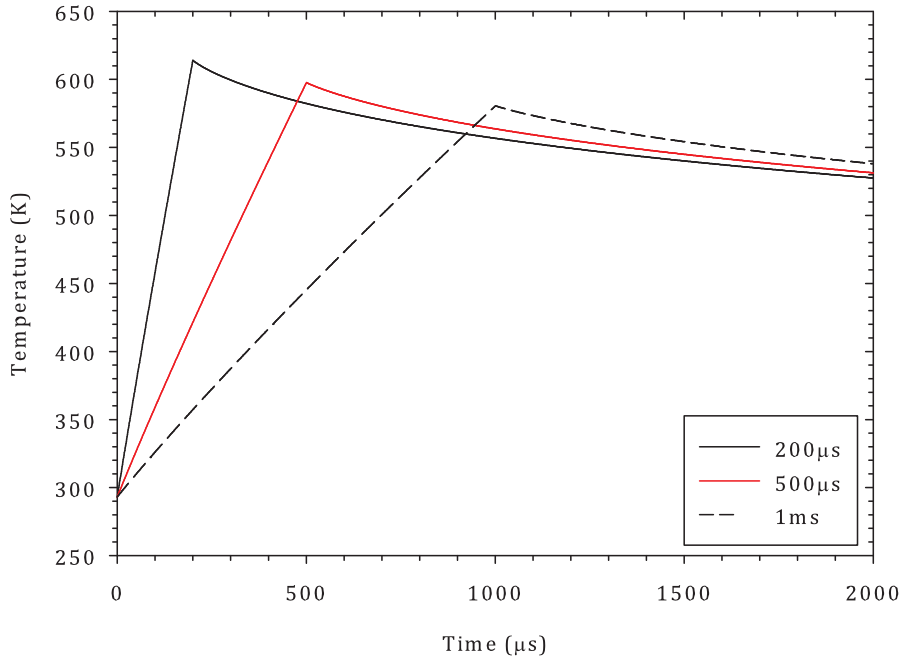

FIGURE 6.1: Temperature as a function of time for the numerical solution of the heat diffusion equation for laser pulse durations of 200μs, 500μs and 1ms. The laser fluence was 2J/cm^2 and the sample thickness was 125μm.

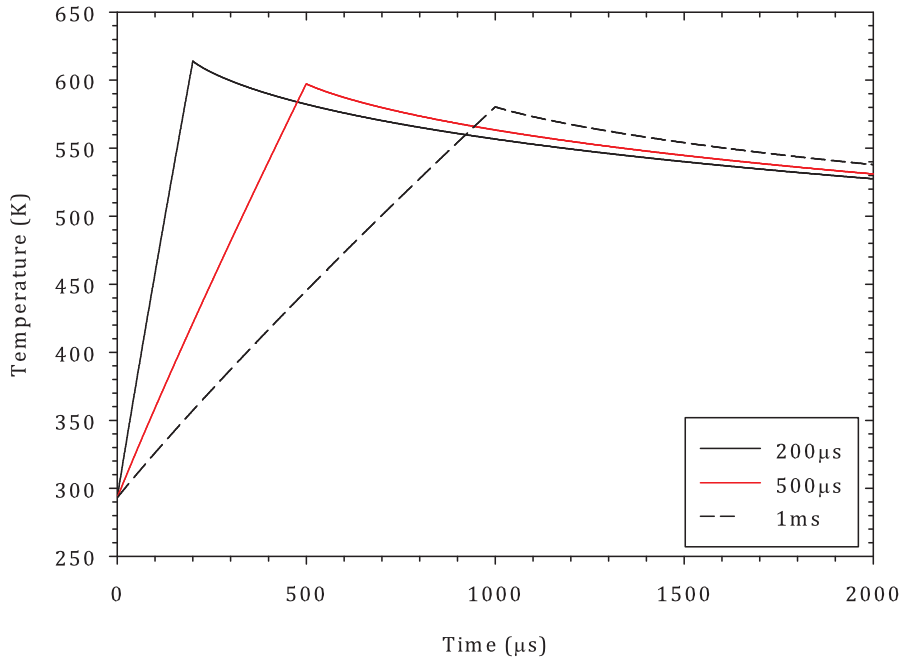

FIGURE 6.2: Temperature as a function of time for the semi-analytical solution of the heat diffusion equation for laser pulse durations of 200µs, 500µs and 1ms. The laser fluence was $2 J/cm^2$.

It is clear that that there was no appreciable difference between the solutions for these conditions and this polymer. The temperature reached at the end of the laser pulse was the same for both solutions over a pulse duration range applicable in this work.

From figure 6.2, cooling was seen to be slow due to the low thermal conductivity of the sample. The temperature reached at the surface was approximately the same for the laser pulse durations used, reaching a maximum at the end of the pulse. As expected due to some small amount of heat flow, the maximum temperature reached for the 1ms pulse was slightly lower than that for the 200µs pulse.

In order to determine the fluence require to reach a sufficient temperature to damage the polymers, the temperature in the semi-analytical solution was set to

the decomposition temperature of PI and PEEK as listed in table 6.1 and the required fluence determined. This fluence was therefore the equivalent of the threshold for damage measured experimentally in the previous chapter. Figures 6.3 and 6.4 show the fluence required to reach the temperature of decomposition as a function of the laser pulse duration. The results are for the top surface of the material.

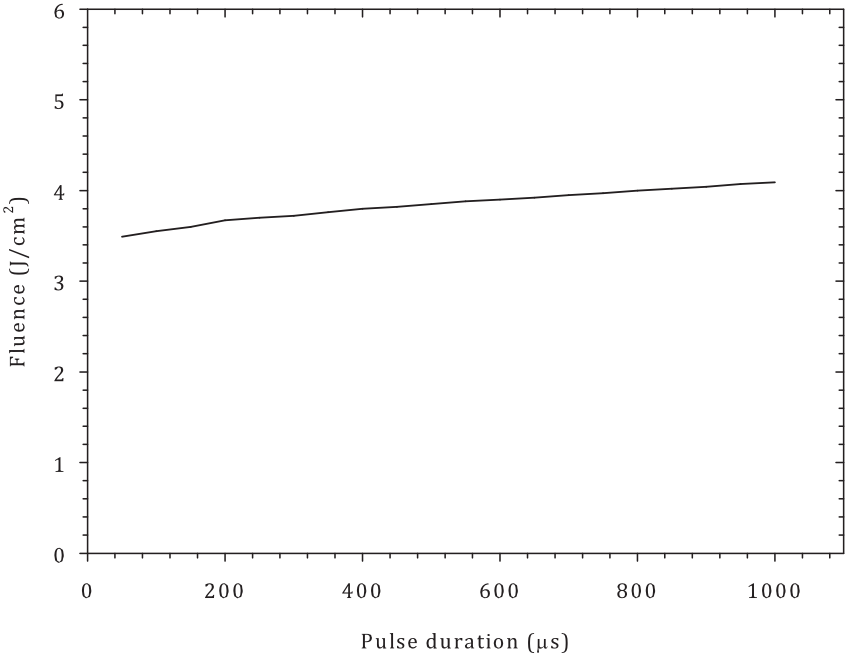

FIGURE 6.3: The laser fluence required to reach the decomposition temperature on the surface of PI as a function of laser pulse duration.

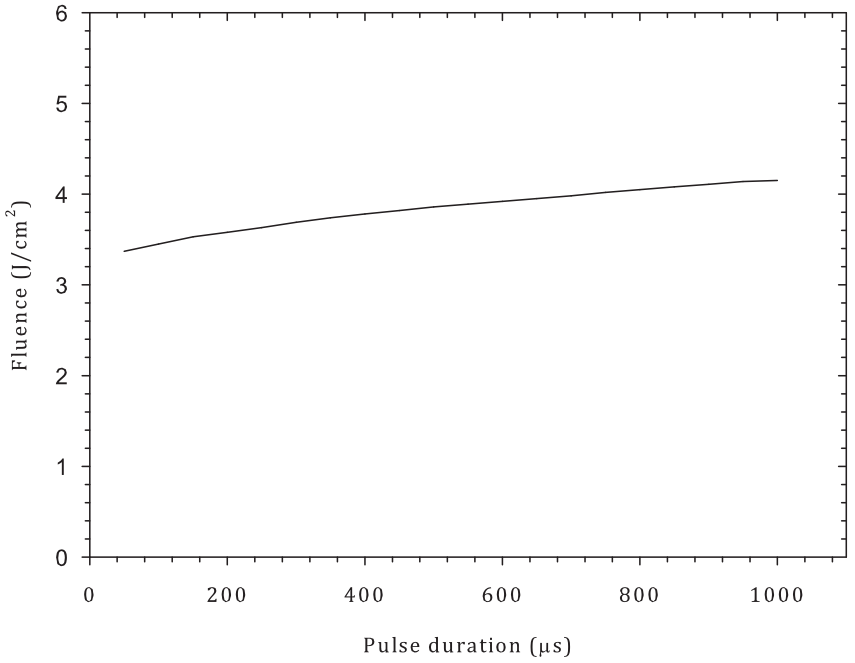

FIGURE 6.4: The laser fluence required to reach the decomposition temperature on the surface of PEEK as a function of laser pulse duration.

The average fluences required to increase the surface temperature of PI and PEEK beyond that for decomposition were calculated to be 3.75J/cm^2 and 3.76J/cm^2 respectively, over a laser pulse duration range of 50μs to 1ms. The graphs shown in figures 6.3 and 6.4 showed a similar behaviour for both polymers, with an increase in fluence at longer pulse durations. This was a small effect, however, and was most likely due to the semi-analytical solution being for a semi-infinite slab and thus allowing heat flow beyond the sample thickness. The calculated fluence was seen to be largely independent of the pulse duration which was in agreement with the results found experimentally in the previous chapter. However, the fluences calculated to reach the decomposition temperatures at the surface of PI and PEEK were much lower than those found experimentally (8.15J/cm^2 and 5.36J/cm^2 respectively).

Decomposition is a heating rate limited process [92]. Therefore, it follows that simply calculating the rise in surface temperature was not sufficient to determine the threshold fluence for damage based on a decomposition process, as the rate of heating was not taken into account. From figures 6.1 and 6.2, heating rates of 10^6–10^7K/s were obtainable with this system, whereas the decomposition measurements made in Chapter 4 were performed at 10s of K/min.

The fraction of bonds remaining in a polymer (N) after a time (t) can be found from equation 6.4. This is the Eyring approach, as used by Burns et al [92] to study the effect of XeCl laser repetition rate on the ablation of polyimide.

$$\mathrm{N} = e^{-\kappa \mathrm{t}} \tag{6.4}$$

In equation 6.4, κ is the decomposition rate and is found in the following way. A rate equation with an Arrhenius form similar to that introduced in the literature review to describe decomposition driven by a photothermal mechanism was used. Strictly speaking, the equation is applicable only to diatomic molecules but is a reasonable estimation for polyatomic dissociations [92].

$$\kappa = \frac{\mathrm{kT}}{\mathrm{h}} e^{\,\mathrm{E_A/kT}} \tag{6.5}$$

Here, k is Boltzmann's constant and T is the temperature, which in this case was calculated using the semi-analytical solution to the heat diffusion equation. $\mathrm{E_A}$ is the activation energy for the rate limited process, in this case decomposition.

For PI this was initially taken to be in the range of 314–418kJ/mol [92, 93] and 201–289kJ/mol for PEEK [63, 94].

The value of N was calculated as a function of the laser fluence at the end of a number of laser pulse durations, with equations 6.4 and 6.5 being directly coupled with equation 6.3 in the computation. For initial calculations, the average activation energy for each polymer was used. Shown in figures 6.5 and 6.6 is the fraction of bonds remaining as a function of the laser fluence for PI and PEEK. Pulse durations of 200µs, 500µs and 1ms are shown as an example of the behaviour observed and are indicated in the legend. The results were for the polymer surface, z=0. Note the expanded scale on the graphs for the fluence axes.

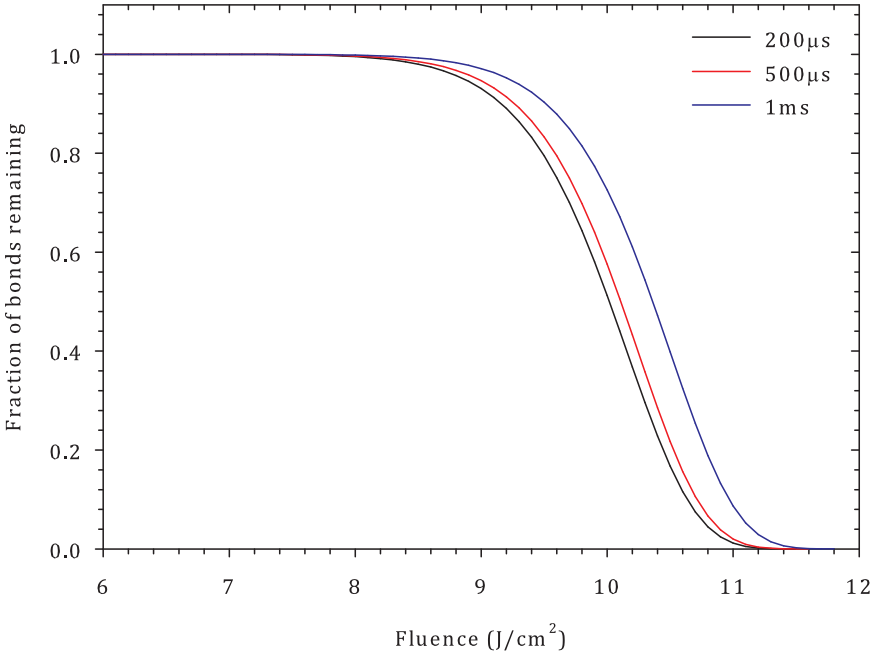

FIGURE 6.5: Fraction of bonds remaining in PI as a function of the laser fluence for laser pulse durations of 200µs, 500µs and 1ms.

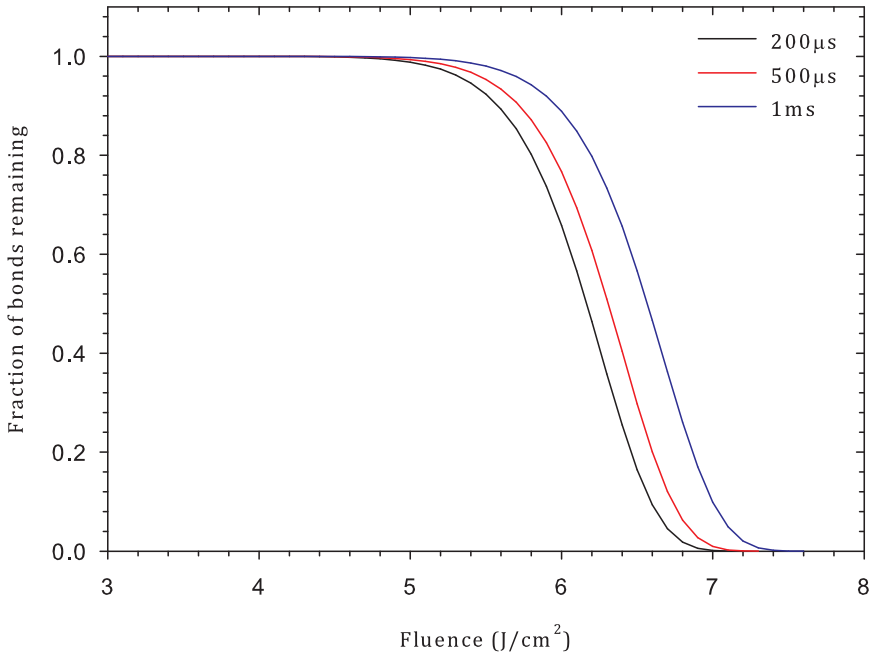

FIGURE 6.6: Fraction of bonds remaining in PEEK as a function of the laser fluence for laser pulse durations of 200µs, 500µs and 1ms.

The results in figures 6.5 and 6.6 indicated that there was an abrupt transition from an intact polymer to a situation where few bonds remained. This was seen to develop over a small range of fluences for each polymer, occurring at approximately 10.38J/cm^2 and 6.33J/cm^2 for PI and PEEK respectively. In order to accurately determine the fluence for significant decomposition based on this analysis, the inflection points of these plots were determined by finding numerically the minimum of the first derivative. This was then the threshold fluence for damage. The calculated results are shown in figures 6.7 and 6.8. Also shown are the experimental results of the threshold fluence for damage of PI and PEEK obtained in the previous chapter, for comparison. Additionally, the activation energies for decomposition were considered in more detail at this point. The large range of

values was seen to give rise to a large uncertainty in the calculated threshold fluence. Therefore, a single activation energy was selected based on the best fit to the experimental results.

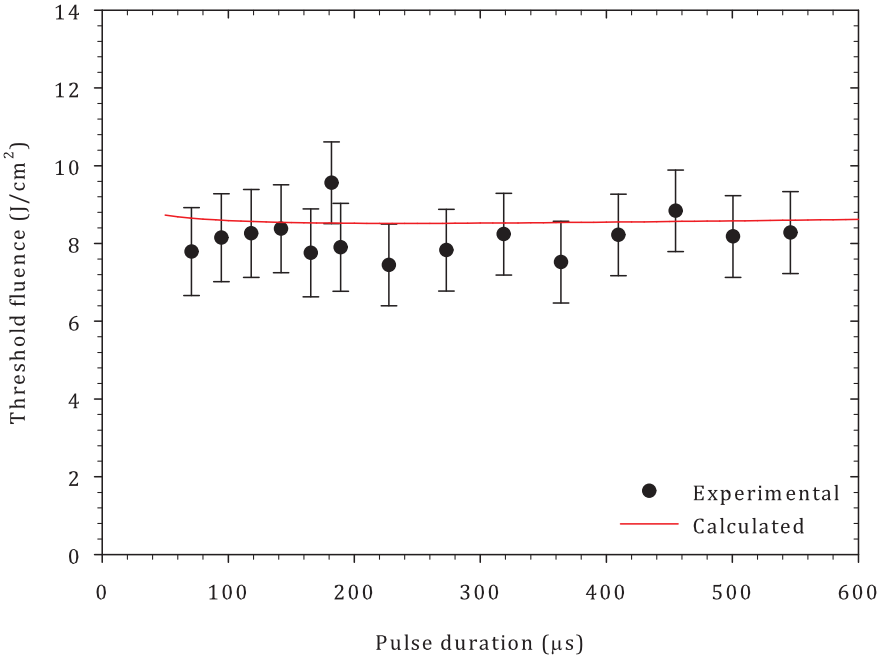

FIGURE 6.7: Threshold fluence for decomposition of PI showing calculated data based on an Eyring approach. Also shown are the experimental results from the previous chapter.

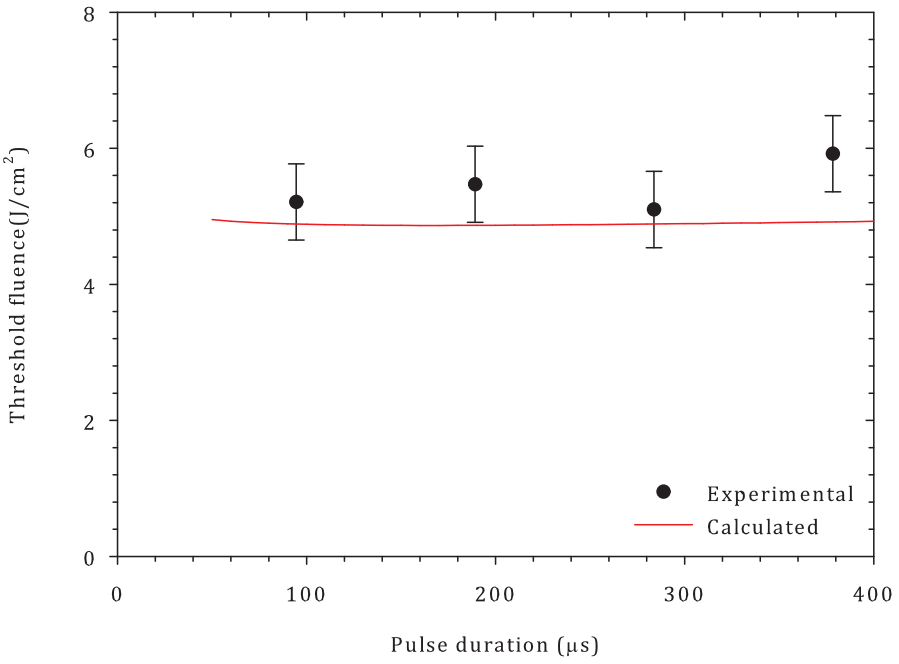

FIGURE 6.8: Threshold fluence for decomposition of PEEK showing calculated data based on an Eyring approach. Also shown are the experimental results from the previous chapter.

There was seen to be good agreement between the experimental and calculated threshold fluence based on the decomposition process. For this agreement, the activation energies selected were 314kJ/mol and 201kJ/mol for PI and PEEK respectively. The activation energy for decomposition of PI was the same as that found in work by Jellinek et al [93]. Similarly for PEEK, Zhang et al [63] and Abate et al [94] both obtained an activation energy of approximately 201kJ/mol.

Figures 6.9 and 6.10 show the fluence required to reach the average melting temperature of PET and PP as a function of the laser pulse duration. The melting temperature for each material was the average of the range given in table 6.1.

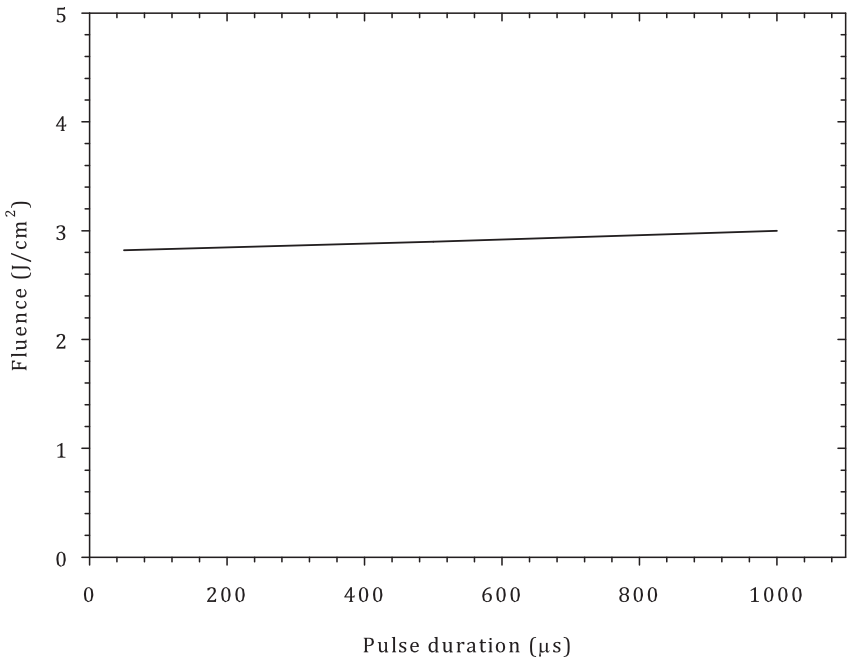

FIGURE 6.9: Fluence required to reach the average melting temperature on the surface of PET as a function of laser pulse duration.

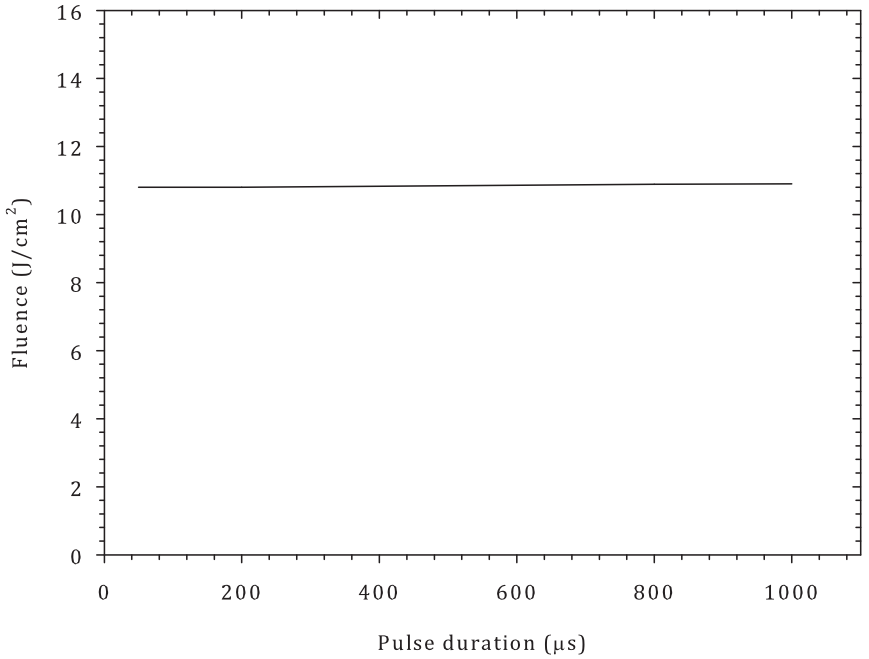

FIGURE 6.10: Fluence required to reach the average melting temperature on the surface of PP as a function of laser pulse duration.

The average fluence required to increase the temperature of PET and PP to their melting points was calculated to be 2.91J/cm^2 and 10.80J/cm^2 respectively, for the pulse duration range of 50μs to 1ms. The fluence was seen to be largely independent on the pulse duration for both polymers, as observed experimentally in Chapter 6. The fluences calculated for PET and PP were approximately the same as the threshold fluence measured experimentally. The experimentally determined diameter of the damage on PET and PP were taken from the edge of the melted region, as shown in the micro-graphs and SEM images in the previous chapter. This was therefore the diameter which was used to infer the threshold fluence for damage and is effectively independent of any decomposition which may have occurred in the middle of the irradiated site. Therefore, the melting temperature was appropriate here and the calculated fluence for melting is now taken to be the threshold for damage.

It should be noted that the latent heat of melting was not included in the model and would mean that more energy would need to be delivered to the sample to account for this. The latent heat (or melting enthalpy) of PET is 17x10^{3}J/kg [27]. The extra temperature rise required to overcome this was found following the approach given by Bäuerle [27] by dividing the latent heat by the specific heat capacity of the material, in this case 1275J/K.kg. This gave the temperature rise if melting had not occurred (and latent heat not required) as approximately 13K, which was small compared to the range of temperatures used for the calculations. The possibility of super-heating due to the heating rate and convection resulting in a complicated melt front were not included in the calculations for simplicity. The

melting temperature of polymers also depends on the heating rate and therefore a detailed experiment to determine the melting point as a function of heating rate would be required to determine this parameter if a more representative model was required. Additionally, the model assumed that the thermal and optical parameters remained constant during heating, which is known not to be the case.

Shown in figures 6.11 and 6.12 are the experimental and calculated results for the threshold fluence for PET and PP shown on the same axes for comparison. The experimental results are those discussed in Chapter 4. Due to the large range in melting temperatures found in the literature for PET and PP, a single value within the range was selected for best fit to the experimental results.

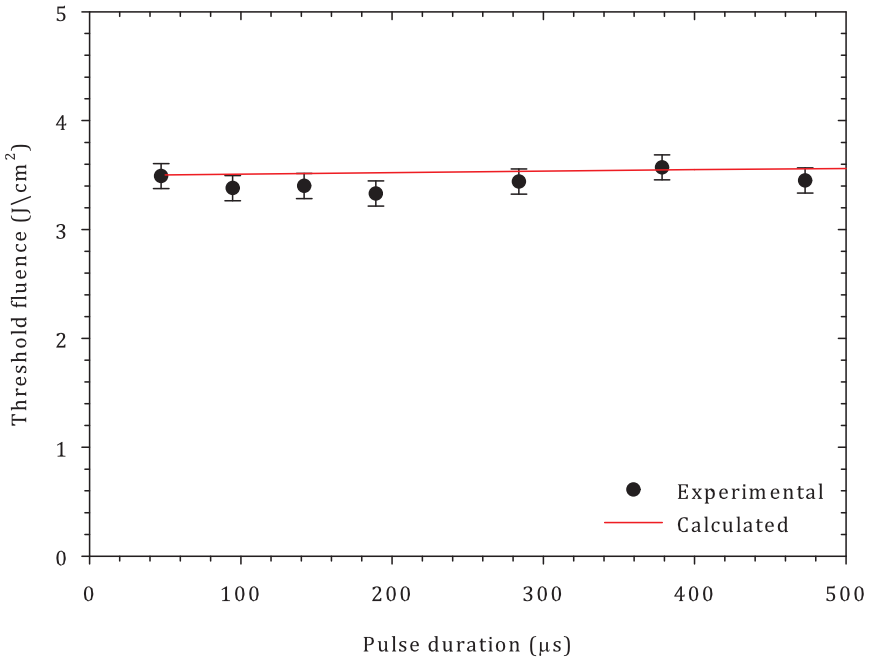

FIGURE 6.11: Threshold fluence required to reach a melting temperature of 520K on the surface of PET as a function of laser pulse duration.

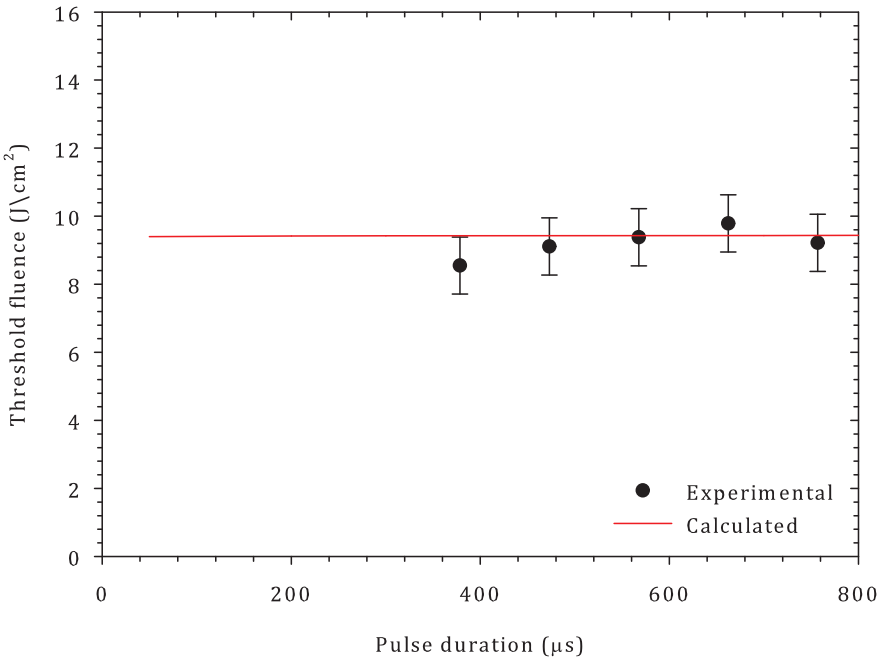

FIGURE 6.12: Threshold fluence required to reach a melting temperature of 404K on the surface of PP as a function of laser pulse duration.

Clearly from figures 6.11 and 6.12 the experimental threshold fluence agrees with the calculated fluences. The melting temperatures used for PET and PP were 520K and 404K respectively, which were in agreement with values found in the literature [51, 80].

It is obvious that a better method of modelling the melting processes would be required to study the subtlety of the mechanisms, but this is beyond the scope of this thesis. Bäuerle [27] gives a detailed account of the various considerations to be made for surface melting. However, without improved data for the melting temperatures of PET and PP, the extra complexity of including detailed melt front kinetics is unlikely to yield improved understanding of the processes.

6.4 Effect of temperature dependent absorption coefficient of PI on calculations

From the preceding data and discussions, it was hypothesised that if PI was heated by the early part of the laser pulse, then its absorption coefficient would drop and the later part of the pulse would penetrate deeper. This would have the effect of lowering the heating rate and possible cooling of the material, leading to improved coupling again. Hence, the heating rate would rise and it might be expected that some oscillation in the surface temperature would occur.

In order to test this, the numerical thermal model was modified in a number of ways.

- The absorption coefficient was replaced with a temperature dependent function which was found by fitting to the results of the absorption coefficient as a function of temperature in Chapter 4.
- The irradiance function in time was made closer to the real pulse shape by using functions to ramp-up and ramp-down the energy delivery in time.
- Finite sample thickness was set to the real polymer film thickness.

The results of this model are shown in figure 6.13 for a laser pulse duration of 200μs and a fluence of $2J/cm^2$.

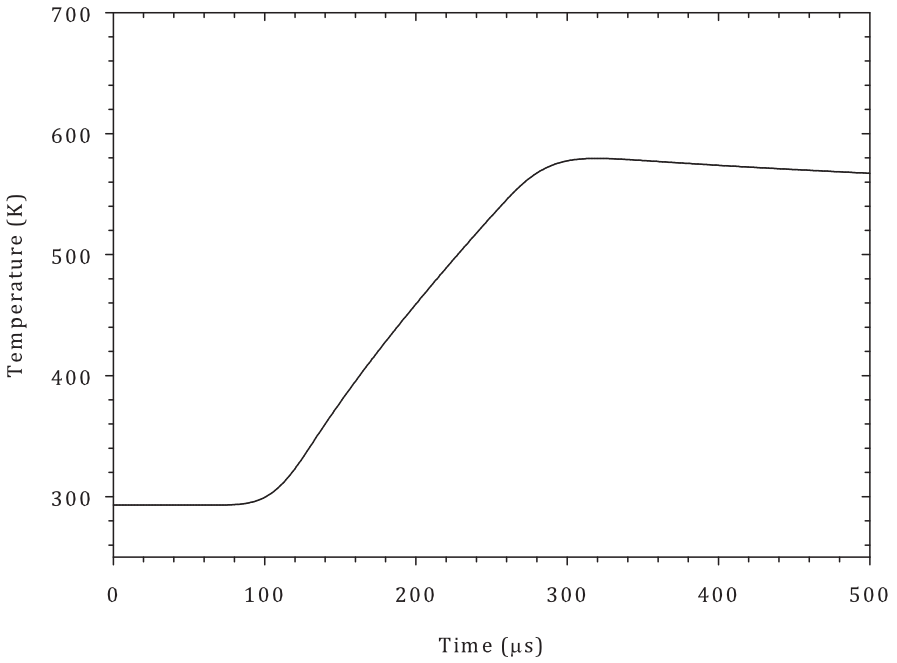

FIGURE 6.13: Temperature as a function of time for the numerical solution of the heat diffusion equation including a function for the absorption coefficient as a function of temperature and an irradiance profile fitted to experimental data of the laser pulse durations. The pulse duration was 200μs and the fluence was 2J/cm^2.

In figure 6.13 the finite rise-time of the irradiance now leads to a slower initial heating rate compared to figures 6.1 and 6.2 and a softer shaped peak. The maximum temperature rise is also reduced, most likely due to a combination of the slower rate of energy delivery and, more significantly, a temperature induced reduction in the absorption coefficient. This is in agreement with the expected result of deeper penetration leading to the laser energy being deposited in a larger volume, thus resulting in a smaller temperature increase. However, oscillation of the surface temperature due to a form of negative feedback is not seen. This can be explained by the consideration of the cooling time. As a crude estimate, the reciprocal of the absorption coefficient is set as the range over which cooling must

occur for a significant drop in the temperature. The time-scale is calculated by rearranging equation 5.8 in terms of time. This gives a time of approximately 6ms for PI, meaning that the time for feedback is too slow for its affect to be seen during the laser pulse.

Carbon formation at the top surface of the material above the threshold fluence would mean that the absorption coefficient of the bulk material as a function of temperature would become unimportant. More information about the time carbon formation occurred for a number of different pulse durations would be required to decide when the temperature dependence of the absorption was significant for coupling and decomposition. Oscillation of the transmission due to feedback was seen to be damped due to the low thermal conductivity of PI coupled with the large volume irradiation.

Work is currently under-way to couple all the significant parts of the laser induced decomposition and melting to try to construct a model which better represents the materials properties and laser characteristics.

6.5 Conclusion

The temperature rise in the polymers was calculated as a function of the laser pulse duration using a semi-analytical solution to the heat diffusion equations for a semi-infinite solid. The results were used to predict the threshold fluence for damage based on a decomposition process for PI and PEEK and a melting process for PET and PP. The threshold fluences were seen to agree well with

the experimental results. Melting temperature, decomposition temperature and activation energy ranges were large but general agreement was found for selected parameters when fitting to experimental data.

Some initial investigation into the effect of the temperature dependent absorption coefficient on the temperature calculations in PI has been carried out. Also, an irradiance profile which better represented the laser pulse in time was included. The numerical solution was used to determine the surface temperature, taking these parameters into account. Using the absorption coefficient as a function of temperature for a laser operating wavelength of 10.59μm, the effect was to reduce the maximum temperature reached, implying that more fluence would have to be supplied to the polymer to raise the temperature by the same amount as the semi-analytical solution predicted.

This is to be expected considering the results shown in figure 4.19 and summarised in table 4.2. The absorption coefficient of PI decreases with increasing temperature so it follows that as the temperature rises, the change in absorption coefficient would result in less absorption and therefore a lower temperature rise.

Chapter 7

Conclusions and Future Work

7.1 Conclusion

The irradiation of PI, PEEK, PET and PP using an RF CO_2 laser operating with pulse durations in the range 50–500μs has been investigated with a view to understanding the interaction. The UV and IR laser ablation of polymers has been widely covered in the literature but not in the pulse duration regime studied here.

The laser was characterised in terms of pulse duration, pulse energy and, perhaps most importantly, operating wavelength. It has been noted by other groups that wavelength hopping can occur during a laser pulse [49]. As such, the laser wavelength was measured here both in a time integrated and time resolved fashion. Time averaged measurements revealed that the laser operated at an number of wavelengths, but predominantly at 10.59μm, as expected. Time resolved measurements during an average laser pulse of duration 189μs showed wavelengths in the range 10.53–10.63μm were present at different times during the pulse. This was a constantly changing effect and thus wherever possible, all wavelengths within the range were used to make calculations, such as the optical absorption length.

The IR absorption of the polymers was studied by FTIR spectroscopy. This was done both at room temperature and as a function of polymer temperature. Room

temperature measurements were found to be broadly consistent with those in existing literature. The temperature dependent absorption coefficient measurements have extended the work by Dyer et al [8] to include the polymers studied here. The effect of temperature rise was characterised by the change in absorption coefficient divided by the change in temperature, approximated by a linear fit to experimental data. This allowed direct comparison of the polymers, despite the measurements having been taken over different temperature ranges. PP showed the least change in absorption coefficient with increasing temperature at all laser wavelengths. PEEK showed the largest effect, with an average change in absorption coefficient of approximately 10% over a temperature rise of 72K. The polymer least affected by temperature rise was PP, with a small change in absorption coefficient over the temperature rise of 47K. At a laser wavelength of 10.55μm, the absorption coefficient increased whereas at 10.63μm it was seen to decrease. This was due to the position of the emission lines on the absorption spectrum which were close to an absorption peak.

The transmission of the laser beam was measured for all the polymers to bring together the results from the measurement of the laser operating wavelength and the absorption coefficient. The transmission was used to calculate an effective absorption coefficient. For PI and PEEK, the inferred absorption coefficient fitted well with the other experimental data. However, due to plastic deformation from laser heating, the absorption coefficients for PET and PP were not within a range that could be explained by changes in the laser emission wavelength or temperature rise affecting the absorption coefficient.

The threshold fluence for damage of the polymers was determined as a function of laser pulse duration. The two were found to be largely independent and this was thought to be due to the small heat diffusion length in each material during the laser pulse. The product of the absorption coefficient and the threshold fluence giving the energy density or damage enthalpy was found to fit well with existing data in the literature for PI and PEEK. However, the energy density for damage of PET and PP was small. This was thought to be due to the method used to measure the threshold fluence in this work being based on damage rather than etch rate. Damage (i.e. melting) occurs at lower fluences than ablation so it follows that etch rate analysis would predict a higher energy density.

SEM micrographs of a selection of damage sites revealed interesting features about the effects of laser irradiation in this regime. Some parallels could be drawn between observations for different lasers in the literature. Of particular interest was the carbon formation observed for PI. This fibrous material has been noted before and adds an interesting problem to the evolution of changes in the laser absorption during irradiation above threshold.

Thermal modelling of the heat rise due to laser irradiation was performed using solutions to the heat diffusion equation. The threshold fluence for damage was predicted for each polymer and shown to fit well with experimental data. The change in absorption coefficient with temperature was included in some preliminary calculations for PI, along with a function for the pulse irradiance in time which better represented the laser pulse duration results. The effect of this was to reduce the maximum temperature reached by the polymer, meaning more energy

would have to be supplied to reach decomposition temperature than predicted by a simpler semi-analytical calculation.

7.2 Future work

The effect of temperature on the absorption coefficient of polymers is an area which is not widely covered in the literature, with the exception of results presented in [8]. The results in the reference offer information which could be informative regarding the type or tuning of lasers in industrial applications and could be extended to include other well known polymers. Additionally, if the thermal response of the absorption coefficient of a polymer is known and the laser wavelength was fixed, it might be possible to tune the polymer by heating the material to shift the absorption features.

The modelling of the system could be improved to better predict the threshold fluence of polymers from their optical, thermal and physical parameters. The importance of the activation energy was highlighted in the calculations of the theoretical threshold fluence using heat diffusion models. The large range of values cited in the literature meant that it was difficult to define a threshold based on a rate limited decomposition process. Finding an activation energy specifically suited for the high rates of heating achieved by laser ablation would be an advantage. For example, the activation energy is most often obtained from TGA data at different heating rates. If this process could be applied to a laser heated system

whereby the rate of heating could be controlled, similar calculations could be used to obtain activation energies for laser irradiation specifically.

Also, the hopping of the laser in wavelength coupled with the effect of temperature rise on the optical coupling could be included in the model. This would allow the threshold fluence for damage of other polymers to be determined to inform experimental decisions.

Extension of the work presented here to include other commercially attractive polymers could be used to help industrial practitioners make informed choices on laser sources in the future. Systems including the laser studied here would be particularly applicable where spot size and resolution were not crucial and where an easy to use and efficient system was required.

References

[1] T. Lippert, "Interaction of photons with polymers: From surface modification to ablation," *Plasma Processes and Polymers*, vol. 2, pp. 525–546, 2005.

[2] P. E. Dyer, "Excimer laser polymer ablation: twenty years on," *Applied Physics A: Materials Science and Processing*, vol. 77, pp. 167–173, 2003.

[3] M. C. Gower, *Laser Processing in Manufacturing, Edited by R. C. Crafer and P. J. Oakley.* Great Britain: Chapman and Hall, 1993.

[4] M. C. Gower, "Industrial applications of laser micromachining," *Optics Express*, vol. 7, pp. 56–67, 2000.

[5] P. E. Dyer, I. Waldeck, and G. C. Roberts, "Rapid communication: Fine-hole drilling in Upilex polyimide and glass by TEA CO_2 laser ablation," *Journal of Physics D: Applied Physics*, vol. 30, pp. L19–L21, 1997.

[6] T. Sumiyoshi, Y. Ninpmiya, H. Ogasawara, M. Obara, and H. Tanaka, "Efficient ablation of organic polymers polyether sulphone and polyether ether ketone by a TEA CO_2 laser with high perforation ability," *Applied Physics A: Materials Science and Processing*, vol. 58, pp. 475–479, 1994.

[7] J. H. Brannon and J. R. Lankard, "Pulsed CO_2 laser etching of polyimide," *Applied Physics Letters*, vol. 48, no. 18, pp. 1226–1228, 1986.

[8] P. E. Dyer, D. M. Karnakis, G. A. Oldershaw, and G. C. Roberts, "TEA CO_2 laser ablation of Upilex polyimide," *Journal of Physics D : Applied Physics*, vol. 29, pp. 2554–2563, 1996.

[9] P. E. Dyer, G. A. Oldershaw, and J. Sidhu, "CO_2 laser ablative etching of polyethylene terephthalate," *Applied Physics B: Photo-physics and Laser Chemistry*, vol. 48, pp. 489–493, 1989.

[10] R. Srinivasan and V. Mayne-Banton, "Self developing photo-etching of poly(ethylene terephthalate) films by far ultraviolet excimer laser radiation," *Applied Physics Letters*, vol. 41, pp. 576–578, 1982.

[11] Y. Kawamura, K. Toyoda, and S. Namba, "Effective deep ultraviolet photoetching of polymethyl methacrylate by an excimer laser," *Applied Physics Letters*, vol. 40, pp. 374–375, 1982.

[12] J. T. C. Yeh, "Laser ablation of polymers," *Journal of Vacuum Science and Technology A:Vacuum Surfaces and Films*, vol. 4, pp. 653–658, 1986.

[13] R. Srinivasan and B. Braren, "Ultraviolet laser ablation of organic polymers," *Chemical Review*, vol. 89, pp. 1303–1316, 1989.

[14] N. Bityurin, "Studies on laser ablation of polymers," *Annual Reports on the Progress of Chemistry - Section C*, vol. 101, pp. 216–247, 2005.

[15] E. E. Said-Galiev and L. N. Nikitin, "Ablation of polymers and composites when exposed to CO_2 laser radiation (review)," *Mechanics of Composite Materials*, vol. 28, pp. 97–114, 1992.

[16] P. E. Dyer, M. Pervolaraki, and T. Lippert, "Experimental studies and thermal modelling of 1064 and 532nm Nd:YVO_4 micro–laser ablation of polyimide," *Applied Physics A: Materials Science and Processing*, vol. 80, pp. 529–536, 2005.

[17] R. Braun, R. Nowak, H. O. P. Hess, and C. Schmidt, "Photoablation of polyimide with IR and UV laser radiation," *Applied Surface Science*, vol. 43, pp. 352–357, 1989.

[18] M. Dadsetan, H. Mirzadeh, and N. Sharifi, "Effect of CO_2 laser radiation on the surface properties of polyethylene terephthalate," *Radiation Physics and Chemistry*, vol. 56, pp. 597–604, 1999.

[19] R. Srinivasan, "Ablation of polyimide (kapton) films by pulsed (ns) ultraviolet and infrared (9.17 μm) lasers," *Applied Physics A: Materials Science and Processing*, vol. 56, pp. 417–423, 1993.

[20] R. Srinivasan, "Ablation of polymethyl methacrylate films by pulsed (ns) ultraviolet and infrared (9.17 μm) lasers: A comparative study by ultrafast imaging," *Journal of Applied Physics*, vol. 73, no. 6, pp. 2743–2750, 1993.

[21] D. W. Zeng and K. C. Yung, "XPS investigation on Upilex-S polyimide ablated by pulse TEA CO_2 laser," *Applied Surface Science*, vol. 180, pp. 280–285, 2001.

[22] K. C. Yung and D. W. Zeng, "Laser ablation of Upilex-S polyimide: influence of laser wavelength on chemical structure and composition in both ablated area and halo," *Surface and Coatings Technology*, vol. 145, pp. 186–193, 2001.

[23] A. Hartwig, J. Hunnekuhl, G. Vitr, S. Dieckhoff, F. Vohwinkel, and O. D. Hennemann, "Influence of CO_2 laser radiation on the surface properties of poly(ether ether ketone)," *Journal of Applied Polymer Science*, vol. 64, pp. 1091–1096, 1997.

[24] P. E. Dyer, *Photochemical processing of electronic materials, Edited by I. W. Boyd and R. B. Jackman.* Great Britain: Academic Press, 1992.

[25] V. Zafiropulos, J. Petrakis, and C. Fotakis, "Photoablation of polyurethane films using UV laser pulses," *Optical and Quantum Electronics*, vol. 27, pp. 1359–1376, 1995.

[26] L. Urech and T. Lippert, *Photochemistry and Photophysics of Polymer Materials, Edited by N. S. Allen.* Great Britain: John Wiley and Sons, Inc, 2010.

[27] D. Bäuerle, *Laser Processing and Chemistry, 2nd Edition.* Germany: Springer, 1996.

[28] T. Dumont, S. Lazare, T. Lippert, and A. Wokaun, "Changes in the etch rate of photosensitive polymers as a function of the pulse number," *Applied Physics A: Materials Science and Processing*, vol. 79, pp. 1271–1274, 2004.

[29] S. Küper, J. Brannon, and K. Brannon, "Threshold behaviour in polyimide photoablation: Single-shot rate measurements and surface temperature modelling," *Applied Physics A: Materials Science and Processing*, vol. 56, pp. 43–50, 1993.

[30] H. H. G. Jellinek and R. Srinivasan, "Theory of etching of polymers by far-ultraviolet, high-intensity pulsed laser and long-term irradiation," *Journal of Physical Chemistry*, vol. 88, pp. 3048–3051, 1984.

[31] N. Bityurin, B. S. Luk'yanchuk, M. H. Hong, and T. C. Chong, "Models for laser ablation of polymers," *Chemical Review*, vol. 103, pp. 519–552, 2003.

[32] P. E. Dyer and J. Sidhu, "Excimer laser ablation and thermal coupling efficiency to polymer films," *Journal of Applied Physics*, vol. 57, pp. 1420–1422, 1985.

[33] G. Gorodetsky, T. G. Kazyaka, R. L. Melcher, and R. Srinivasan, "Calorimetric and acoustic study of ultraviolet laser ablation of polymers," *Applied Physics Letters*, vol. 46, pp. 828–830, 1985.

[34] G. A. Oldershaw, "Excimer laser ablation of polyethylene terephthalate: Predication of threshold fluences from thermolysis rates," *Chemical Physics Letters*, vol. 186, pp. 23–26, 1991.

[35] D. Pham, L. Tonge, J. Cao, J. Wright, M. Papiernik, E. Harvey, and D. Nicolau, "Effects of polymer properties on laser ablation behaviour," *Smart Materials and Structures*, vol. 11, pp. 668–674, 2002.

[36] V. N. Tokarev, J. Lopez, S. Lazare, and F. Weisbuch, "High-aspect-ratio micro-drilling of polymers with UV laser ablation: experiment with analytical model," *Applied Physics A: Materials Science and Processing*, vol. 76, p. 385396, 2003.

[37] Y. Feng, J. Gottmann, and E. W. Kreutz, "Structuring of polyetheretherketone by ArF excimer laser radiation in different atmospheres," *Applied Surface Science*, vol. 211, pp. 68–75, 2003.

[38] P. Laurens, B. Sadras, F. Decobert, F. Arefi-Khonsari, and J. Amouroux, "Laser induced surface modifications of poly(ether ether ketone):influence of

the excimer laser wavelength," *Journal of Adhesion Science and Technology*, vol. 13, pp. 983–997, 1999.

[39] P. E. Dyer, G. A. Oldershaw, and D. Schudel, "XeCl laser ablation of polyetheretherketone," *Applied Physics B: Photophysics and Laser Chemistry*, vol. 51, pp. 314–316, 1990.

[40] P. E. Dyer, G. A. Oldershaw, and D. Schudel, "157nm F_2 laser ablation of polyethylene terephthalate," *Journal of Physics D: Applied Physics*, vol. 26, pp. 323–325, 1993.

[41] E. Bormashenko, R. Pogreb, S. Avigdor, S. Sutovski, A. Shulzinger, R. Kerbel, and L. Nachum, "Resonance absorption of coherent infrared radiation by thin polypropylene films and its technological applications," *Applied Surface Science*, vol. 220, pp. 125–135, 2003.

[42] I. B. Sohn, Y. C. Noh, Y. S. Kim, D. K. Ko, and J. Lee, "Laser ablation of polypropylene using nanosecond, picosecond and femtosecond laser," *Journal of the Optical Society of Korea*, vol. 12, pp. 38–41, 2008.

[43] D. Hall and P. E. Jackson, *The Physics and Technology of Laser Resonators*. USA: Taylor and Francis, 1990.

[44] P. W. Kruse, L. D. McGlauchlin, and R. B. McQuistan, *Elements of Infrared Technology: Generation, Transmission and Detection*. USA: Wiley, 1962.

[45] J. Wilson and J. F. B. Hawkes, *Lasers: Principles and Applications*. UK: Prentice Hall, 1987.

[46] J. T. Luxon and D. E. Parker, *Industrial Lasers And Their Applications*. USA: Prentice-Hall, 1985.

[47] J. Hecht, *The Laser Guidebook*. USA: McGraw-Hill, 1986.

[48] *Optical Engineering CO_2 Laser Spectrum Analyser Instruction Manual and Wavelength Tables, Optical Engineering Inc., California*.

[49] E. F. Plinski, J. S. Witkowski, B. W. Majewski, and K. M. Abramski, "The laser pulse from a RF waveguide CO_2 laser," *Applied Physics B: Lasers and Optics*, vol. 76, pp. 375–382, 2003.

[50] W. Koechner, *Solid–state laser engineering*. USA: Springer Science and Business Media, Sixth Revised and Updated Edition 2006.

[51] J. R. Fried, *Polymer Science and Technology*. USA: Prentice Hall PTR, 1995.

[52] X. D. Huang, S. M. Bhangale, P. M. Moran, N. L. Yakovlev, and J. Pan, "Surface modification studies of Kapton HN polyimide films," *Polymer International*, vol. 52, pp. 1064–1069, 2003.

[53] Goodfellow Cambridge Ltd, *PEEK manufacturer technical information (www.goodfellow.com/E/Polyetheretherketone.html), Ermine Business Park, Huntingdon, England*.

[54] L. M. Robeson, *Polymer blends: a comprehensive review*. Germany: Carl Hanser Verlag, 2007.

[55] S. R. Shukla and K. S. Kulkarni, "Depolymerization of poly(ethylene terephthalate) waste," *Journal of Applied Polymer Science*, vol. 85, pp. 1765–1770, 2002.

[56] M. P. Stevens, *Polymer Chemistry – An Introduction, 3rd Edition.* USA: Oxford University Press Inc., 1999.

[57] M. K. Seo and S. J. Park, "Electrical resistivity and rheological behaviors of carbon nanotubes-filled polypropylene composites," *Chemical Physics Letters*, vol. 395, pp. 44–48, 2004.

[58] R. J. Young and P. A. Lovell, *Introduction to polymers.* GB: Chapman and Hall, 1991.

[59] A. Oshima, F. Shiraki, H. Fujita, and M. Washio, "Surface modification of polymeric materials using ultra low energy electron beam irradiation," *Radiation Physics and Chemistry*, vol. 8, pp. 196–200, 2011.

[60] H. Konno, T. Nakahashi, and M. Inagaki, "State analysis of nitrogen in carbon film derived from polyimide Kapton," *Carbon*, vol. 35, pp. 669–674, 1997.

[61] K. P. Pramoda, T. S. Chung, S. L. Liu, H. Oikawa, and A. Yamaguchic, "Characterization and thermal degradation of polyimide and polyamide liquid crystalline polymers," *Polymer Degradation and Stability*, vol. 67, pp. 365–374, 2000.

[62] R. K. Goyal, Y. S. Negi, and A. N. Tiwari, "Preparation of high performance composites based on aluminium nitride/poly (ether ether ketone) and their properties," *European Polymer Journal*, vol. 41, pp. 2034–2044, 2005.

[63] M. O. Zhang, Z. P. Lut, and K. Friedrich, "Thermal analysis of the wear debris of polyetheretherketone," *Tribology International*, vol. 30:2, pp. 103–111, 1997.

[64] P. Patel, T. R. Hull, R. W. McCabe, D. Flath, J. Grasmeder, and M. Percy, "Mechanism of thermal decomposition of poly(ether ether ketone) (PEEK) from a review of decomposition studies," *Polymer Degradation and Stability*, vol. 95, pp. 709–718, 2010.

[65] H. Liu, R. Wang, and X. Xu, "Thermal stability and flame retardancy of PET/magnesium salt composites," *Polymer Degradation and Stability*, vol. 95, pp. 1466–1470, 2010.

[66] J. Bandyopadhyay, S. S. Ray, and M. Bousmina, "Thermal and thermo-mechanical properties of poly(ethylene terephthalate) nanocomposites," *Journal of Industrial and Engineering Chemistry*, vol. 13, pp. 614–623, 2007.

[67] X. Chen, J. Yu, and S. Guo, "Thermal oxidative degradation kinetics of PP and PP/$Mg(OH)_2$ flame-retardant composites," *Journal of Applied Polymer Science*, vol. 106, pp. 1978–1984, 2007.

[68] Z. Fang, P. Song, L. Tong, and Z. Guo, "Thermal degradation and flame retardancy of polypropylene/C_{60} nanocomposites," *Thermochimica Acta*, vol. 473, pp. 106–108, 2008.

[69] D. A. Skoog and J. J. Leary, *Principles of Instrumental Analysis, 4th Edition.* USA: Saunders College Publishing, 1992.

[70] Z. M. Zhang, G. Lefever-Button, and F. R. Powell, "Infrared refractive index and extinction coefficient of polyimide films," *International Journal of Thermophysics*, vol. 19, no. 3, pp. 905–916, 1998.

[71] M. A. El-Bakary, "An interferometric method for determining the mean refractive indices of highly birefringent fibres," *Optics and Laser Technology*, vol. 42, pp. 1004–1009, 2010.

[72] G. Kampffineyer, "Self-supporting thin-film beam splitter for far-infrared interferometers," *Applied Physics*, vol. 14, pp. 313–317, 1977.

[73] E. Bormashenko, R. Pogreb, S. Avigdor, S. Sutovski, A. Shulzinger, R. Kerbel, and L. Nachum, "Resonance absorption of coherent infrared radiation by thin polypropylene films and production of highly developed surface reliefs," *Polymeric Materials*, vol. 88, pp. 258–259, 2003.

[74] J. M. P. Coelho, M. A. Abreu, and F. C. Rodrigues, "Methodologies for determining thermoplastic films optical paramters at 10.6μm laser wavelength," *Polymer Testing*, vol. 23, pp. 307–312, 2004.

[75] G. M. Hale and M. R. Querry, "Optical constants of water in the 200nm to 200μm wavelength region," *Applied Optics*, vol. 12, pp. 555–563, 1973.

[76] Goodfellow Cambridge Ltd, *PI manufacturer technical information (http://www.goodfellow.com/E/Polyimide.html), Ermine Business Park, Huntingdon, England.*

[77] G. Vasconcelos, R. L. Mazur, E. C. Botelho, M. C. Rezende, and M. L. Costa, "Evaluation of crystallization kinetics of poly(ether-ketone-ketone)

and poly(ether-ether-ketone) by DSC," *Journal of Aerospace Technology and Management*, vol. 2, pp. 155–162, 2010.

[78] G. Baschek, G. Hartwig, and F. Zahradnik, "Effect of water absorption in polymers at low and high temperatures," *Polymer*, vol. 40, pp. 3433–3441, 1999.

[79] Goodfellow Cambridge Ltd, *PET manufacturer technical information (www.goodfellow.com/E/Polyethylene-terephthalate.html), Ermine Business Park, Huntingdon, England.*

[80] Goodfellow Cambridge Ltd, *PP manufacturer technical information (www.goodfellow.com/E/Polypropylene.html), Ermine Business Park, Huntingdon, England.*

[81] J. M. Lui, "Simple technique for measurements of pulsed gaussian-beam spot sizes," *Optics Letters*, vol. 7, pp. 196–198, 1981.

[82] F. Yergeau, S. L. Chin, and P. Lavigne, "Multiple ionisation of rare-gas atoms by an intense CO_2 laser," *Journal of Physics B: Atomic, Molecular and Optical Physics*, vol. 20, pp. 723–739, 1987.

[83] J. E. Decker, W. Xiong, F. Yergeau, and S. L. Chin, "Spot-size measurement of an intense CO_2 laser beam," *Applied Optics*, vol. 31, pp. 1912–1913, 1992.

[84] E. Marin, "Characteristic dimensions for heat transfer," *Latin-American Journal of Physics Education*, vol. 4, pp. 56–60, 2010.

[85] R. F. Cozzens and R. B. Fox, "Infrared laser ablation of polymers," *Polymer Engineering and Science*, vol. 18, pp. 900–904, 1978.

[86] Z. Ball, T. Feurer, D. L. Callahan, and R. Sauerbrey, "Thermal and mechanical coupling between successive pulses in KrF–excimer–laser ablation of polyimide," *Applies Physics A: Materials Science and Processing*, vol. 62, pp. 203–211, 1996.

[87] R. Srinivasan, "Etching polymer films with ultraviolet laser pulses of long (10-400μs) duration," *Journal of Applied Physics*, vol. 72, pp. 1651–1653, 1992.

[88] P. Hariharan, *Basics of Interferometry*. USA: Academic Press, 2007.

[89] M. V. Allmen and A. Blatter, *Laser–beam Interactions with Materials: Physical Principles and Applications*. Germany: Springer-Verlag Berlin and Heidelberg GmbH and Co. KG, 1995.

[90] H. S. Carslaw and J. C. Jaeger, *Conduction of Heat in Solids, 2nd Edition*. GB: Oxford University Press, 1959.

[91] L. H. Sperling, *Introduction to Physical Polymer Science, 2nd Edition*. Canada: Wiley and Sons Inc, 1992.

[92] F. C. Burns and S. R. Cain, "The effect of pulse repetition rate on laser ablation of polyimide and polymethylmethacrylate-based polymers," *Journal of Physics D: Applied Physics*, vol. 29, pp. 1349–1355, 1996.

[93] H. H. G. Jellinek and S. R. Dunkle, "HCN evolution from thermal and oxidative degredation of poly(diphenyl methane pyromellitimide) at high temperatures," *Journal of Polymer Science*, vol. 21, pp. 2111–2131, 1983.

[94] L. Abate, S. Calanna, A. Pollicino, and A. Recca, "Thermal stability of a novel poly(ether ether ketone ketone) (pk99)," *Polymer Engineering and Science*, vol. 36, pp. 1782–1788, 1996.